



Virginia Commonwealth University  
VCU Scholars Compass

---

Theses and Dissertations

Graduate School

---

2023

# I. Preparation of Strategic Synthetic Building Blocks for World Health Organization Essential Medicines. II. Applying the Principles of Process Intensification to the Synthesis of Fluoroquinolone Antibiotics.

Jeffrey M. Noble  
*Virginia Commonwealth University*

Follow this and additional works at: <https://scholarscompass.vcu.edu/etd>

 Part of the [Organic Chemistry Commons](#)

© Jeffrey Michael Noble

---

Downloaded from

<https://scholarscompass.vcu.edu/etd/7294>

This Dissertation is brought to you for free and open access by the Graduate School at VCU Scholars Compass. It has been accepted for inclusion in Theses and Dissertations by an authorized administrator of VCU Scholars Compass. For more information, please contact [libcompass@vcu.edu](mailto:libcompass@vcu.edu).

**I. Preparation of Strategic Synthetic  
Building Blocks for World Health  
Organization Essential Medicines**  
**II. Applying the Principles of Process  
Intensification to the Synthesis of  
Fluoroquinolone Antibiotics**

A dissertation submitted in partial fulfillment of the requirements for the degree  
of Doctor of Philosophy at Virginia Commonwealth University

By

Jeffrey Michael Noble  
Bachelor of Science, University of Richmond, 2018

Advisor and Dissertation Director: B. Frank Gupton  
Chair, Department of Chemical and Life Science Engineering

Committee: Dr. B. Frank Gupton, Dr. Everett Carpenter, Dr. Joshua Sieber, Dr. Keith Ellis

Virginia Commonwealth University

Richmond, Virginia

April 2023

© Jeffrey M. Noble 2023

All Rights Reserved

## Acknowledgements

I would like to take a moment to thank all of the people both within the university and without who have made the past five years an incredible experience of educational, professional, and personal advancement. I would never have been able to complete this work without each of you.

First, I would like to thank my committee for their generous time and insight into the projects I have worked on.

Dr. Gupton, without you this work would truly have never been possible. It was luck that I was directed to your lab in the first place, but it was your ingenuity and dedication that made Medicines for All and incredible place to work and study.

My fellow Gupton students, John and Erin. Your friendship and support over the last four years has been one of the brightest spots of VCU. Your willingness to help with problems and instrument training has been invaluable in me reaching this point. Without the two of you, I would never have been able to make it to the end and for that, I cannot thank you enough.

The members of the Massey Lab at M4All, for their help and support in guiding my graduate career and the work I performed.

Dr. Tai Yue, for being a mentor and friend. Your oversight and teaching has helped to make me a better scientist and a better person. I will never be able to repay all the hours of work you have invested into myself and the other graduate students here at M4All. You have been instrumental over the last few years and it was your effort that helped to move me across the finish line.

Amy Miner, Madelyn Lorenz, Chuky Spivey, and Maria Kubick, our fearless lab managers who helped to support not only the work we do but the graduate students, both professionally and personally.

Will Carrick and Adrian Matthews, two of our lab techs who were extremely helpful in performing reactions and a joy to be around.

Dr. John Saathof and Dr. David Snead, your help in defining my early years of graduate school shaped the scientist that I have become.

My girlfriend, Rachel, whose years of support and love have steadied me throughout the highs and lows of graduate school. You are as important to this work as any of the chemistry.

My parents, Chris and Audrey, for all the love and support they have given to me my entire life. Your belief in me was the impetus for all that I have achieved here and will achieve for years to come. I could never have become the person I am today without everything you have given me.

My brother Bryan, who has been a role model for me my entire life and showed me how hard work and never giving up can bring you so far in life. To my sister-in-law Lauren, I have known you so long and have always felt your love and support for me and my family.

All of my grandparents, aunts, uncles, and cousins who have made me laugh and cared for me. Your love and support over the years and the time we have spent together has been invaluable in making me who I am and in helping me achieve this goal.

Alex Richard, who has introduced me to so many new hobbies, has been an incredible friend and fellow graduate student. My other friends, Sean, Jake, and Griffin, our weekly trivia nights and our D&D sessions have always brought me enjoyment and I will always appreciate the friendship we have built over the years.

Lastly, I would like to thank the myriad of hobbies, foods, drinks, and caffeine that helped me get through the last five years.

Thank you for reading.

This work is dedicated to

Audrey Noble

Christopher Noble

## **Abstract**

The synthesis of active pharmaceutical ingredients is often a time-consuming and expensive process. Due to the nature of pharmaceutical manufacturing, these costs are carried forward to the final purchase price by the consumer. Although there are many factors which are involved in the final costing of a pharmaceutical, the cost associated with the synthesis is the primary one which can be managed by chemists and engineers.

This work discusses the synthetic routes of four active pharmaceutical ingredients as well as the synthetic techniques and equipment used with an emphasis on how the application of specific techniques can be applied to decrease the cost of the drug. Four main factors: reagent cost, reaction yield, atom and step economy, and operation costs, are used to guide the work being performed and the routes which are chosen.

Using these variables, we apply process intensification to the synthesis of dolutegravir, glycidyl pivalate, albuterol, and the fluoroquinolone class of antibiotics. Through this, we are able to optimize reaction conditions to improve the final yield of reactions as well as improve purification to allow for direct utilization of our material in solution for subsequent reactions. We also utilize continuous flow chemistry techniques to streamline the synthesis of pharmaceuticals through the application of different flow reactor vessels and peripheral devices.

Lastly, in order to address factors outside of science's control, we develop an alternative synthesis in order to strengthen the drug synthesis against shifts in availability and costing of currently available reagents. By identifying a convergent synthesis using different starting materials and reagents early in the synthesis, the overall synthesis is protected from unexpected or sudden increases in the costs of the current route's starting materials.

## Table of Contents

Acknowledgements.....	iii
Dedication.....	v
Abstract.....	vi
Table of Contents.....	vii
List of Figures.....	ix
List of Schemes.....	xi
List of Tables.....	xii
List of Equations.....	xiii
List of NMR Spectra.....	xiv
List of Abbreviations.....	xv
1. Preparation of Strategic Building Blocks for WHO Essential Medicines.....	1
1.1. Introduction to Techniques.....	1
1.1.1. Considerations for Cost Reduction.....	1
1.2. Dolutegravir.....	6
1.2.1. Introduction.....	6
1.2.2. Prior Art.....	7
1.2.3. Synthesis of ( <i>R</i> )-3-aminobutanol.....	8
1.2.3.1. $\gamma$ -Butyrolactone Route.....	8
1.2.3.2. Chiral Pool Approach.....	9
1.3. <i>S</i> -Glycidyl Pivalate as an Intermediate Towards Pretomanid.....	16
1.3.1. Introduction.....	16
1.3.2. Initial Route Scouting.....	17
1.3.3. Reaction Optimization.....	19
1.3.4. Isolation.....	20
1.3.5. Conclusion and Next Steps.....	23
1.4. A Brief Introduction to Continuous Flow Synthesis.....	24
1.4.1. Continuous Stirred Tank Reactors.....	25
1.4.2. Plug Flow Reactors.....	28
1.4.3. Packed Bed Reactors.....	31
1.4.3. Picking Your Poison.....	32
1.5. Application of Continuous Flow to the Synthesis of Albuterol Sulfate.....	33



1.5.1. Background .....	33
1.5.2. Current Synthesis and Improvements .....	34
1.5.4. Transfer of Synthesis into Continuous Flow .....	35
1.5.5. Albuterol Conclusions and Next Steps .....	50
1.6. Cost Mitigation of WHO Essential Medicines .....	51
1.7. General Procedures and Experimental Data .....	52
1.7.1. General Information.....	52
1.7.2. Procedures and Data towards ( <i>R</i> )-3-Aminobutanol.....	53
1.7.3. Procedures and Data Towards ( <i>S</i> )-Glycidyl Pivalate.....	65
1.7.4. Procedures and Data Towards Albuterol .....	70
2. Applying the Principles of Process Intensification to Fluoroquinolone Antibiotics .....	77
2.1. Background .....	77
2.1.1. Process Intensification .....	77
2.1.2. Fluoroquinolone Antibiotics .....	78
2.2. Prior Art .....	82
2.3. Early Gupton Work <sup>83</sup> .....	83
2.4. Friedel-Crafts Acylation for the Synthesis of Fluoroquinolone Antibiotics.....	85
2.4.1. Introduction.....	85
2.4.2. Meldrum's Acid .....	86
2.4.3. Step by Step Formation of the Backbone .....	87
2.5. <i>S<sub>N</sub>Ar</i> of Fluoroquinolone Antibiotic Intermediates .....	98
2.6. Conclusions and Next Steps .....	102
2.7. General Procedures and Experimental Data .....	104
2.7.1. General Information.....	104
2.7.2. Procedures and Data Towards the Synthesis of Fluoroquinolone Antibiotics .....	105
References .....	128

## List of Figures

Figure 1. Structure of Dolutegravir.....	6
Figure 2. Use of Verbenone as Precursor to the Natural Product Onoseriolide .....	9
Figure 3. Equivalence screens of NaH.....	11
Figure 4. Solvent Screens towards amino alcohol 4 .....	11
Figure 5. Wipe Film Evaporator (WFE).....	13
Figure 6. Yield and Purity Comparison Between Thin-Film Evaporator (Batches 1-4) and Short-Path Distillation (Batches 5-10).....	14
Figure 7. Cost of ( <i>R</i> )-3-aminobutanol dependent on $\beta$ -amino-acid starting material cost and reaction yield.....	15
Figure 8. Retrosynthesis of pretomanid from substituted glycidols .....	16
Figure 9. Semi-continuous distillation of epichlorohydrin .....	21
Figure 10. <i>In situ</i> distillation of epichlorohydrin .....	22
Figure 11. Example of a Continuous Stirred Tank Reactor.....	25
Figure 12. Image of an Example Plug Flow Reaction Instrument used in the Gupton Lab .....	28
Figure 13. Structure of <i>rac</i> -Albuterol Sulfate.....	33
Figure 14. Process Flow Diagram (PFD) for the continuous flow synthesis of albuterol sulfate. Red = Amination and HCl Salt formation; Green = hydrogenation; Blue = crystallization; and Yellow = filtrations, solvent swaps, and solvent removal. ....	36
Figure 15. Tertiary Amine Impurity <b>22b</b> and its reduced counterpart <b>20b</b> in the Synthesis of Albuterol .....	40
Figure 16. ThalesNano H-Cube Mini .....	42
Figure 17. Example of an In-line Static Mixer .....	43
Figure 18. PFD Diagram for our PFR Synthesis of Albuterol.....	44
Figure 19. Additions of Diol in Series .....	45
Figure 20. Split-line Filtration .....	46
Figure 21. Chromatograms of the desired Aminoalcohol enantiomer (A) and the racemic mixture (B). ....	63
Figure 22. Chromatogram for Derivatized products <b>43</b> and <b>44</b> from Enantioenriched Glycidyl Pivalate.....	68
Figure 23. Chromatogram for Derivatized products <b>43</b> and <b>44</b> from Racemic Glycidyl Pivalate .....	68
Figure 24. General Structure of Fluoroquinolones .....	78
Figure 25. Select Collection of Fluoroquinolone Antibiotics.....	80
Figure 26. C-acylation and N-acylation Products.....	84
Figure 27. Friedel-Crafts Acylation of DCFB Performed in a Sealed Tube .....	89
Figure 28. Initial Coordination of AlCl <sub>3</sub> with Acetyl Chloride in a Friedel-Crafts Acylation Mechanism.....	90
Figure 29. Proposed FQAs from Different Halogenated Acetophenones .....	91
Figure 30. Alternate Halobenzenes for Friedel-Crafts Acylation.....	91
Figure 31. Acylation of Halobenzenes Using Acetyl Bromide .....	92
Figure 32. <sup>1</sup> H NMR Spectra Zoom (6.63-6.88 ppm) for the Aromatic Protons of 2,3,6-trifluorophenol <b>44</b> . ....	93
Figure 33. Possible Products of FCA of Trifluorophenol <b>44</b> with Acetyl Bromide.....	93
Figure 34. <sup>1</sup> H NMR Spectra Zoom (7.47-7.53 ppm) for the Aromatic Proton of Crude Reaction Mixture Believed to Contain <b>46b</b> . ....	95

Figure 35. Crystal formation of $\beta$ -ketoester 40 after Column Chromatography .....	97
Figure 36. Ciprofloxacin ( <b>29</b> ) and the Undesired Side-product of $S_NAr$ ( <b>42</b> ) .....	98
Figure 37. Resonance Structures Showing Activation of C7 and C6 Sites of Fluoroquinolone Precursor .....	99
Figure 38. GCMS of Crude Reaction Mixture in the Synthesis of 2,4-dichloro-5- fluoroacetophenone <b>39</b> .....	113
Figure 39. GCMS of Crude Reaction Mixture in the Attempted Synthesis of 1-(2,3,5-trifluoro-4- hydroxyphenyl)ethan-1-one <b>46b</b> .....	115
Figure 40. GCMS of Crude reaction mixture in the Attempted Synthesis of 1,3,4- Trifluoroacetophenone <b>43b</b> .....	118
Figure 41. GCMS of Crude reaction mixture in the Attempted Synthesis of 1,2,3,4- Tetrafluoroacetophenone <b>45b</b> .....	119

## List of Schemes

Scheme 1. Three Step Synthesis to DTG-OMe using ( <i>R</i> )-3-aminobutanol.....	7
Scheme 2. Final Step in the GSK Process of Cabotegravir .....	7
Scheme 3. Synthesis of ( <i>R</i> )-3-aminobutanol starting with $\gamma$ -butyrolactone. <sup>a</sup> Isolated Yield <sup>b</sup> Purity by LCMS Area %.....	8
Scheme 4. Synthesis of ( <i>R</i> )-3-aminobutanol <b>4</b> from homo-beta-alanine.....	10
Scheme 5. Traditional synthesis of albuterol.....	34
Scheme 6. Streamlined synthesis of albuterol starting from bromo-keto-diol <b>21</b> .....	38
Scheme 7. Derivatization of Glycidyl Pivalate for Analysis of Enantiomeric Purity. ....	66
Scheme 8. Chemical Transformations in the Synthesis towards Ciprofloxacin.....	82
Scheme 9. Gupton Route to Ciprofloxacin .....	83
Scheme 10. Initial Retrosynthetic Strategy to Ciprofloxacin .....	85
Scheme 11. Proposed Synthesis Towards Vinyl Ether from Meldrum's Acid.....	86
Scheme 12. Reassessed Meldrum's Acid Route.....	86
Scheme 13. Friedel-Crafts Acylation Route Towards Stepwise Formation of the Fluoroquinolone Backbone.....	87
Scheme 14. Synthesis of Common Intermediate <b>26c</b> towards Norfloxacin over Two Steps .....	97

## List of Tables

Table 1. Costing Analysis for the Synthesis of ( <i>R</i> )-3-Aminobutanol using ( <i>R</i> )-3-aminobutanoic acid.....	14
Table 2. Base and Condition Screens for Glycidyl Pivalate.....	17
Table 3. Glycidyl Pivalate Formation with Epichlorohydrin Recovery .....	18
Table 4. Temperature and equivalent condition screens for glycidyl pivalate .....	19
Table 5. Direct distillation of glycidyl pivalate .....	22
Table 6. Retention times, Area % and Assigned Compounds for the Chromatograms.....	68
Table 7. MIC <sub>90</sub> Values of Selected Fluoroquinolone Antibiotics.....	81
Table 8. LA Catalyst Screens in DMSO.....	100
Table 9. LA catalyst Screens in Pyridine.....	101
Table 10. Equivalent screens of Tin (IV) LA Catalysts.....	102

## List of Equations

Equation 1. Equation for Residence Time .....	29
---	----

## List of NMR Spectra

NMR Spectra 1. <sup>1</sup> H NMR Spectra of $\gamma$ -butyrolactone sodium enolate <b>9</b> .....	54
NMR Spectra 2. <sup>1</sup> H NMR Spectra of $\alpha$ -methylene- $\gamma$ -butyrolactone <b>10</b> .....	56
NMR Spectra 3. <sup>1</sup> H NMR Spectra of 3-methyltetrahydro-2-furanone <b>11</b> .....	58
NMR Spectra 4. <sup>13</sup> C NMR Spectra of 3-methyltetrahydro-2-furanone <b>11</b> .....	58
NMR Spectra 5. <sup>1</sup> H NMR Spectra of 4-hydroxy-2-methylbutanamide <b>12</b> .....	60
NMR Spectra 6. <sup>1</sup> H NMR Spectra of (R)-3-aminobutanol <b>4</b> .....	64
NMR Spectra 7. <sup>13</sup> C NMR Spectra of (R)-3-aminobutanol <b>4</b> .....	64
NMR Spectra 8. <sup>1</sup> H NMR of Glycidyl Pivalate <b>16</b> .....	69
NMR Spectra 9. <sup>13</sup> C NMR of Glycidyl Pivalate <b>16</b> .....	69
NMR Spectra 10. <sup>1</sup> H NMR Spectra of Amino-keto-aldehyde salt <b>19</b> .....	71
NMR Spectra 11. <sup>1</sup> H NMR Spectra for Amino-keto-diol <b>22</b> .....	74
NMR Spectra 12. <sup>1</sup> H NMR of Meldrum's Acid Vinyl Methyl Ether <b>32</b> .....	106
NMR Spectra 13. <sup>13</sup> C NMR of Meldrum's Acid Vinyl Methyl Ether <b>32</b> .....	106
NMR Spectra 14. <sup>1</sup> H NMR of Meldrum's Acid Vinyl Ethyl Ether <b>32</b> .....	107
NMR Spectra 15. <sup>1</sup> H of Meldrum's Acid Vinyl Cyclopropylamide <b>35</b> .....	109
NMR Spectra 16. <sup>1</sup> H of Cyclopropyl Vinylogous Carbamate <b>36</b> .....	111
NMR Spectra 17. <sup>13</sup> C of Cyclopropyl Vinylogous Carbamate <b>36</b> .....	111
NMR Spectra 18. <sup>1</sup> H NMR of 2,4-dichloro-5-fluoroacetophenone <b>39</b> .....	114
NMR Spectra 19. <sup>1</sup> H NMR of 1-(2,3,5-trifluoro-4-hydroxyphenyl)ethan-1-one <b>46b</b> .....	116
NMR Spectra 20. <sup>19</sup> F NMR of 1-(2,3,5-trifluoro-4-hydroxyphenyl)ethan-1-one <b>46b</b> .....	117
NMR Spectra 21. <sup>1</sup> H NMR of 2,4-dichloro-5-fluorobenzene- $\beta$ -ketoester <b>40</b> .....	121
NMR Spectra 22. <sup>13</sup> C NMR of 2,4-dichloro-5-fluorobenzene- $\beta$ -ketoester <b>40</b> .....	122
NMR Spectra 23. <sup>19</sup> F NMR of 2,4-dichloro-5-fluorobenzene- $\beta$ -ketoester <b>40</b> .....	123
NMR Spectra 24. <sup>1</sup> H NMR of Cyclopropyl Vinylogous Amide <b>26a</b> .....	125
NMR Spectra 25. <sup>1</sup> H NMR of Ethyl Vinylogous Amide <b>26b</b> .....	126

## List of Abbreviations

API	Active Pharmaceutical Ingredient
CDI	Cost Driving Intermediate
COPD	Chronic Obstructive Pulmonary Disease
CPME	Cyclopentyl Methyl Ether
CSTR	Continuous Stirred Tank Reactor
DCFA	Dichlorofluoro-acetophenone
DCFB	2,4-Dichlorofluorobenzene
DCFBC	Dichlorofluorobenzoyl Chloride
DI	Deionized
DTG	Dolutegravir
EOR	End of Reaction
FCA	Friedel-Crafts Acylation
FDA	United States Food and Drug Administration
FQA	Fluoroquinolone Antibiotic
GSK	GlaxoSmithKline
HBA	Homo-beta-alanine
IPA	Isopropyl Alcohol
IY	Isolated Yield
LA	Lewis Acid
LAH	Lithium Aluminum Hydride
LC	Liquid Chromatography
LCAP	Liquid Chromatography Area Percent
LLE	Liquid-Liquid Extraction
MA	Meldrum's Acid
MS	Mass Spectrometry
MTBE	Methyl Tert-butyl Ether
NAH	Sodium Aluminum Hydride
NaOMe	Sodium Methoxide
NMR	Nuclear Magnetic Resonance
PBR	Packed Bed Reactors
PFD	Process Flow Diagram
PFR	Plug Flow Reactors
PI	Process Intensification
PPE	Personal Protective Equipment
ppm	Parts per Million
QNMR	Quantitative Nuclear Magnetic Resonance
$S_NAr$	Nucleophilic Aromatic Substitution
TB	Tuberculosis
TFE	Thin-Film Evaporator
THF	Tetrahydrofuran
TMAC	Tetramethyl Ammonium Chloride
TMS	Tetramethylsilane
UTI	Urinary Tract Infection
WHO	World Health Organization



# **1. Preparation of Strategic Building Blocks for WHO Essential**

## **Medicines**

### **1.1. Introduction to Techniques**

#### **1.1.1. Considerations for Cost Reduction**

Pharmaceutical manufacturing is a billion-dollar industry which affects lives across the globe.<sup>1</sup> Access to pharmaceuticals can be improved, especially in lower-income areas and countries, through reduction of the cost of active pharmaceutical ingredients (APIs). According to the United States Food and Drug Administration (FDA), active pharmaceutical ingredient is defined as “any substance that is intended for incorporation into a finished drug product and is intended to furnish pharmacological activity or other direct effect in the diagnosis, cure, mitigation, treatment, or prevention of disease, or to affect the structure or any function of the body. Active pharmaceutical ingredient does not include intermediates used in the synthesis of the substance.”<sup>2</sup> Although the synthesis of APIs can be expensive throughout the entirety of their manufacturing process, it is also observed that specific intermediates can be major cost-drivers. The impact of these cost-driving intermediates (CDIs) can be attributed to a wide range of variables which can be broadly simplified to reagent cost, reaction yield, atom and step economy, and operation costs.

##### **1.1.1.1. Reagent Cost**

Reagent cost is the most straightforward of the variables which affect CDIs. Higher cost of starting materials is, of course, important in the total synthesis of APIs and CDIs, but reagents used in the synthesis can be equally impactful to the final cost. In order to decrease the cost of CDIs, attention must be paid to the purchase price of starting materials and reagents. At a laboratory

scale, reagents and starting materials are often purchased from vendors at relatively low volumes compared to the volumes purchased for the large-scale manufacturing of APIs. These low volume purchases often do not accurately reflect the cost of the materials in bulk, and the use of import/export databases can be helpful in identifying the real-world price of large (multiple kilogram) shipments of desired reagents and starting materials.

Reagent cost can also be volatile over time, so it is good practice to consistently monitor the prices of reagents and starting materials within a synthesis. Not only should the cost of the currently defined synthesis be monitored, alternate syntheses which were more expensive should be monitored in case they become more economically viable. This particular volatility, which exists outside of a single synthetic process, is a major support for the method of identifying multiple syntheses to a single API. By identifying multiple syntheses, effect of price volatility can be minimized by switching to one of the alternate syntheses if it is advantageous. Reagent cost can also be volatile in situations where there is a single manufacturer or very few manufacturers of the material. This can lead to large and sudden price changes in material as well as higher susceptibility to external factors such as starting material supplies, shipping costs, natural disasters, and geographical location factors.

#### 1.1.1.2. Reaction Yield

Reaction yield is another straightforward variable; higher yielding reactions will result in more material manufactured for the same reagent cost. By performing reaction optimization, it is possible to increase the yield of the reactions, and therefore, lower the cost of the synthesis. Another aspect of reaction yield, which should be considered to lower costs is, when possible, to utilize more expensive reagents later in the synthesis to conserve the costs. Very few syntheses, especially multi-step syntheses, produce ideal one-hundred percent yield. Therefore, any yield

below one-hundred percent correlates to an increase in the final cost. In order to minimize the effect on cost that this loss of material results in, the use of more expensive reagents should be performed as late in the synthesis as possible. Although this may not always be possible, it can result in a decrease in CDI cost when applied correctly.

### 1.1.1.3. Atom & Step Economy

Another major factor which defines a synthesis can be broken down into two main aspects, atom economy and step count.<sup>3</sup> Atom economy focuses on the number of atoms being utilized in a synthesis and is weighed against the number of atoms that are in the final product of the synthesis.<sup>4</sup> Since the generation of byproducts is an unfortunate necessity of synthesis, a goal of cost reduction and green chemistry is to minimize the waste generated by these byproducts.<sup>5</sup> Meanwhile, minimization of step count can also have an impact on the cost of the synthesis. Generally, each individual step of a synthesis will require its own reagents, a process for isolation and purification, which inherently leads to some yield loss, and will frequently have some loss of material if the yield is not quantitative. By developing a synthetic route which has fewer steps than an alternative route, the overall cost of the synthesis will likely decrease. The step count is also tied to the atom economy of a reaction. Installation of unnecessary atoms can increase the step count as in the case of protecting groups where a protection step and subsequent deprotection adds two additional steps to the synthesis. Optimization of these reaction economy parameters can be significant in driving down the cost of CDIs as well as lowering the environmental impact of the synthesis.

### 1.1.1.4. Operation Costs

Since the purpose of CDI cost reduction is to make APIs more affordable, we must also consider how synthetic routes will scale-up to the volumes required for large-scale pharmaceutical

manufacturing. Due to the significant differences between lab-scale and kilo-scale manufacturing, such as safety concerns, reagent handling at large scale, and temperature control of reactions, it can be difficult to make decisions on synthetic routes with these operational factors. Some aspects, however, are straightforward and can also be modified to decrease costs at gram scale. In addition to this, developing syntheses which are robust, reproducible, and scalable is just as important. Reactions that require a very narrow range of operating conditions are not preferred since small changes in manufacturing controls could then result in batches which are low-yielding or produce product in lower purity that cannot be used for subsequent reaction steps. The other factor of operation costs that can be applied at lab-scale is a focus on safe and controllable reactions. This aspect can range from the use of appropriate personal protective equipment (PPE) to the use of safer and less volatile reagents in the synthesis as well as order of addition to consume volatile reagents immediately to prevent accumulation. Proper safety practices and an emphasis on running safe reactions can prevent lost time from accidents, and fines or shutdowns as a result of health and safety incidents.

Some aspects of operation costs are not as obvious at laboratory scale but can be important at larger scales. The first of this, which ties into safety, is the control of reactions, especially those with exotherms. At small scale, the control of exothermic reactions is much easier and the consequences of a “runaway” reaction are less dangerous. Syntheses that require particular care to prevent runaway reactions are less favored at industrial scale since additional effort and precautionary measures are required to safely run them. These precautions and the time to implement them for each reaction step will add cost to the synthesis. In addition to safety, there are also chemical procedures that are routinely performed at laboratory scale but are not practical at plant scale. Two examples are cryogenic conditions and the use of traditional column

chromatography for product purification. In batch reactions, cryogenic reactions and chromatographic purifications require large amounts of cooling or purification material respectively. Cooling at smaller scales is more efficient than plant scale due to higher surface to volume ratio. The use of these cryogens can add significant costs to reactions at manufacturing scale.

Chromatographic purifications, specifically column chromatography for the purpose of isolating the desired product from a crude reaction mixture is expensive on large scale due to the cost of the silica, or other stationary phase, required for the column as well as the large volumes of solvents used as the mobile phase. In addition to the raw material cost of the technique, it is also time intensive and requires active attention, increasing the cost as well. As a result, purification techniques that are less resource-intensive, such as distillation and crystallization, are preferred.

Other factors affecting operating costs include the costs of staffing for operating and maintenance of the manufacturing site, rent and utilities, and waste treatment and disposal. Although these costs are significantly different from a laboratory synthesis set-up, it is still possible to decrease the associated costs when determining the best synthetic route. Shorter reaction steps can make the overall synthesis shorter as well, decreasing the labor costs for the synthesis. The use of fewer reaction vessels or vessels with a smaller footprint is another way to decrease costs. By decreasing the physical space occupied by one complete synthesis within a facility, more than one API can be manufactured in the same location, spreading the cost for the space out between them.

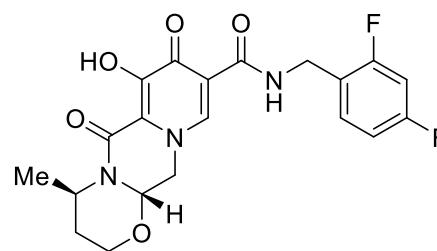
All of these considerations are indefinite and syntheses may be altered during the scale-up process from laboratory to manufacturing regardless of the effort put into optimization in the early steps. However, the synthetic decisions that are made early on in the process can also help determine how the scale-up proceeds and whether it is successful in addition to its financial

efficacy. For these reasons, operation costs are an important factor when trying to improve accessibility of an API.

## 1.2. Dolutegravir

### 1.2.1. Introduction

Dolutegravir (DTG) is an integrase inhibitor used in the treatment of human immunodeficiency virus (HIV) and acquired immunodeficiency syndrome (AIDS).<sup>6</sup> Integrase inhibitors prevent the insertion of HIV viral RNA into the host's chromosomes by blocking

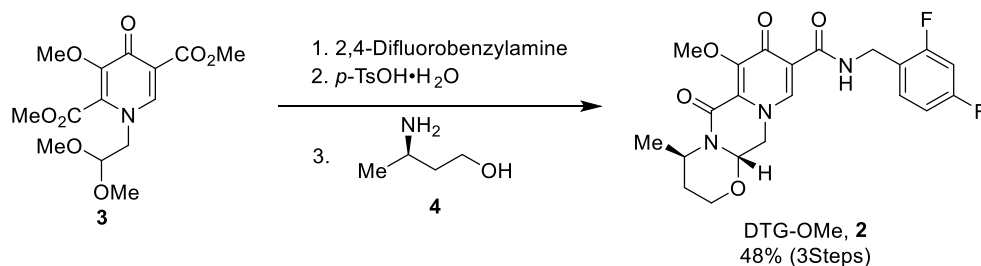


Dolutegravir, 1

Figure 1. Structure of Dolutegravir

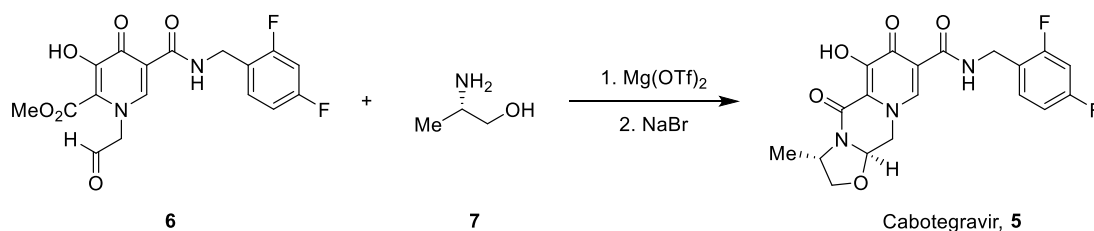
transesterification which is vital for replication and spread of the disease.<sup>7</sup> Due to its effectiveness in combatting HIV, DTG is included on the World Health Organization's (WHO) list of essential medicines. In addition to single dose administration, DTG is also an API in combination drug therapies such as with rilpivirine.<sup>8</sup> In addition to dolutegravir, there are a number of other analogs, for example, cabotegravir, which are being explored for HIV/AIDS treatment.<sup>9</sup> The primary difference between these APIs is the size of the nitrogen and oxygen containing heterocyclic ring present in the molecules.

## 1.2.2. Prior Art



**Scheme 1.** Three Step Synthesis to DTG-OMe using (*R*)-3-aminobutanol

The pharmaceutical company GlaxoSmithKline (GSK) developed DTG and some of its analogs.<sup>9</sup> They have published some of the work on their syntheses, which has allowed for external investigation into the optimization of the synthesis and exploration towards decreasing the cost of the APIs. The Roper research group at VCU identified a continuous flow synthesis over seven steps with an overall yield of 24%.<sup>10</sup> During route exploration, (*R*)-3-aminobutanol (**4**), which is installed during the final step of a three-step telescoped synthesis to form methoxylated DTG **2** (Scheme 1), was identified as a CDI, making up ~30% of the cost of DTG. The DTG-OMe **2** could then be demethylated to give the final API, dolutegravir (**1**). In GSK's synthesis of cabotegravir (**5**, Scheme 2), which has a five-membered oxazole ring, they utilize a shorter chain aminoalcohol



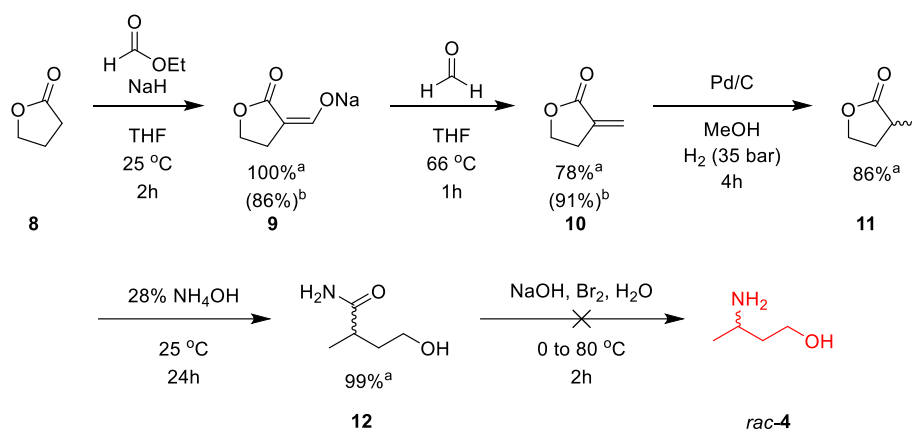
**Scheme 2.** Final Step in the GSK Process of Cabotegravir

(**7**) obtained from the amino acid L-alanine. The synthesis towards dolutegravir, however, requires a longer-chain aminoalcohol to form the six-membered oxazine ring of the molecule. Since this intermediate was determined to be such a large portion of the expense for dolutegravir, we envisioned that it would be prudent to explore alternate syntheses toward this chiral aminoalcohol.

### 1.2.3. Synthesis of (*R*)-3-aminobutanol

#### 1.2.3.1. $\gamma$ -Butyrolactone Route

After identifying (*R*)-3-aminobutanol as the CDI, we approached the synthesis of the intermediate with the intent of decreasing its total cost. Our focus was in the use of low-cost and



widely available starting materials and reagents. Therefore, we initially settled on a synthetic route beginning with  $\gamma$ -butyrolactone (**8**). Our proposed synthesis (Scheme 3) utilized cost-effective materials, with the exception of the palladium catalyst in step 3. However, the palladium catalyst was used at low catalyst loading (10 mol %) and could be recycled after filtration since it was a heterogeneous reaction. As shown in Scheme 3, we observed high yields and moderately high purities for most of our reaction steps. The biggest hurdle associated with this synthesis stemmed from the need for high enantiopurity of the final aminoalcohol. Our developed route established the stereochemistry during the reduction of the exomethylene group at step three. We had been using palladium on carbon without any chiral ligands resulting in a racemic mixture of  $\alpha$ -methylbutyrolactone **11**.

In order for our synthetic route to produce enantioenriched aminoalcohols, an additional step, most likely through the formation of a tartrate salt, would be required and would have a



maximum yield of 50%. We did begin to consider the use of chiral catalysis for an enantioselective hydrogenation; however, these initial screens did not provide good selectivity and drove the cost of the synthesis higher than we had intended. In addition, as we explored alternative stereoselective syntheses, we ran into trouble with the final Hofmann rearrangement step caused by issues with purification of amide **12**.<sup>11</sup> Since preparation of the amide was run under aqueous conditions, the isolation of pure amide was challenging. Initially we were able to obtain a crude mixture of the amide through azeotropic distillation to remove water using methanol and toluene. This crude mixture was subjected to the Hofmann conditions which showed no conversion of starting material. We also explored ion-exchange chromatography which resulted in decomposition of the amide product. We next proposed a modification through a Schotten-Baumann reaction with an acyl chloride on the crude distilled mixture.<sup>12</sup> However, due to mounting complications and perceived cost increases, this route was abandoned as we identified an alternate synthetic route which we believed showed more promise towards lowering the cost of the aminoalcohol CDI.

### 1.2.3.2. Chiral Pool Approach

Chiral pool is an effective synthetic strategy that can provide cost-effective approaches through exploitation of the built-in

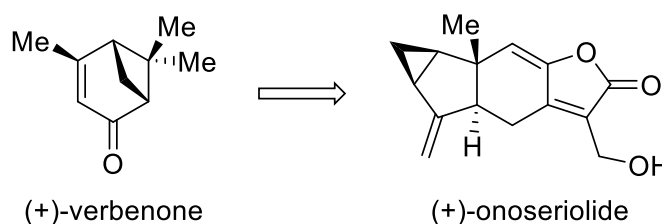


**Figure 2.** Use of Verbenone as Precursor to the Natural Product Onoserialide

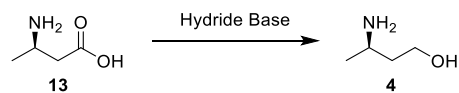
stereochemistry of the starting raw materials to be used. The basis for the technique is the utilization of enantiopure small molecules that are found in nature for installation into larger molecules.<sup>13</sup> Since the stereocenter is already present in the small molecule, it can be carried forward in the synthesis without the use of chiral catalysts or tartrate salt formations. This

technique has been applied to a variety of complex syntheses, including chemotherapy drugs such as onoseriolide (Figure 2).<sup>14</sup>

We believed that the synthesis of cabotegravir **5** was based on the chiral pool technique since the aminoalcohol **7** used in the final step can most likely be synthesized from the  $\alpha$ -amino-acid alanine. However, the  $\beta$ -amino-acid that we required is not natural and is therefore much more expensive. That led us to an initial foray into the butyrolactone route (*vide supra*). However, in the midst of our route development using butyrolactone, a collaborator informed us that they could provide our desired  $\beta$ -amino-acid **4** at a much lower cost (~\$50/kg) than previously expected. Although the material was slightly more expensive than  $\gamma$ -butyrolactone, it would require far fewer steps to obtain our product and would not require any enantioselective reactions as the desired stereocenter was already present within the molecule. As such, the required amino alcohol would have a lower overall cost of goods when made through the  $\beta$ -amino-acid.

#### 1.2.3.3. (*R*)-3-Aminobutanoic Acid (**13**)

Using (*R*)-3-Aminobutanoic acid (**13**), or homo- $\beta$



**Scheme 4.** Synthesis of (*R*)-3-aminobutanol **4**

-alanine (HBA), we developed a procedure based on the

single-step reduction of the carboxylic acid to the desired alcohol (Scheme 4). We began exploration into this reduction using lithium aluminum hydride (LAH).<sup>15</sup> Initially, we performed the reaction with an excess (3 equivalents) of LAH and observed complete conversion of HBA to aminobutanol **4**. However, this reaction had safety issues as the potentially hazardous and reactive reagent, LAH, was used. We also found that the quenching of the reaction and isolation of our material was difficult due to the formation of lithium and aluminum salts. Lastly, the high price of lithium led us to search for alternative reducing agents to perform this reaction.

### 1.2.3.3.1. Condition Screens

We identified an alternative reducing agent, sodium aluminum hydride (NAH), as a suitable alternative. NAH (\$9.7/kg) is significantly less expensive than LAH (\$507/kg), resulting in a decrease in the synthetic cost.<sup>1</sup> In order to determine the efficacy of NAH as a replacement for LAH, we performed two main screens: equivalents of NAH and solvent choice.

Our first screen focused on the equivalents of NAH that were required to observe

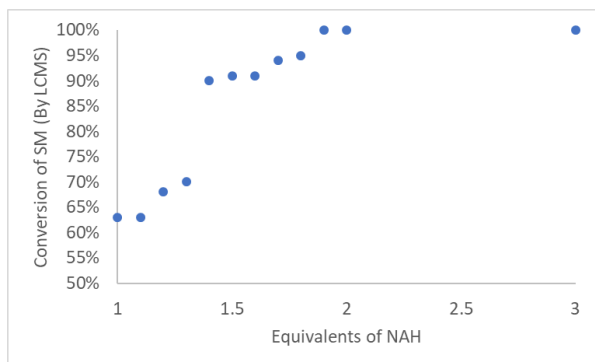


**Figure 3.** Equivalence screens of NAH

high conversion of material. We began our screens following the literature procedure we had found for LAH and performed 12 experiments using between one and three equivalents of NAH. As seen in Figure 3, NAH performed well under the literature conditions of three equivalents, and

we observed similar conversion of ~100% at two equivalents. There was a significant drop off in conversion below 1.9 equivalents which led us to establish two equivalents of NAH as the standard for our reaction moving forward.

Secondly, we investigated solvent effect which would result in high-conversion (Figure 4). We originally performed this reaction using tetrahydrofuran (THF) as the solvent, which is sometimes avoided at large scale due

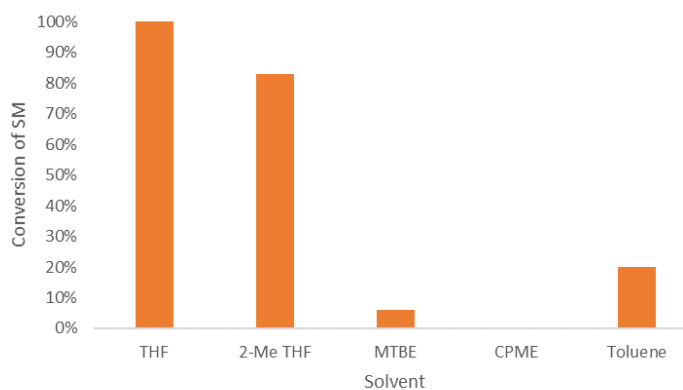


**Figure 4.** Solvent Screens towards amino alcohol **4**

<sup>1</sup> Costing data from Indian import/export databases

to its propensity to form dangerous peroxides. Although THF with BHT added as a peroxide inhibitor can be used safely, we explored alternative ether solvents which form peroxides less readily. Following a screen of 3 alternative ether solvents, 2-Me THF, methyl *tert*-butyl ether (MTBE), and cyclopentyl methyl ether (CPME), as well as toluene (Figure 4), we determined that THF was the most effective solvent for the reaction. Using 2-Me-THF, we did observe conversion over 80%. The other three solvents showed significantly lower conversions ( $\leq 20\%$ ). Although this loss of conversion in 2-Me-THF is significant, it may be that the safety considerations of THF make the loss acceptable. Nevertheless, for the purpose of our small-scale work, we chose to continue with the use of THF for the solvent as we moved forward to isolation of the aminoalcohol **4**.

#### 1.2.3.3.2. Purification & Isolation

The work-up procedure of this reaction required quenching of unreacted NAH by the slow addition of 10% sodium hydroxide solution which generated sodium hydroxide, aluminum hydroxide, and hydrogen gas. This addition was performed slowly and at low temperatures ( $<10$  °C) to control the exotherm. After all excess NAH was quenched, as confirmed by the cessation of effervescence from hydrogen evolution, additional sodium hydroxide solution was added to dissolve remaining aluminum salts. A liquid-liquid extraction (LLE) was then performed, washing the aqueous layer with THF two additional times before collecting the organic layers and carrying them toward purification.

We isolated our desired material by removal of excess THF solvent and performing a short-path distillation on the residual crude mixture. Following this procedure, we were able to reproducibly purify (*R*)-3-aminobutanol (**4**) with  $>60\%$  yield and  $>95\%$  purity (Figure 6, Batches 5-10). These results showed great promise and we believe that larger-scale distillations could

increase the yield with minimal impact on purity. However, due to the necessity to remove THF prior to the distillation, we sought to explore an alternative method for reaction purification, thin-film evaporation (Figure 5).

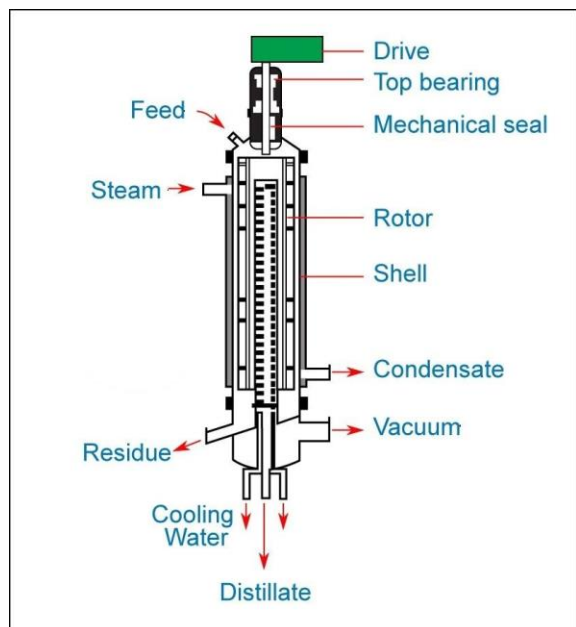


**Figure 5.** Wipe Film Evaporator (WFE). Photo: <https://www.conceptprocess.com/wiped-film-evaporator/>

Wiped-film evaporation (WFE) is a technique which can provide semi-continuous distillation and separation of up to three components. The equipment has three main outlets for material, as seen in Figure 5. In our case, the organic phase of our liquid-liquid extraction (LLE), enters the system through the “feed” valve. From here, the solution drops down along the heated outer column, where rotating blades spread the mixture into a thin-film to maximize the surface

area to heat ratio. The compounds within the heated material can now go one of three places which is controlled by the temperature and vacuum within the system. The most volatile component, in our case THF, would be expelled from the system as vapor and be removed, often using a condenser to collect the material. The second most volatile, in our case the aminobutanol product, is evaporated, but then condenses on a cooled inner column of glass, where it travels downward and is collected in the “distillate” collection flask as purified material. Lastly, any compounds that are less volatile than our product remain on the outer wall where they travel down and are collected in the “residue” collection flask. This technique requires a significant amount of fine tuning, but due to its nature, it is only inherently limited in volume by the volume of each collection flask, meaning it can be readily scaled-up and used for large volume reactions.

We explored the use of the TFE for purification of (*R*)-3-aminobutanol directly from our extracted reaction mixture in THF. We found that the TFE purification (Figure 6, Batch 1-4) typically resulted in slightly higher yield

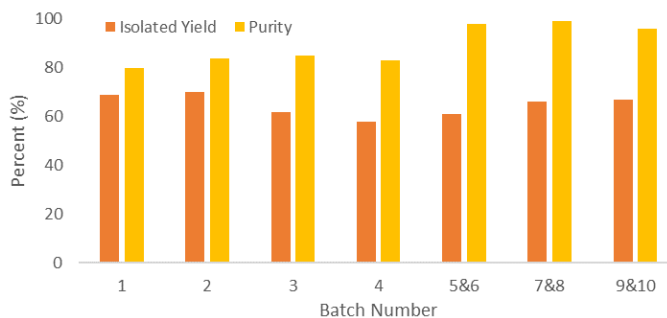


**Figure 6.** Yield and Purity Comparison Between Thin-Film Evaporator (Batches 1-4) and Short-Path Distillation (Batches 5-10). Purity by QNMR.

compared to a short-path distillation, but gave lower product purity (80-85 mol %). Although this technique may be improved using a larger TFE system to allow for better differentiation of components within the mixture, we determined that short-path distillation was more effective for our application.

#### 1.2.3.3.3. Costing Analysis

The most important aspect of this synthesis was the cost of the aminoalcohol. In order to determine the cost (\$/kg) of our synthesis, we needed to factor in all relevant aspects of the reaction and its conditions to provide a cost-of-goods (COG) value. As shown in Table 1, we have the cost per kilogram of each individual reagent and solvent and the amounts of each material

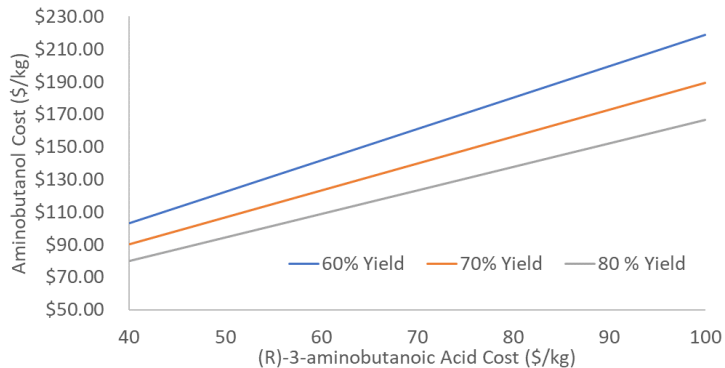
**Table 1.** Costing Analysis for the Synthesis of (*R*)-3-Aminobutanol using (*R*)-3-aminobutanoic acid.

Raw materials	M.Wt.	Amount /mole alanine	Amount /kg product	Equivalents	RM Price \$/Kg	RM Cost \$/batch	RM Cost \$/Kg Product
( <i>R</i> )-3-aminobutanoic acid	103.12	103.12	1.65	1	\$ 50.00	\$ 5,156.00	\$ 82.63
Sodium aluminium Hydride	54	108.00	1.73	2	\$ 5.00	\$ 540.00	\$ 8.65
Tetrahydrofuran	72.11	73.42	11.8	8V	\$ 1.40	\$ 102.79	\$ 1.65
Tetrahydrofuran	72.11	146.84	23.5	16V	\$ 1.40	\$ 205.58	\$ 3.29
Sodium Hydroxide (10%)	40	40.00	0.64	1	\$ 0.30	\$ 12.00	\$ 0.19
Water	18	1031.20	16.53	10V	\$ 0.01	\$ 6.19	\$ 0.10
Product: R-3-amino-butanol-1	89.14	62.40	1			\$ 6,022.56	\$ 96.52
Yield = 70%						Conversion Cost =	\$ 10.00
Recycle Solvent = 90%						Total Cost =	\$ 106.52

used in the synthesis in relation to the final product. Some other aspects of the calculation which are less intuitive are the solvent recycle and conversion cost. The solvent recycle we used was an estimated 90% since the THF used would be recollected after its removal, presumably with high purity, allowing it to be used again in a subsequent reaction. This estimate is based on the experience our costing team members have in large-scale small molecule synthesis. The conversion cost, which is an estimate for the operation costs of the synthesis, was assumed to be on average \$10/kg of product based on experience with multiple manufacturers.

At the time that this work was being performed, a recent transaction registered in an Indian import/export database listed the cost of 400 kg of (*R*)-3-aminobutanol at ~\$345/kg. Using this information, and an assumed cost of \$50/kg of our aminobutanoic acid starting material as shown in Table 1, we can manufacture the aminoalcohol for ~\$107/kg. The cost for the aminobutanoic acid was an estimated price provided to us by our collaborators, TCG Green Chem,

so we wanted to make sure that fluctuations in the price of the starting material would not result in increasing the cost of our synthesis above the standard synthesis. As seen in Figure 7,



even with a cost of starting material

**Figure 7.** Cost of (*R*)-3-aminobutanol dependent on  $\beta$ -amino-acid starting material cost and reaction yield

double our estimate, the manufacturing cost would be about \$190 per kilogram, 45% below the current cost of \$345 per kilogram. Similarly, should the process have fluctuations in final yield, possibly due to issues with distillation, a lower yield of 60% would still only result in a cost around \$220 per kilogram (36% cost reduction). One problem with this process is that currently, our collaborators seem to be the only suppliers of the amino-acid which can result in significant price

fluctuations. However, we believe that due to the drastic cost savings observed from our synthesis, other manufacturers will begin synthesizing the amino-acid in large quantities. Overall, we feel that the application of our synthetic route and purification technique to the manufacturing of the key CDI of dolutegravir provides an opportunity to drastically decrease the cost of the final API and broaden access to it around the world.

### 1.3. S-Glycidyl Pivalate as an Intermediate Towards Pretomanid

#### 1.3.1. Introduction

Tuberculosis (TB) is one of the leading global causes of mortality, and it is believed that one third of the world population suffers from latent TB.<sup>16,17</sup> Pretomanid is a therapy for treatment of tuberculosis, and was recently approved by the US FDA under the Limited

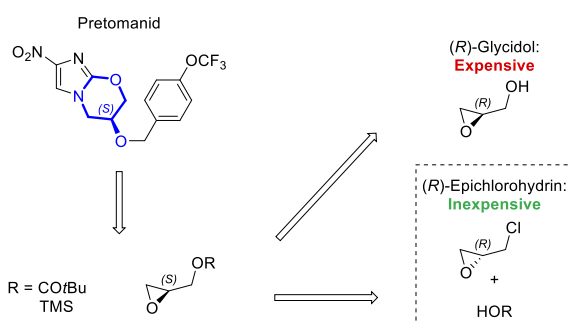


**Figure 8.** Retrosynthesis of pretomanid from substituted glycidols

Population Pathway (LPAD Pathway) for treatment of extensively drug resistant (XDR) tuberculosis in combination with bedaquiline and linezolid.<sup>18</sup> It works as a respiratory poison against bacteria by releasing nitric oxide under anaerobic conditions.

Given the large quantities of drug substance that could be required to treat tuberculosis throughout the world, cost-effective syntheses are highly desirable. A key structural feature of pretomanid is the dihydro-1,3-oxazine containing an oxygen-substituted asymmetric center on the C<sub>3</sub> unit (Figure 8). One could foresee installation of this fragment from an (*R*)-glycidol derivative, and not surprisingly many of the current pretomanid routes make use of functionalized glycidols.<sup>19–22</sup>



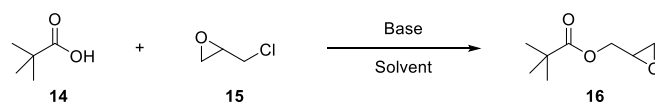
Glycidyl pivalate appears to be a particularly important variant<sup>ii</sup>. Enantiomers of optically active glycidol are of considerable expense, and their construction from less expensive precursors would be desirable. Epichlorohydrin is a feedstock chemical, and its pure enantiomers are readily available. (*R*)-epichlorohydrin is approximately 5-6% of the cost<sup>iii</sup> of (*S*)-glycidol and thus forms the basis for our more cost-effective route to this intermediate.

Numerous reports describe reaction of racemic epichlorohydrin with carboxylates, particularly sterically hindered carboxylates, as the ensuing glycidyl esters are used in alkyd resins, paints, coatings, and acrylate monomer compositions.<sup>23-25</sup> Fewer reports detail the reaction of enantiopure epichlorohydrin with carboxylic acid derivatives. This work describes the development of a practical route to (*S*)-glycidyl pivalate from low-cost and readily available (*R*)-epichlorohydrin and pivalic acid.

### 1.3.2. Initial Route Scouting

Our investigation began with a screen of typical conditions used to couple acids with racemic epichlorohydrin (Table 2<sup>26-31</sup>). We explored equivalents of starting material, preformation of the carboxylate, solvent, variable temperature, and reaction time. We observed that introducing an excess of epichlorohydrin was advantageous. Furthermore, after removal

**Table 2.** Base and Condition Screens for Glycidyl Pivalate



Entry	Epi. (Equiv.)	Base (Equiv.)	Temp. (°C)	Time (hr)	Solvent	Prod. (LCAP)
1	0.6	NaOH (0.25)	55	2	EtOH/H <sub>2</sub> O (1:1)	ND
2 <sup>a</sup>	0.9	NaOH (1)	110	12	Toluene	ND
3 <sup>b</sup>	1.08	NaOH (1.5)	70	1-25	-	ND
4 <sup>a</sup>	2	K <sub>2</sub> CO <sub>3</sub> (2)	80	12	MeCN	9% <sup>d</sup>
5	5	K <sub>2</sub> CO <sub>3</sub> (0.02)	90	2	H <sub>2</sub> O	ND
6 <sup>c</sup>	10	NaOH (1)	120	2	-	<b>96%</b>

<sup>a</sup>) 20 mol% tetrabutylammonium bromide (TBAB). <sup>b</sup>) 8 mol% tetramethylammonium chloride (TMAC, 50% aq.). <sup>c</sup>) 1.5 mol% tetramethylammonium chloride. <sup>d</sup>) % Yield determined by qNMR using 1,3,5-trimethoxybenzene as internal standard.

<sup>ii</sup> Private Correspondence

<sup>iii</sup> Market costs and volumes taken from Indian import/export databases (Zauba and Datamyne)

of exogeneous solvent, we observed the best results, giving glycidyl ester **16** in greater than 95% assay yield (AY) by quantitative  $^1\text{H}$  NMR spectroscopy. While a high molar ratio of epichlorohydrin was employed, we were encouraged that these conditions could be rendered economical if excess starting material were to be recovered.

We subsequently shifted our focus on isolation of the desired compound from the reaction mixture, and the reaction scale was increased to 20 g of pivalic acid and 182 g (10 Eq.) of (*S*)-epichlorohydrin (Table 3). The reaction of sodium pivalate with epichlorohydrin produced one equivalent of sodium chloride which was easily removed by filtration. Next, epichlorohydrin (bp 118 °C) was evaporated and collected. A high proportion (143 g, 87%) of the theoretical amount was collected, an important consideration in rendering an economically viable synthesis. The residual crude glycidyl pivalate (33 g, contained 6% epichlorohydrin) was distilled twice at 50-70 °C under vacuum (~6-10 Torr), resulting in 74% isolated yield of the pure glycidyl pivalate. The compound appeared to be heat sensitive at high concentration, and thus heat history was minimized. The product showed high optical activity ( $-21.87^\circ$ ,  $\text{CHCl}_3$ , 25 °C) as compared to literature values for (*S*)-glycidyl pivalate ( $20.7^\circ$ )<sup>32</sup>. However, the sign of rotation was inverted indicating that the undesired (*R*)-enantiomer had been made. Starting from (*R*)-epichlorohydrin led to (*S*)-glycidyl pivalate samples with  $[\alpha]_D$  values of  $18.8^\circ$  and  $18.9^\circ$ . Attack of the pivalate

**Table 3.** Glycidyl Pivalate Formation with Epichlorohydrin Recovery.<sup>36</sup>

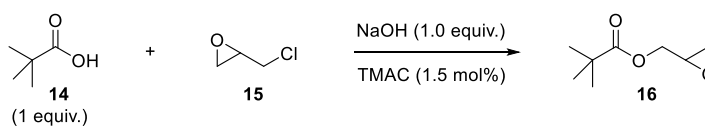
Scale (g)	Isolated Yield, (g, %)	$[\alpha]_D^{25}$ (lit.: ( <i>S</i> )-Glycidol)	Epichlorohydrin Recovery	Recovered Epi. er
20 g	23 g, 74%	$-21.87$ ( $20.7$ )	143 g, 87%	1:1

anion on the methylene carbon of the epoxide rather than the primary chloride rationalizes this observation and has been observed previously.<sup>33</sup> Despite these encouraging results, analysis of the recovered epichlorohydrin revealed that the epichlorohydrin racemized over the course of the reaction.

### 1.3.3. Reaction Optimization

Further reaction optimization was required to identify a cost-effective system due to the racemization of recovered epichlorohydrin. Our goals were to suppress epichlorohydrin racemization and reduce the equivalents of epichlorohydrin to avoid recycling of this starting material (Table 4). We first explored suppression of racemization with the hypothesis that at lower temperatures, the rate

**Table 4.** Temperature and equivalent condition screens for glycidyl pivalate



Entry	Epi. (Equiv.)	Temp. (°C)	Time (hr)	AY	Epichlorohydrin er (R:S) <sup>c</sup>
1	10	120	3	96%	50:50
2	10	60	3	98%	90:10
3	10	50	17	96%	95:5
4	6	120	3	62%	-
5	3	120	3	13%	-
6 <sup>b</sup>	6	120	3	88%	-
7 <sup>b</sup>	3	120	3	80%	-
8	6	60	3	76%	-
9	6	60	24	98%	-
10	3	60	3	61%	-
11	3	60	24	93%	-

<sup>a</sup>) 1 g of pivalic acid combined with epichlorohydrin. NaOH (0.39 g, 1.0 equiv.) and TMAC (0.021 g, 1.5 mol%) added. 1,3,5-trimethoxybenzene (0.165 g, 1.0 equiv.) added as an internal standard. Reaction heated and monitored by quantitative NMR. <sup>b</sup>) Chlorobenzene added as solvent to reach volume equivalent to reaction volume at 10 equiv. of epichlorohydrin. <sup>c</sup>) er determined using derivatization and chiral HPLC.

of racemization might be slower. The alkylation was run at 60 °C which gave high assay yield (entry 2). At this temperature, the enantiomeric ratio increased from 50:50 to 90:10 (Table 4, entry 1 vs 2). While this was a positive development, further improvements were required. The high assay yield was maintained at 50 °C, and enantiomeric ratio was elevated to 95:5 (Table 4, Entry

3). This moved the conditions toward economic viability, however, even slight erosion of optical activity in epichlorohydrin limits the usefulness of its recycling.

Removing the need for the epichlorohydrin recycle would be preferable as it would simplify operations. If the epichlorohydrin equivalency could be reduced, the economic driver for recycle of the starting material would be eliminated. However, simply reducing the equivalents of epichlorohydrin led to much lower yields, and a large amount of decomposition was observed (Table 4, Entries 4-5). The root cause was believed to be its heat sensitivity, where degradation of the product most likely accelerated at elevated concentrations. To evaluate this hypothesis, the reaction run with 3 or 6 equivalents of epichlorohydrin was simply diluted with inert chlorobenzene to a volume equivalent to that of 10 equivalents of epichlorohydrin. This did indeed provide a significant increase to yield at and above 80% (Entries 6-7). Decreasing temperature to 60 °C (Entries 8-11) was found to be the best solution as it further increases yield, avoids the need for exogenous solvent, greatly increases throughput of material, and renders the system highly economical as compared to glycidol.

#### 1.3.4. Isolation

Now that we have identified new conditions for the reaction, we sought to isolate the glycidyl pivalate. Our initial technique was to perform a standard vacuum distillation using a short-path distillation head. Using this method, we observed efficient removal of epichlorohydrin, but low isolated yields of the glycidyl pivalate. We believe this is a result of the same bimolecular degradation of the product that was observed during the reactions ran with lower volumes of epichlorohydrin (Table 4, Entries 4-5).

In response to these results, we identified two feasible solutions: isolate the glycidyl pivalate as a solution in an appropriate solvent, or modifying the distillation to yield a higher purity

glycidyl pivalate. Each of these solutions had benefits and drawbacks. The in solution method was desirable as we believed it could be accomplished in a solution of toluene, a solvent that is used in subsequent steps of pretomanid synthesis<sup>iv</sup> and would maximize the yield by limiting the heat history and concentration of the epoxide. However, this technique would not provide isolated glycidyl pivalate in the same way an optimized distillation would.

#### 1.3.4.1. In Situ Purification

Isolation of glycidyl pivalate as a solution was explored first (Figure 9). A solvent swap to toluene was carried out as toluene could be used in the subsequent steps. In first attempts toward this goal, epichlorohydrin was directly distilled from the reaction mixture under vacuum, then toluene

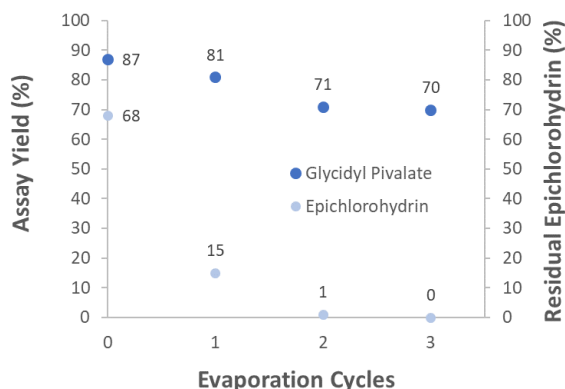


**Figure 9.** Semi-continuous distillation of epichlorohydrin was added intermittently to make-up the volume lost from epichlorohydrin evaporation. Volatiles

were then fully removed to give a glycidyl pivalate residue. The process was repeated three times. This led to a loss of active glycidyl pivalate in solution as observed by decrease in the assay strength (10-15%) and the observation of unidentified by-products (Figure 9).

---

<sup>iv</sup> Unpublished work

Again, heat and concentration sensitivities were suspected to cause the loss in yield. If the solvent swap could be conducted while maintaining constant volume, the decomposition was expected to be mitigated by maintaining concentration and lower temperature. This was accomplished by adding toluene continuously to a stirred solution of the glycidyl pivalate reaction mixture which was

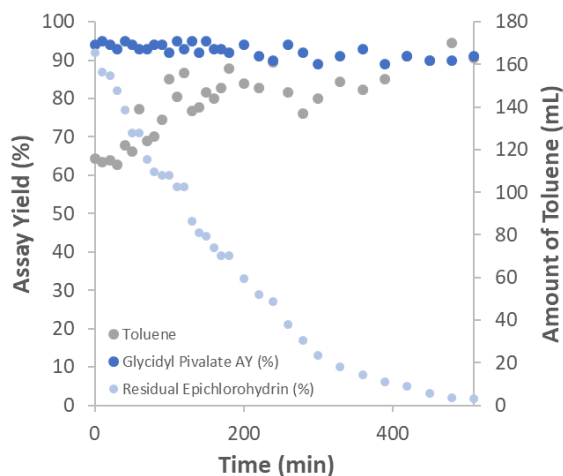


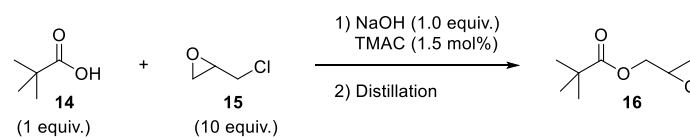
Figure 10. *In situ* distillation of epichlorohydrin

under vacuum (Figure 10). Performing the solvent swap in this manner largely prevented the loss of active glycidyl pivalate to decomposition products. The reaction mixture had a 94% AY at the end of reaction and a 90% AY after removal of epichlorohydrin through a toluene solvent swap. This yields a solution of epoxide **16** which could then be used for the subsequent alkylation step.<sup>19</sup> Although this technique was effective in decreasing the loss of glycidyl pivalate and removing residual epichlorohydrin, its applications were limited since it did not provide pure, isolated glycidyl pivalate and would only be functional for subsequent synthetic steps run in toluene.

#### 1.3.4.2. Direct Distillation

With the goal of broadening the applications of our work, we attempted to isolate glycidyl pivalate in high purity by direct distillation<sup>34</sup> (Table 5). First, sodium chloride was removed from the reaction mixture by filtration, and then

Table 5. Direct distillation of glycidyl pivalate



Entry	Scale (g)	AY, EOR	AY, Epi. Removal	IY	Assay (wt%)	Residual Epi.
1	10	98%	81%	40%	99%	1.0%
2	20	90%	83%	66%	96%	0.0%
3	40	92%	87%	76%	95%	0.2%

epichlorohydrin was evaporated from the filtrate. Care was taken to evaporate epichlorohydrin at minimal temperature under high vacuum (< 10 torr) so that vapors of epichlorohydrin did not exceed 60 °C. After evaporation, the assay yield of the crude glycidyl pivalate residue was 87%. The product was then distilled. Again, it was important to apply maximum levels of vacuum so that the temperature of glycidyl pivalate did not exceed 70 °C. At higher temperature, lower yields were observed as a result of product decomposition. Conditions used in this work were to distill at 50 °C and 6 Torr. This is likely a function of system configuration which can be further optimized upon implementation and might benefit from a continuous distillation system such as a thin-film evaporator so as to minimize thermal history of the heat sensitive compound. Isolated yield reached 76% with material of 95 wt% purity.

Optical activity of the epoxide samples was confirmed through derivatization with 4-nitro-2-bromo-imidazole. The derivatives synthesized from enantiopure epichlorohydrin were compared against those of racemic epichlorohydrin by HPLC or supercritical fluid. The Supercritical Fluid (SFC) traces indicated an enantiomeric ratio of 97:3, which was consistent with the high optical activity observed from the specific rotation.

### 1.3.5. Conclusion and Next Steps

In conclusion, we have developed an efficient method for the preparation of enantiopure (*S*)-glycidyl pivalate from (*R*)-epichlorohydrin and pivalic acid using readily available and inexpensive materials. This work provides an alternative to the synthesis of this important CDI of pretomanid. During the process of this work, we demonstrated the application of multiple techniques for CDI/API cost reduction. Although the primary focus was on the considerable cost savings that come from switching to epichlorohydrin from glycidol, the route would not have been successful without the application of other techniques as well.

This work demonstrated the application of high reaction yield and a consideration for the operation costs of the synthesis. Our high isolated yields were a direct result of our development of two different methods for glycidyl pivalate purification. The first could be reasonably applied to large scale synthesis through a direct introduction of the *in situ* glycidyl pivalate into the next reaction step towards pretomanid. Our second method allows for a broader application of our chemistry to syntheses that do not utilize toluene. In addition to supporting the efficacy of our distillation technique, we also demonstrated its ability to scale and showed an increase in isolated yield as we increased our scale. This technique can be readily performed in the large-scale synthesis of glycidyl pivalate. Further work exploring the synthesis of other glycidol derivatives through epichlorohydrin could provide an opportunity for application of our work to a broader array of APIs.<sup>20</sup>

#### **1.4. A Brief Introduction to Continuous Flow Synthesis**

Continuous flow synthesis refers to a broad range of chemical reactions and processes that occur in a constant stream through a system of reactors to afford a desired.<sup>35</sup> This is in itself an incomplete definition as the continuous flow can refer to a single step which mixes two or more reagents within a line of tubing or to an entire process which passes continuously from one reactor to the next, behaving more similarly to batch processes rather than what is typically imagined when discussing flow. The following account by no means exhausts the discussion surrounding flow chemistry, but we hope to introduce the techniques as well as the factors that led to the decisions we have made.<sup>36</sup>

The most important aspect of continuous flow is its divergence from a traditional batch reactor. A traditional batch reactor is typically a vessel in which discrete reaction operations are



completed. Once a single reaction is performed, the reaction must be ceased, and the material within the vessel must be completely removed before the next reaction can be performed in it. In a continuous flow reactor, more material can be continuously added to the reaction vessel without cessation of the reaction. Some of the vessels used for continuous flow are continuous stirred tank reactors, plug flow reactors, and packed bed reactors.<sup>35</sup> In general, continuous stirred tank reactors look and perform similarly to batch reactors, while plug flow reactors perform the chemical interactions through constant flowing of material within small-diameter tubing. Packed-bed reactors are often cylindrical cartridges that contain reagents, often facilitating heterogeneous solid/liquid phase reactions. These three vessel types are not an exhaustive list, but are the most applicable to the chemistry performed in this work.

#### 1.4.1. Continuous Stirred Tank Reactors

Continuous Stirred Tank reactors (CSTRs) are one class of reactors that are utilized in multi-step continuous flow syntheses. CSTRs, such as in Figure 11 are applied similarly to a traditional batch reactor, with the primary difference being the presence of an outlet for product to flow out of the reactor and into subsequent steps.<sup>37</sup> Similar to batch reactors, CSTRs achieve their mixing through an internal stirring mechanism whether it be an overhead stirring device or an internal

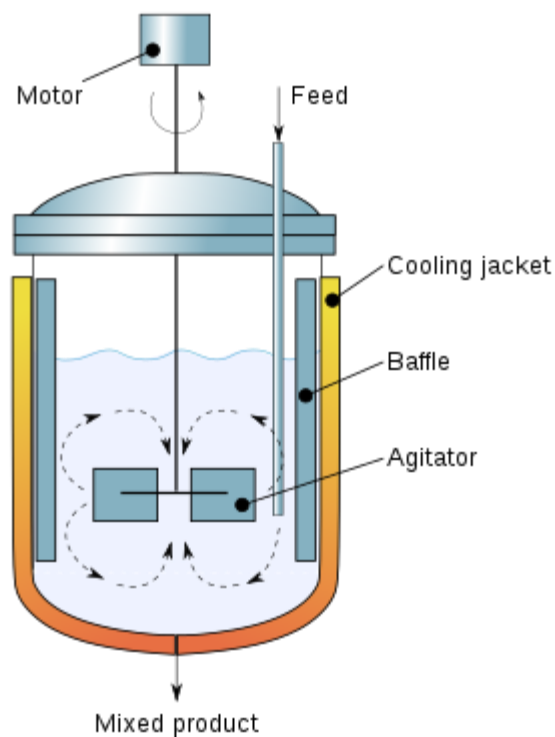


**Figure 11.** Example of a Continuous Stirred Tank Reactor. Image source: Wikipedia ([https://en.wikipedia.org/wiki/Continuous\\_stirred-tank\\_reactor](https://en.wikipedia.org/wiki/Continuous_stirred-tank_reactor))

magnetic stirrer. Reagents are continuously added to the CSTR and allowed to react in an environment of controlled temperature, pressure, atmosphere, and mixing. Material is continuously removed at an equal rate to maintain a consistent reactor volume.<sup>37</sup>

A major benefit of CSTRs is its similarity to batch reactors, which often results in minimal changes in the reaction when transferring the process from batch into continuous flow. In CSTRs, residence time can be equated to the time it takes the traditional batch reaction to occur. Starting material feed and product removal rates are equal to preserve the reactor volume. Flow rate is determined based on the reactor volume and the time required for the desired reaction. Initial conditions for reaction in a CSTR can easily be based on batch conditions but optimization should always be expected to be necessary.<sup>38</sup>

CSTRs offer an opportunity to perform continuous flow on reaction steps which are otherwise difficult to perform continuously. One of the major advantages of using a CSTR for continuous flow over plug-flow reactors is the ability of the reactor to handle heterogeneous mixtures and generation of precipitates during the course of a reaction.<sup>39</sup> Since the CSTR is designed similarly to a standard batch reactor, heterogeneous mixtures can be stirred in the same way, and if necessary, solids can be filtered out prior to removal from the CSTR or, using appropriate pathways, can be carried through to membrane filters.

The use of filtration following a CSTR can allow for a wider variety of reactions to be transferred to continuous flow including those where the desired product precipitates out of solution and can be washed by solvent addition at the subsequent filtration step. This process is preferable to precipitation within standard flow tubing as it allows for a slurry to be formed prior to moving through the tubing instead of precipitation occurring within the tubing itself causing

blockages. Although plug flow reactors can handle some precipitation, it requires a much more tightly controlled system.<sup>40</sup>

The ability to filter reaction mixtures as they are being removed from the CSTR also provides an advantage when working with heterogeneous catalytic reactions. Catalyst is charged to the CSTR prior to the addition of solvent or other reagents. Due to regeneration of the catalyst during the reaction process, it can be maintained in the CSTR as reactive material for extended periods of time. When the catalyst has become deactivated, it can be removed from the CSTR for regeneration.<sup>41</sup>

Although CSTRs can provide a simpler transfer of a synthesis from batch into continuous flow, they do not typically offer the same control over the reaction or safety benefits that are observed in tubing-based continuous processes. Due to these short-comings, it is beneficial to perform continuous flow reactions in plug flow reactors when possible.

## 1.4.2. Plug Flow Reactors

Traditionally, when imagining a continuous flow system, one would expect to see the use of plug flow reactors (PFRs). PFRs can be broad in their complexities, ranging from a simple tubing setup with syringe pumps, all the way up to complex large-scale manufacturing reactors with hundreds of feet of tubing inside of them.<sup>35</sup> Some systems do not involve tubing at all, but are instead composed of glass mixing plates where the reactions are performed. However, all of these systems offer the same basic ability: flowing material through a system and allowing for reaction to take place



**Figure 12.** Image of an Example Plug Flow Reaction Instrument used in the Gupton Lab

within. PFRs offer a wide range of controls to this basic set-up which can provide monumental differences in the transfer of a batch process into continuous flow.<sup>35</sup>

Reaction conditions such as temperature, time, and mixing can be altered based on the type of flow reactor being used and better control over these variables is provided in PFR systems than in some batch and CSTR systems.<sup>35,37</sup> Temperature is a factor which can be significantly different between batch systems and PFRs, due to the higher surface to volume ratio for tubing compared to a traditional batch reactor. A PFR tubing system immersed in a heated oil bath is more evenly heated throughout the reaction than a round bottom flask of the same total volume immersed in the same bath. This is due to the fact that the oil bath is only heating the outer “skin” of the reaction

flask and is in direct contact with a much lower volume at any time point than in the PFR system. Although stirring within the flask reaction can help to improve heat distribution, it is still not as efficient as a PFR system. This improved heat distribution in PFRs can result in faster reactions and greater overall temperature control.<sup>42,43</sup>

Reaction time is another variable that can be precisely controlled within a PFR system using a combination of two main factors, flow rate and reactor volume. Flow rate refers to the

**Equation 1. Equation for Residence Time**

$$T_R = \frac{\text{Reactor Volume}}{\text{Flow Rate}}$$

speed that the material is flowing through the tubing system and can be measured generally using volume per time. Reactor volume is the internal volume of the portion of the reactor where the reaction is occurring, such as a heated zone. Together, these two variables determine the residence time ( $T_R$ ) of the reaction in the system.

The residence time can be controlled by altering either of the two variables, which allows for very fine tuning of reaction conditions and closely ties into the mixing that is observed within the reaction system. Mixing in flow, under ideal conditions, is assumed to occur in only the radial direction and not axially through diffusion.<sup>35</sup> However, as flow rates decrease, this assumption becomes less true and there can be more diffusion-based mixing than radial mixing. Diffusion-based mixing can decrease the precision of the residence time calculation since it can occur in both the forward and backward direction, extending or shortening a particular plug's residence time. Therefore, when making significant changes to  $T_R$ , it is preferable to change the reactor volume rather than the flow rate, especially for increasing  $T_R$ .

Although reactor volume is the most important for determining reaction conditions, the total system volume, which includes the reactor volume as well as non-reactor volume, must be

considered. Typically, there is some transfer tubing to carry the materials from their source flasks to where they mix, as well as tubing leading into and out of the reactor. At reactions which occur at or near room temperature, the lead-in tube volume can be important since it is likely there is some reaction occurring between mixing and where heat is applied. In these situations, minimizing the tube volume between mixing and reactor is important for having accurate reaction control.

Understanding of these variables allows for more accurate fine-tuning of reaction conditions and can be combined with peripheral devices to improve the reaction profile or achieve otherwise unavailable reactions. One such peripheral device is a static mixer, which can be added within a flow line to promote turbidity within the line.<sup>44</sup> Static mixers often consist of a stationary, helical structure within a wide tube which causes material flowing through the line to mix better than would occur within a standard flow tube. This can help to prevent the formation of small pockets of unreacted reagents forming.

Peripheral devices can also be used to allow for the transfer of syntheses into flow that would be difficult to do in a standard system. One such peripheral is an in-line membrane separator. The membrane separator is an in-line porous filter which can perform liquid-liquid separations, solid-liquid separations, and gas-liquid separations.<sup>45</sup> This separation technique is a potent tool for the isolation of desired material and removal of undesired precipitates, reagents, or side-products which could hinder later steps of the reaction.

Altogether, PFRs can be customized to support a wide range of reactions and novel techniques. Devices are commonly being added as the field increases in popularity. In addition to reactions that require precise control, PFRs can also provide a safer alternative to conducting hazardous reactions in batch conditions, especially on industrial scale. This advantage is related to the temperature control of the flow system and the high surface to volume ratio in PFRs.<sup>43</sup> Highly

exothermic reactions, with the risk of runaway reactions, must be carefully controlled on large-scale. Due to the nature of PFRs, the risk of runaway reactions is greatly decreased, as an exothermic reaction is less likely to initiate nearby exotherms since axial mixing through diffusion is decreased, localizing the reaction to a single “plug” within the tubing. In addition, the small volume and the higher surface to volume ratio in a PFR system allows for more efficient cooling and heat dissipation of the reaction, making it less likely to pose a safety problem.<sup>46</sup>

The use of PFRs does not only mitigate the risk of running exothermic reactions. Chemistry which involves the generation of dangerous, hazardous, or unstable intermediates can be performed safely in continuous flow. For example, flash chemistry, which is chemistry which generates or requires unstable intermediates is amenable to PFRs.<sup>47</sup> PFRs allow for these unstable intermediates that would otherwise collapse or react in an undesired way to be trapped by the desired reactant. Intermediates such as aziridines<sup>48,49</sup> and benzyne<sup>50</sup> which are difficult or unsafe to generate in large scale batch reactions can be utilized in a PFR where fast subsequent reactions can occur.

### 1.4.3. Packed Bed Reactors

Packed bed reactors (PBRs) are a type of continuous reaction vessel which can be used for assisting in different applications within continuous flow. In our work, we focus on applying PBRs to heterogeneous catalysis reactions and in-line filtrations. In general, a packed bed reactor consists of a cylinder which is filled with some sort of material or solid support, and most importantly with a filter to prevent the carrying of material out of the cartridge.<sup>35</sup>

For use in heterogeneous catalysis or reactions with solid-supports, the PBR cartridge is packed with catalyst or other reagent, and the reaction mixture is flowed through the cartridge

similarly to a PFR reaction. The use of regenerating catalysts for PBRs is beneficial as a large volume of reaction mixture can be passed through the cartridge with a small loading of the catalyst, helping to keep costs down. Eventually, the catalyst will need to be removed for regeneration, at which point a new cartridge can be installed.<sup>51</sup>

Filtration using a packed bed is less common, but can be useful for isolating small amounts of insoluble side-products from a flowing reaction mixture. This process can be employed by preparing an empty cartridge with a frit of some sort which can stop flow of the solid particulates within the reaction. This can be modified to include specific filter material such as silica, celite, charcoal, or other solids. These filter designs are commonly used in at-home water filtrations.<sup>52</sup> The filter will need to be regularly replaced and cleaned for continued application. This can cause down-time within the flow system and remove some of the benefits of flow including automation and lack of operation processes.

### 1.4.3. Picking Your Poison

Continuous flow synthesis provides an opportunity to allow traditional batch syntheses to be streamlined in favor of a more controllable, safer, and cost-effective technique.<sup>53</sup> However, continuous flow is not always the right answer, especially for very slow (multi-day) reactions. Once the transition to flow begins, it is important to keep in mind the benefits and disadvantages that come with the two reactor types discussed. CSTRs provide a more similar environment to batch, but they are still limited in their application to continuous flow. Transfer from batch into a CSTR can be relatively simple, but CSTRs do not mitigate dangerous or high-energy reactions as well as PFRs. CSTRs do allow for some level of filtration depending on the reaction, but it must also be kept in mind that excessive precipitation or inert solids in the reaction vessel can result in clogging of the tubing or the filter and thus require constant cleaning, negating the benefits of



continuous flow. PFRs offer many improvements and opportunities for cost savings compared to many batch and CSTR syntheses, but a range of factors can limit their efficacy. For instance, it is difficult to carry crude material forward without purification to subsequent synthetic steps. Although some in-line work-ups are possible, such as continuous extractions, continuous distillations, and in-line filtrations, these techniques are not perfect and must be applied judiciously for what is best for each individual synthetic route. Overall, continuous flow is a powerful tool when applied appropriately, but significant consideration must be taken to begin the process.

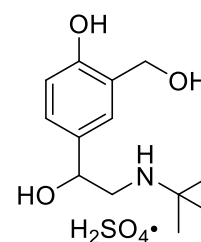
## 1.5. Application of Continuous Flow to the Synthesis of Albuterol Sulfate

### 1.5.1. Background

A powerful technique for cost reduction of APIs is in the identification of major cost-driving intermediates involved in their synthesis followed by process intensification on that specific molecule. However, some APIs are simpler than others and may not have a specific CDI. In these cases, one can take the considerations for cost reduction to CDIs and instead apply them to the entire API synthesis. This is

particularly effective when the synthesis of the API is short and does not involve a large number of different reagents or multiple intermediates. One such API that we have applied these principles to is albuterol sulfate.

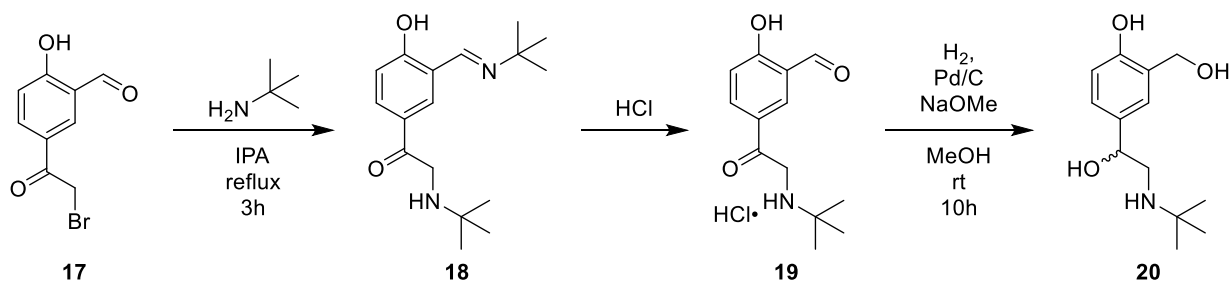
Albuterol sulfate, also known as salbutamol sulfate, is a potent  $\beta_2$ -adrenergic receptor agonist which is used in the treatment of asthma and chronic obstructive pulmonary disease (COPD).<sup>54</sup> Albuterol is listed as an essential medicine by the WHO and it is used across the globe.<sup>55</sup> It is widely available and is synthesized through a traditional batch chemistry process which



*rac*-Albuterol Sulfate  
**Figure 13.** Structure of  
*rac*-Albuterol Sulfate

completes in the addition of sulfuric acid to a solution of the intermediate compound **20** (Scheme 5) to form the API, albuterol sulfate (Figure 13).<sup>56</sup> We identified this process as having potential for transference into a continuous flow synthesis which will facilitate the manufacturing and formulation of the final drug product for distribution.

### 1.5.2. Current Synthesis and Improvements



**Scheme 5.** Traditional synthesis of albuterol.

The current synthesis<sup>56</sup> of albuterol sulfate utilizes bromo-keto-aldehyde **17** as its starting material (Scheme 5). Amination of this starting material with stoichiometric *tert*-butylamine results in an undesired imine formation at the aldehyde. Subsequent addition of excess *tert*-butylamine and mixing at reflux results in the desired S<sub>N</sub>2 reaction of the  $\alpha$ -bromide. We found that these two steps could be completed in a single unit operation using a large excess of *tert*-butylamine (4 equiv) and heating the mixture to reflux (Scheme 5, Step 1) to provide **18**. The imine functional group can be cleaved using hydrochloric acid, which reverts the imine back to the aldehyde, at the same time forming the amine hydrochloride (**19**). This salt showed low solubility in isopropyl alcohol (IPA), resulting in precipitation of high purity **19** (54% yield, 90% purity). After isolation, salt break was performed using NaOMe/MeOH followed by direct carbonyl reduction Pd/C and H<sub>2</sub>. This reaction resulted in the racemic free base of albuterol (**20**). Although there is some evidence showing the activity of (*R*)-albuterol to be higher than (*S*)-albuterol, the current standard for albuterol API is as a racemic mixture.<sup>57</sup> Addition of sulfuric acid results in the

formation of the final API, albuterol sulfate. Albuterol sulfate can then be made into solutions in water, and is often prepared in a pressurized vial for use as an inhalant.

#### 1.5.4. Transfer of Synthesis into Continuous Flow

Based on its short synthesis, we embarked upon the adjustment of the synthesis into a continuous flow process. Based on literature techniques<sup>56</sup> and our own initial reaction screens, we observed that formation of the HCl salt intermediate could be accomplished in a single-pot reaction where the imine formation and amination were allowed to occur followed by addition of concentrated HCl to form the salt intermediate as a precipitate (*vide supra*). The following neutralization of the salt and subsequent hydrogenation could also occur in a single pot together, leaving us with two individual reaction steps followed by an addition of sulfuric acid to form the API. Since these steps require few reagents and unit operations and have been demonstrated in separate single-pot systems, the synthesis could be made compatible with continuous flow.

### 1.5.4.1. Continuous Stirred Tank Reactor Process

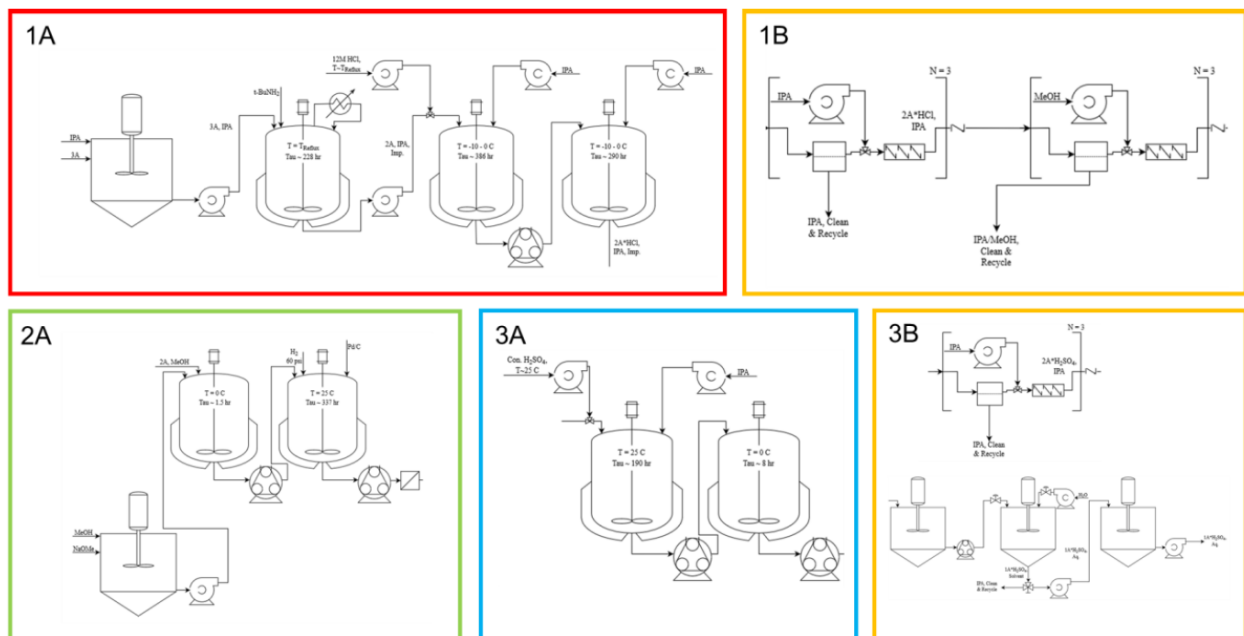


**Figure 14.** Process Flow Diagram (PFD) for the continuous flow synthesis of albuterol sulfate. Red = Amination and HCl Salt formation; Green = hydrogenation; Blue = crystallization; and Yellow = filtrations, solvent swaps, and solvent removal.

As we began this endeavor, we identified the formation of the HCl salt intermediate as a major factor in how we would be able to proceed. Since the precipitation of this salt is spontaneous upon addition of hydrochloric acid, we projected that the best way to transfer this synthesis would be through the use of CSTRs. Using CSTRs provides the easiest transition of the process and allows some control over the precipitation of the salt. During the designing of our CSTR process, a process flow diagram (PFD) of the process was created (Figure 14). In this figure, each of the colored boxes indicates a different type of reaction or unit operation within the process. Red is the amination and HCl salt formation step, green is the hydrogenation, blue is the crystallization, and the yellow boxes are the filtration, solvent swap, and solvent removal steps.

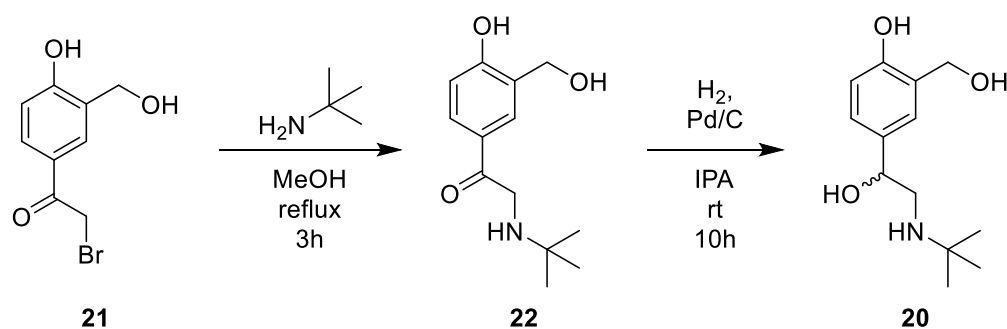
The development of this process was predicated by the low solubility of the intermediate HCl salt **19** in IPA. Therefore, our proposed plan was to generate the imine-amine product **18** in a CSTR and then combine the imine-amine product **18** with HCl in a second CSTR at room temperature. After initial formation of the salt, the slurry of material would be transferred to

another CSTR that is cooled to 0 °C, decreasing the solubility of the salt and promoting more precipitation and increasing yield. The slurry would then be moved into our second module (Figure 14, 1B) where the salt would be washed three times with additional IPA through the use of a membrane filter. The purified material would undergo a solvent swap from IPA to methanol through the use of another membrane filter before being carried forward to the next module for hydrogenation. In the next module, the synthesis again requires the use of CSTRs since the salt and the sodium methoxide added to the reaction mixture are not fully soluble in methanol. The neutralization of the salt occurs in one CSTR, and the mixture is then moved forward to a second CSTR pre-charged with palladium on carbon. Hydrogen is introduced at this stage and hydrogenation is allowed to occur. After the required residence time, which is calculated based on batch conditions, but would be fine-tuned based on experimental results, the reaction mixture is carried forward to the third module. In the third module, we introduce sulfuric acid and IPA at room temperature and then carry the sulfate salt material into a cooled reactor where further precipitation of albuterol sulfate can occur. This material is transferred to our final module, undergoing a similar filtration as in 1B followed by a filter dryer which aims to remove all volatile organic solvents so that the sulfate salt can be suspended in water and carried forward to the formulation modules being explored by our collaborators.

This process is expected to be effective in continuous flow and offers additional opportunities for optimization and streamlining. There are multiple unit operations that can be condensed, especially the triple wash of methanol in 1B that is used as a solvent swap. Although the literature procedure utilized IPA for the amination and methanol for the hydrogenation, we believed we could utilize a single solvent throughout the synthesis. Initial results demonstrated that the amination and HCl salt formation steps could be performed in methanol and resulted in

high purity, albeit slightly lower yields (54% yield, 90% purity). The processing point where we would need to see a switch to a single solvent is in the sulfate salt formation, which was planned to occur with addition of IPA along with the sulfuric acid. This IPA addition added complexity due to the formation of a two-solvent reaction system as well as decreasing the concentration of the salt mixture, resulting in a loss of more material as albuterol sulfate has some solubility in both methanol and IPA. Experiments were performed to determine that albuterol sulfate, although slightly less soluble in IPA (0.0225 mg/g), could still be precipitated out of a neat methanol (0.85 mg/g) system, allowing us to change our synthetic design to use methanol throughout the entire synthesis.

The second, and perhaps more important, opportunity for improvement of the process was removing the requirement for CSTRs and transferring the process, or at least the amination and hydrogenation steps into PFRs. This alteration would help to streamline the synthesis and address the long residence time required by some of the reaction steps.



**Scheme 6.** Streamlined synthesis of albuterol starting from bromo-keto-diol **21**

#### 1.5.4.2. Modification of the Route

Our first step towards transfer into plug flow reactors was bypassing the HCl salt intermediate as that precipitation product and its subsequent neutralization are the primary reasons for requiring CSTRs to perform the synthesis. We found that we could utilize an alternate starting

material, a bromo-keto-diol (**21**, Scheme 6), for the amination reaction due to its lack of a competing site for imine formation. This step resulted in no major precipitation of material **22** and gave high conversion (75%) by LC area percent (LCAP). Since no HCl salt was formed in this process, the hydrogenation could also be transferred into a PFR through the use of a packed bed of palladium on carbon and the use of a flow hydrogenation unit which generates H<sub>2</sub> through electrolysis of water. The initial conversion of the flow hydrogenation was low (~5% LCAP), but we believed we could improve the results through optimization.

For our initial exploration into flow hydrogenation, the ThalesNano H-Cube Mini packed-bed reactor system was used. This system is a “kit system” which is user friendly and allows for simple walk-up use of the instrument. Other than internal variable controls, the only external operation is preparation of the catalyst cartridge which must be packed with the desired catalyst, in our case palladium on carbon. This easier use also helps make the system safer than custom equipment for the typical user. Ease of use is beneficial in the unit operation, but it does sacrifice some control over the reaction process.

As transition of the hydrogenation into flow is performed, considerations must be taken for the technical restriction of flow hydrogenation. In a standard PFR system, if modifications need to be made, changes such as altering temperature, flow rate, and pressure can be performed. However, due to the fixed size of the packed bed, other variables of PFR conditions such as tube volume and tube diameter cannot be easily changed in this flow hydrogenation equipment. The system is also limited in catalyst loading as a result of the fixed cartridge size. Because of these factors, the use of in-line packed bed hydrogenation units is heavily reliant on the specific equipment that is chosen. Using our ThalesNano H-Cube Mini, we have been able to successfully consume all starting material, however, with major production (50% LCAP) of an unknown impurity which

was speculated to be a side-reaction of our amino-keto-diol intermediate (**22**) with oxygen or water. This is attributed to oxygen or water due to the observation of increased degradation following aqueous workups or after sitting under atmospheric conditions. We have performed a number of experiments to determine the cause and circumvent this side-product. These experiments focused on reaction kinetics, utilizing the crude reaction mixture immediately upon amination completion, and maintaining air and water-free environments. We have observed success in mitigating the presence of the impurity using these techniques but have still been unable to characterize it. Attempts at isolation through chromatography were unsuccessful as the product further degraded into another unknown impurity.

#### 1.5.4.3. Batch Synthesis

Our modified synthetic route was initially performed in batch experiments in order to provide us with a better understanding of the reaction conditions and to determine its viability in continuous flow. We performed our amination step following the same procedure as the imine-forming literature route. These conditions showed promising results as we observed ~75% LCAP of our desired product **22**, with the major impurity (~15% LCAP) being the formation of a tertiary amine **22b** caused by reaction of our starting material with the product of the reaction. The remainder of material seemed to be a result of polymerization that also occurred between our product and starting material (<2% LCAP). Lastly, though not detectable using LCMS analysis due to extremely low solubility, we observed some precipitation over the course

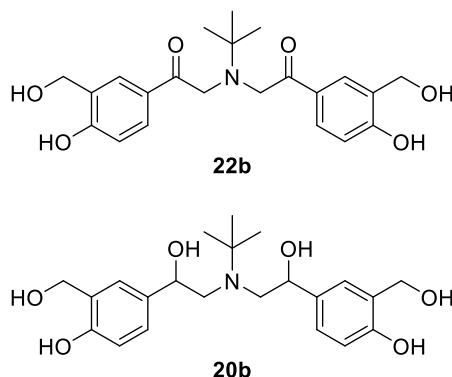


**Figure 15.** Tertiary Amine Impurity **22b** and its reduced counterpart **20b** in the Synthesis of Albuterol



of the reaction. These results were promising, and as a result we decided to move forward to exploring the hydrogenation.

The hydrogenation of compound **22** initially led to low conversion as a result of a side product observed by LCMS (168 m/z), though further characterization of the product has been unsuccessful. In addition, some tertiary amine side-product **22b** was carried forward from the amination and reduced to **20b**. Initial reaction conditions performed following the literature hydrogenation of the HCl salt intermediate, without neutralization, resulted in low yielding reactions (0-5%). These experiments showed low conversion to product, and primarily starting material was observed following the completion of the reaction. To address this, we ran the reaction under more rigorous conditions by increasing the temperature and the hydrogen pressure. Initial experiments showed formation of product, and at times, complete conversion of starting material. It was at this point that we started observing the mass which we later attributed to an oxidation side-reaction of our amine-keto-diol intermediate **22**. Under our best batch conditions, we observed total consumption of starting material and significant generation of product **20** (45% LCAP), but also some of the side-product (20% LCAP). Unfortunately, during the process of optimizing conditions, our batch hydrogenation equipment failed, and we could no longer explore this in batch. Since we had observed conversion to product, we were confident in transferring this procedure into continuous flow and perform our optimization there.

#### 1.5.4.4. H-Cube Hydrogenation and Continuous Amination

Due to the loss of our batch hydrogenation system, we decided to first explore the hydrogenation in continuous flow and work our way backwards to the amination step. For continuous hydrogenation, we utilized a ThalesNano H-Cube Mini system (Figure 16) which carries reaction mixture through tubing and

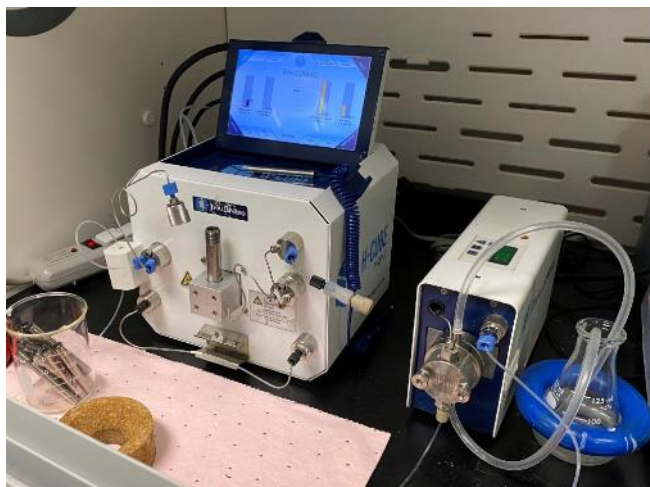


Figure 16. ThalesNano H-Cube Mini

through a packed cartridge of catalyst. In our case, we continued to use 10 wt% palladium on carbon as our catalyst and for the purpose of maintaining continuity between experiments, used a loading mass of 150 mg. Our initial runs, mimicking conditions from our early batch hydrogenations, resulted in no conversion to product. Through a wide variety of conditions, we eventually observed full conversion of starting material **22** to ~25% (LCAP) of our desired product **20**, and ~47% (LCAP) of the product of the side-reaction. Prior to using the H-Cube, we believed this impurity to be a side-product of the hydrogenation itself and not an independent reaction. During the conducting of the H-Cube experiments, we realized that this side-product was being generated spontaneously in our amination reaction mixtures, and was therefore, independent from the hydrogenation. Further discussion of this impurity and potential solutions will be addressed in the troubleshooting section.

After confirming that the hydrogenation could be accomplished in continuous flow, though needing optimization, we began to perform the amination step in continuous flow as well. Initially, we performed the reaction as close to our batch conditions as possible, flowing our diol starting

material **21** in methanol at a rate of 1.61 mL/min and the tert-butylamine neat at a rate of 0.06 mL/min with a residence time of one hour. This reaction was unsuccessful and only showed a conversion to ~5% of product **22**. We assumed that this was due to poor mixing and the lack of axial diffusion within the flow tubing during the reaction. In order to promote improved mixing of the reagents, we performed another experiment where both reagents were in solution in methanol and were programmed to flow together at the same rate. This initial experiment was much more successful and resulted in an LCAP of ~55%. The remainder of material in the mixture consists of ~30% starting material **21**, ~9% tertiary amine impurity **22b**, and small amounts of dimers, trimers, and other polymers which are also observed in our batch conditions.

The considerable increase in conversion is most likely due to improved mixing of the reagents within the flow system. In order to further improve this system, the use of an in-line static mixer (Figure 17) would further improve the mixing and result in better conversion, possibly complete consumption of the starting



**Figure 17.** Example of an In-line Static Mixer. (Photo: koflo.com)

material like in our batch conditions. In-line static mixers are tubular pieces of equipment which contain some sort of regular or spiral structure within that impedes the flow of the system. This flow impediment results in axial mixing within a flow system and can be effective in improving interactions between reagents. The use of a static mixer may also decrease the presence of the tertiary amine impurity, which appears to be formed through the reaction between product and residual starting material. Therefore, improvement of the conversion to product and decreasing the interaction time between product and unreacted starting material would result in less generation of the impurity. Unfortunately, we have been unable to purchase a static mixer that works in our current system due to cost restraints and thus have been unable to test our theory.

### 1.5.4.5. Plug Flow and Packed Bed Reactors

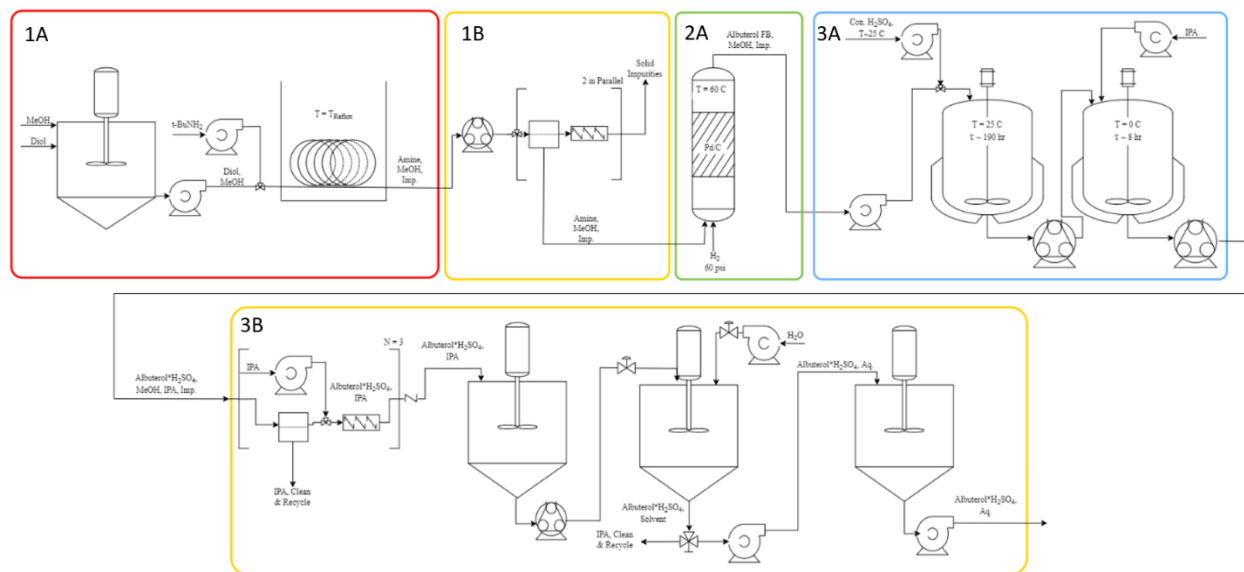


**Figure 18.** PFD Diagram for our PFR Synthesis of Albuterol

With our initial condition screens completed, we determined that by using the bromo-keto-diol as our starting material, we had the opportunity to transfer part of the synthesis of albuterol into plug flow reactors instead of CSTRs (Figure 18). By using PFRs, we were able to remove five CSTRs from the required setup and remove both of the washing and solvent swap operations, greatly decreasing the footprint of our equipment, and the impact of high initial costs for the multiple CSTRs. We did require the addition of an in-line filtration set-up (Figure 18, 1B) to remove the polymer precipitate from the amination, but due to its low level of formation, this should not add excessive strain into our system. Following the filtration, our reaction mixture could proceed into the packed-bed reactor for hydrogenation before converging with the original route with sulfuric acid addition and filter-drying. Unfortunately, the final two modules (3A & 3B) cannot be altered as the formation of the sulfate salt is a necessary step and the filtration is required to produce the purest possible material before transfer to our collaborators.

#### 1.5.4.6. Addressing Synthetic Challenges

An initial observation of our synthetic route leaves much to be desired since we have relatively low yields of our albuterol product in solution and a large excess of an undesired side-product after our second reaction step. In order to address these issues, we must take a closer look at the experiments which helped us understand these problems, the initial steps we have taken to mitigate them, and how we are looking to continue the optimization of both reaction steps.

##### 1.5.4.6.1. Amination Troubleshooting & Understanding

The amination reaction performed well under batch conditions (~75% LCAP) with the major impurity being the tertiary amine which forms when the amine product reacts with the starting material. Other impurities consisted of polymers generated from the starting material and product. It was hypothesized that a slow addition of the diol to a solution of tert-butylamine would decrease the presence of the tertiary amine at the end of the reaction system. This technique is achievable in batch conditions, since diol can be added slowly into a reaction flask, but this becomes challenging when transferring into a PFR system. One technique to adapt this into flow is to incorporate multiple additions of diol in series (Figure 19). Ideally, the addressing of the tertiary amine impurity issue will also address the issue of polymeric impurities as well since we should hopefully see a decrease in interactions between the starting material and product which we believe are forming the polymers.

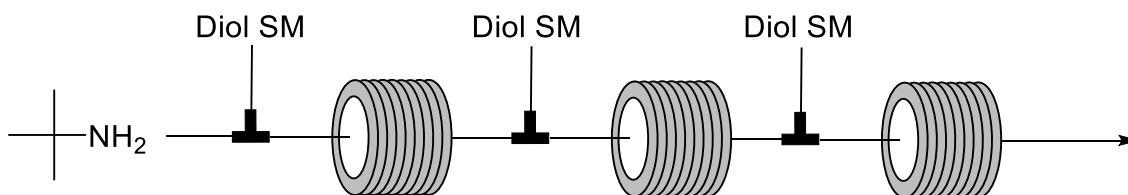


**Figure 19.** Additions of Diol in Series

Another problem for our transfer into continuous flow, as we have seen in our batch studies, is a precipitate which forms during the course of the reaction. Initially, we attempted to identify the precipitate using LCMS and NMR spectroscopy. Our working theory was that the precipitate was the HBr salt of *tert*-butylamine from acid/base reaction with the HBr generated during the reaction. However, the precipitate was a brown color, in dissonance with the literature reported white solid of *tert*-butylamine HBr. More importantly, the *tert*-butylamine salt was reported to be soluble in water, which our precipitate was not. In addition to insolubility in water, we found that it was insoluble in dichloromethane, dimethyl sulfoxide, chloroform, hexanes, toluene, acetonitrile, methanol, isopropanol, and ethyl acetate. As a result of this extreme insolubility, we were unable to identify it via LCMS or NMR. At this time, we believe the precipitate is a polymer of our starting material and dimer. During our attempts at identification, we determined that it was a minor impurity as the collected mass through filtration was only ~40 mg in a reaction using 3 g of our diol starting material. Since the precipitate could be easily removed through filtration, we decided that we could incorporate an in-line filtration between the amination and hydrogenation steps in continuous flow. Although this is not desired, it is a technique that is known to address issues in flow like we are anticipating.

The main drawback of incorporating an in-line filter is the buildup of material within it requiring more hand-on interaction between the operator and the equipment than is typically the goal when transferring a synthesis into continuous flow. This problem has been addressed using a split-line filtration technique where two or more filters are placed in parallel

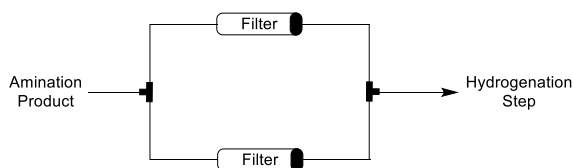


**Figure 20.** Split-line Filtration

with a flow controller directing flow to only a single filter line at one time (Figure 20). Once one filter is filled with the filtered-out precipitate,

then the flow direction can be switched to the next filter in the process. This allows for more time in between filter swaps and all of the filters can be swapped at one time instead of switching them individually as they fill. Since we are seeing such a small amount of precipitate during our reaction, this technique should be effective in removing the undesired precipitate from the reaction mixture before moving to the next step using only a fritted filter and possibly a small celite plug in each filter. Assuming the conditions occur similarly in flow, we would only need to filter ~13 g for every kilogram of starting material that is reacted. This should be the maximum amount of material we see, since our efforts to decrease the tertiary amine and other polymers will also decrease the presence of this precipitate, which we believe is a polymer of the starting material and product.

Overall, the amination performs well in batch conditions and our efforts to transfer the synthesis into continuous flow have made significant headway towards an efficient reaction process. Although our conversion is low, we have a specific plan towards addressing the issues that are causing the problems and the integration of these techniques will continue as the project progresses.

#### 1.5.4.6.2. Hydrogenation Troubleshooting & Reaction Understanding

Our main issue with the reaction process has come from the transfer of the hydrogenation step into continuous flow. As I mentioned before, the breakdown of our batch hydrogenation equipment prevented us from further exploring the optimization of the conditions before transferring them into continuous flow. During our initial transfer of the process into continuous flow, we have been utilizing an H-Cube which supplies hydrogen through the electrolysis of water, a technique which will be relevant later on. In our first H-Cube experiments, we ran using the conditions of the literature route to albuterol, which was room temperature and 60 PSI (~4 bar) of hydrogen. The batch literature reaction was run for 10 hours, but due to the

nature of flow, we used our first experiment to attempt flow rates for the reaction of 0.3 mL/min (the lowest the instrument can go), 0.8 mL/min, and 1.3 mL/min. We saw no generation of product from any of these flow rates, but we also did not see any of the impurity (LCMS - 168 m/z) present.

In order to determine whether the issue was reaction kinetics, we decided to run another reaction using the lowest flow rate (0.3 mL/min) and increasing the temperature to 60 °C. We once again wanted to observe different conditions so we collected fractions that passed through the H-Cube with hydrogen pressures of 10 bar, 30 bar, and 50 bar. For this reaction, to conserve material, we used the combined fractions from the previous H-cube run since no reaction had been observed. When we ran the variable pressure conditions, we saw ~5% (LCAP) of our desired product in all three fractions, residual starting material, and most interestingly, a significant amount of the impurity identified by its mass of 168 m/z. When we took samples of each fraction, we also took a sample of the starting reaction mixture as the fractions were combined from the previous reaction that had sat for a few days, and we observed the same impurity present which had not been present in the analysis of the prior experiment. This led us to realize that the impurity was not a direct side product of the hydrogenation as we had originally thought, but was instead the result of degradation of the amine-keto-diol intermediate **22**.

In order to better understand the conditions that led to this impurity, we performed a complete work-up of our amination product. This workup consisted of filtering off the precipitate, removing the methanol solvent via rotary evaporator, dissolving the residual oil in ethyl acetate, then performing a liquid-liquid extraction with deionized (DI) water. After the organic fractions were collected, anhydrous sodium sulfate and activated charcoal was added, and then removed via filtration. Ethyl acetate was then removed using the rotary evaporator again and the residual oil was dissolved back into methanol for use in another H-Cube experiment. The entirety of the work-



up took ~2 hours. This material was passed through the H-Cube again using conditions of 60 °C, 30 bar H<sub>2</sub> pressure, and 0.3 mL/min flow rate. We also performed a recirculation of the material instead of collecting separate fractions. This was achieved by passing material through the H-Cube, collecting it, and then passing it through again. During this run, we saw complete consumption of our starting material and ~25% (LCAP) of our product. The vast majority of material observed (~55% LCAP), however, was the impurity. Based on these results, we believe the impurity is the result of a side-reaction of the amination product with air or water. This would explain why the impurity was only observed after longer periods of time, since it gave more time for moisture or oxygen in the air to react with the material. In our work-up procedure, we performed an extraction with water which would've introduced moisture into the system and caused the impurity.

To test whether this was a viable theory, instead of performing the full work-up, we performed an amination reaction, removed the methanol solvent and residual *tert*-butylamine on the rotary evaporator, and then dissolved the crude reaction back into methanol and performed an experiment on the H-Cube. This resulted in similar observation of product, some starting material still remaining, and only ~25% of the impurity. This supported our theory, but we were unsure why we were still seeing such large amounts of the impurity. After controlling for every other source of water into the system, we determined that the H-Cube itself must be responsible for allowing water to pass into the system. The equipment is supposed to be designed in a way that prevents most moisture from passing into the reaction, but since the hydrogen is isolated through the electrolysis of water, we knew there was a chance that excess water was being carried through with the hydrogen gas. In order to determine to what extent this was occurring, we ran a test experiment using dichloromethane on its own and setting the instrument to the same parameters

as our prior reaction. We observed that in the course of collecting ~15 mL of dichloromethane from the instrument, we also collected 2-3 mL of water, which was immediately visible as the two separated in our collection vial. This showed that a significant amount of water was entering into our system from the electrolytic cell and the oxidation reaction to the impurity was most likely catalyzed by the high heat in the system causing its prevalence in all of our experiments.

Once again, we found ourselves unable to use a piece of equipment for hydrogenation, although for a much different reason. Now that we have identified the source of the impurity and can thus better account for the factors which cause it, we are looking into alternative flow hydrogenation techniques which use canisters of hydrogen gas instead of electrolysis. We believe that these instruments will provide us with an improved hydrogenation process and allow us to form the albuterol API in high yield.

#### 1.5.5. Albuterol Conclusions and Next Steps

The transfer of a synthesis for albuterol sulfate into continuous flow has been difficult and required significant time and effort into identifying novel conditions in batch and transferring them into flow. Although the project is not complete, we have made significant headway towards the flow process and identifying both the problems involved and solutions which will address them. Now that we have determined the synthetic route, continued work will be assisted by chemical engineers who will be able to choose and modify the best instruments to perform the chemical transformations within the process as well as carry the material forward to its salt formation and subsequent purifications.

## 1.6. Cost Mitigation of WHO Essential Medicines

In this chapter a number of techniques have been introduced which can be used to decrease the costs of APIs and CDIs in the synthesis of essential medicines. Throughout the three projects I have discussed, we have applied these techniques throughout the synthetic process in the pursuit of more cost-effective medicines. One of the best techniques, which we applied for the synthesis of dolutegravir and *S*-glycidyl pivalate is the use of cost-effective starting materials. By opting for more cost-effective starting materials and reagents, we immediately put ourselves in a better position for cost decreases than in trying to just increase yields and perform other optimizations of an already established synthetic route. Although we used more available starting materials, the choice of reagents is also important and finding similar reagents that are less expensive as in our dolutegravir work when we modified the synthesis to use sodium aluminum hydride instead of the significantly more expensive lithium aluminum hydride.

Although these projects are still recent, and it is difficult to see direct effects of cost mitigation in the cost of manufactured pharmaceuticals, we have seen some decrease in the price of dolutegravir since our route to the aminoalcohol **4** was developed. Through communications with our industry partners, we have been made aware that our route to the aminoalcohol was being applied to the synthesis of dolutegravir. Since the date of our information transfer, there has been a significant drop in the cost of dolutegravir from \$750-800 per kilogram to as low as \$247 per kilogram based on the Datamyne import/export database. Although the decrease in cost cannot be exclusively attributed to our work, it is reasonable to believe that the decrease in cost of a major CDI resulted in the lowered price of the API itself as well as the possible utilization of the previous continuous flow work performed by the Roper lab at VCU.<sup>10</sup>

Although cost of materials is an extremely important factor in cost mitigation, it is also a factor of the synthesis which must be continuously reevaluated in order to make sure that the current synthesis remains the most cost-effective. New techniques, new industrial processes, and new trends both in the realm of synthetic chemistry and in the world as a whole can alter the availability of starting materials and reagents of a synthesis, resulting in significant cost changes over time. For example, although lithium may have been a reasonable choice as a reagent, the increase in electric vehicle technologies has put a larger strain on lithium sources for use in vehicle batteries. This change in vehicle trends and other battery technologies has resulted in a high uptick in the cost of lithium making it a poor choice in reagent if another alkali metal reagent will work, even at the cost of conversion or yield.<sup>58</sup> For this reason, it is important to not only have a cost-effective synthetic route, but to also have multiple known routes using different starting materials and reagents in order to be less affected by changes in the cost of reagents. Although a process may not be economically viable at its inception, changes in circumstances can make it a better choice.

## **1.7. General Procedures and Experimental Data**

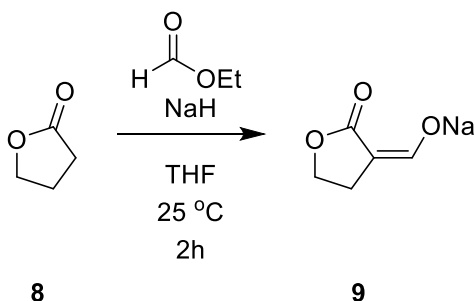
### **1.7.1. General Information**

All commercially available reagents and solvents were purchased from Acros Organics, Sigma-Aldrich, TCI, Alfa Aesar, Combi-Blocks, or Oakwood Chemical and used as received. All ether solvents, unless otherwise noted contained trace BHT as a peroxide inhibitor. Proton nuclear magnetic resonance (<sup>1</sup>H NMR) spectra and carbon nuclear magnetic resonance (<sup>13</sup>C NMR) were recorded on a Bruker Ascend-600MHz. Chemical shifts for protons are reported in parts per million (ppm) downfield from tetramethylsilane (TMS) or referenced to residual solvent. Chemical shifts

for carbon are reported in ppm downfield from TMS or referenced to residual solvent. Data are represented as follows: chemical shift, multiplicity (br = broad, s = singlet, d = doublet, t = triplet, q = quartet, m = multiplet), coupling constant in Hertz (Hz), integration.

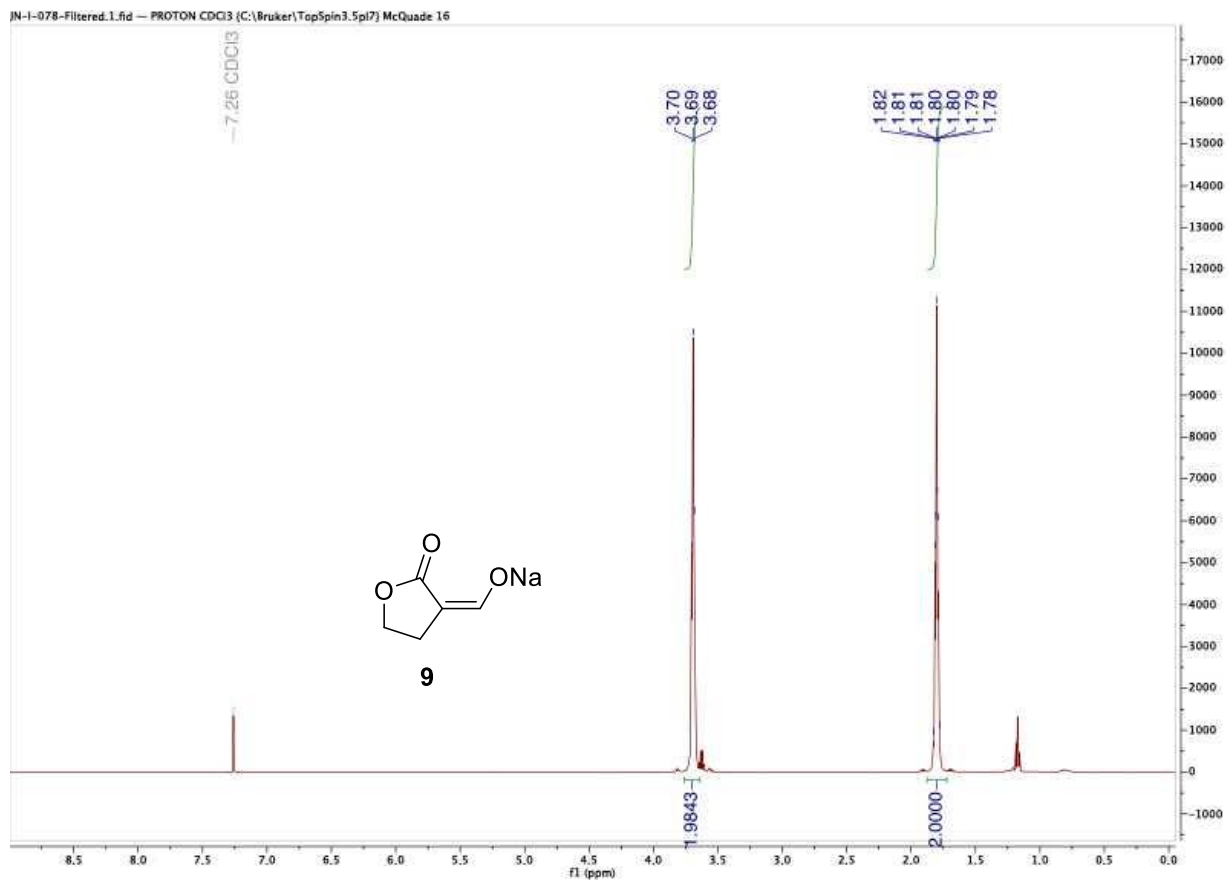
## 1.7.2. Procedures and Data towards (*R*)-3-Aminobutanol

### 1.7.2.1. $\gamma$ -Butyrolactone Route

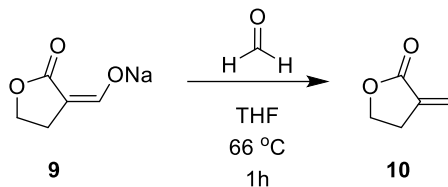


$\gamma$ -butyrolactone sodium enolate **9**: A suspension of sodium hydride (9.0 g, 0.225 mol) (60% wt dispersion in mineral oil) and THF (125mL) was prepared under nitrogen and ethanol (0.9 mL) was added to the stirring suspension. In an addition funnel,  $\gamma$ -butyrolactone (12 mL, 0.15 mol) (**8**) and ethyl formate (12.1 mL, 0.15 mol) were combined. This solution was then added over one hour to the stirring suspension allowing for a steady formation of H<sub>2</sub>. After addition of the butyrolactone solution completed, the suspension was allowed to stir for an additional hour. Upon completion, the suspension was filtered, washed with THF and dried to yield the sodium formyl salt as a white powder (100.3% yield, 86% purity by LCMS Area %). This solid is then moved to the next step without further purification.

<sup>1</sup>H NMR (600 MHz, Chloroform-*d*)  $\delta$  3.7 (t, *J*= 6.4 Hz, 2H), 1.82-1.78 (m, 2H).

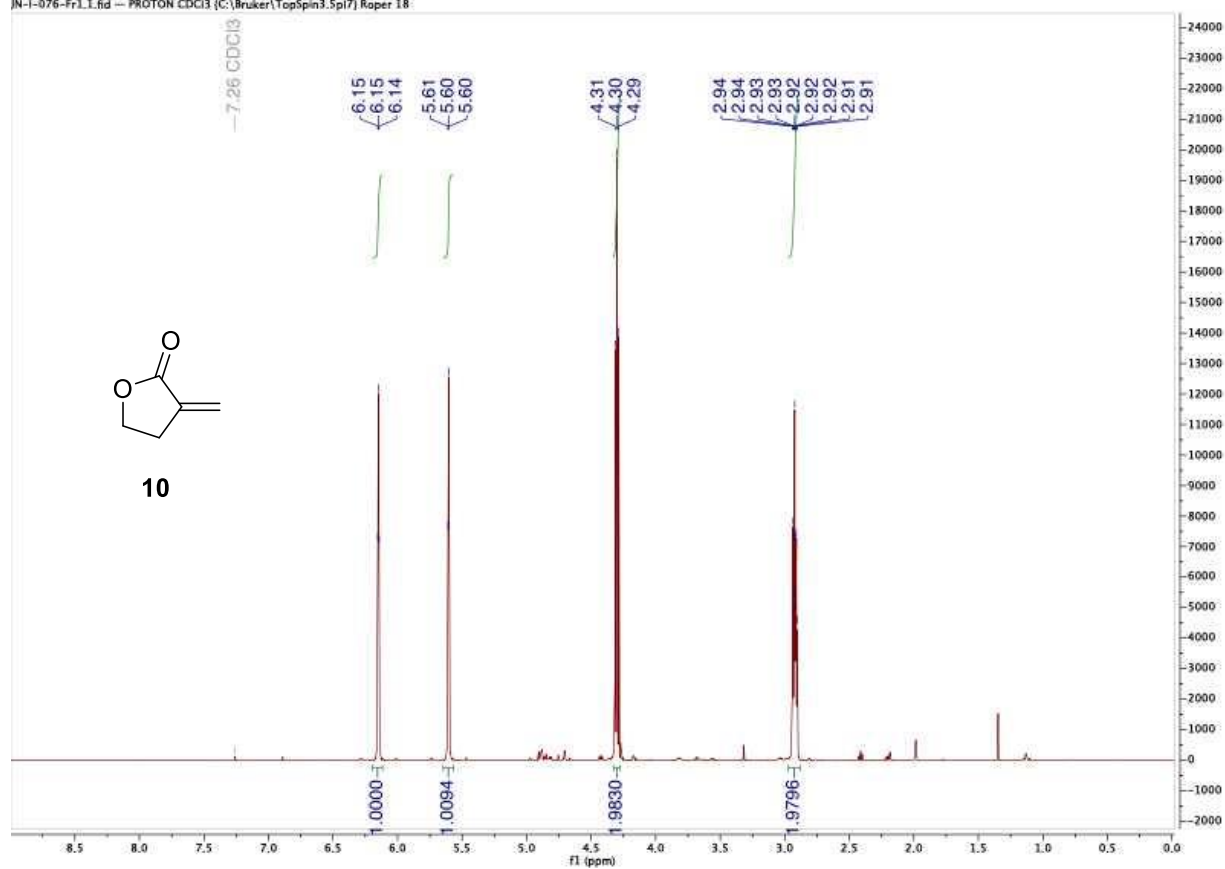


**NMR Spectra 1.**  $^1\text{H}$  NMR Spectra of  $\gamma$ -butyrolactone sodium enolate **9**.



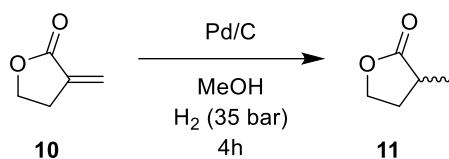
$\alpha$ -methylene- $\gamma$ -butyrolactone **10**: The sodium formyl salt (**9**) (14.3g, 0.105 mol) was combined with paraformaldehyde (14.2g, 0.473 mol) and THF (150 mL) under nitrogen. The suspension was heated to reflux and allowed to reflux for one hour. After one hour, the reaction was cooled to 10°C. Once cooled, a mixture of 1M potassium carbonate (25 mL) and MTBE (75mL) was added. The organic layer was separated, dried with magnesium sulfate, and the solvent was evaporated to give a yellow oil (8.003 g, 78% yield). The oil was vacuum distilled and pure methylene butyrolactone (**10**) was obtained (1.73g, 17% yield, 97% purity by LCMS).

$^1\text{H}$  NMR (600 MHz, Chloroform-*d*)  $\delta$  6.15 (t,  $J$ = 2.9 Hz, 1H), 5.60 (t,  $J$ = 2.6 Hz, 1H), 4.30 (t,  $J$ = 7.4 Hz, 2H), 2.94-2.91 (m, 2H). Spectra recorded was in agreement with prior literature.<sup>59</sup>



NMR Spectra 2. <sup>1</sup>H NMR Spectra of  $\alpha$ -methylene- $\gamma$ -butyrolactone **10**.

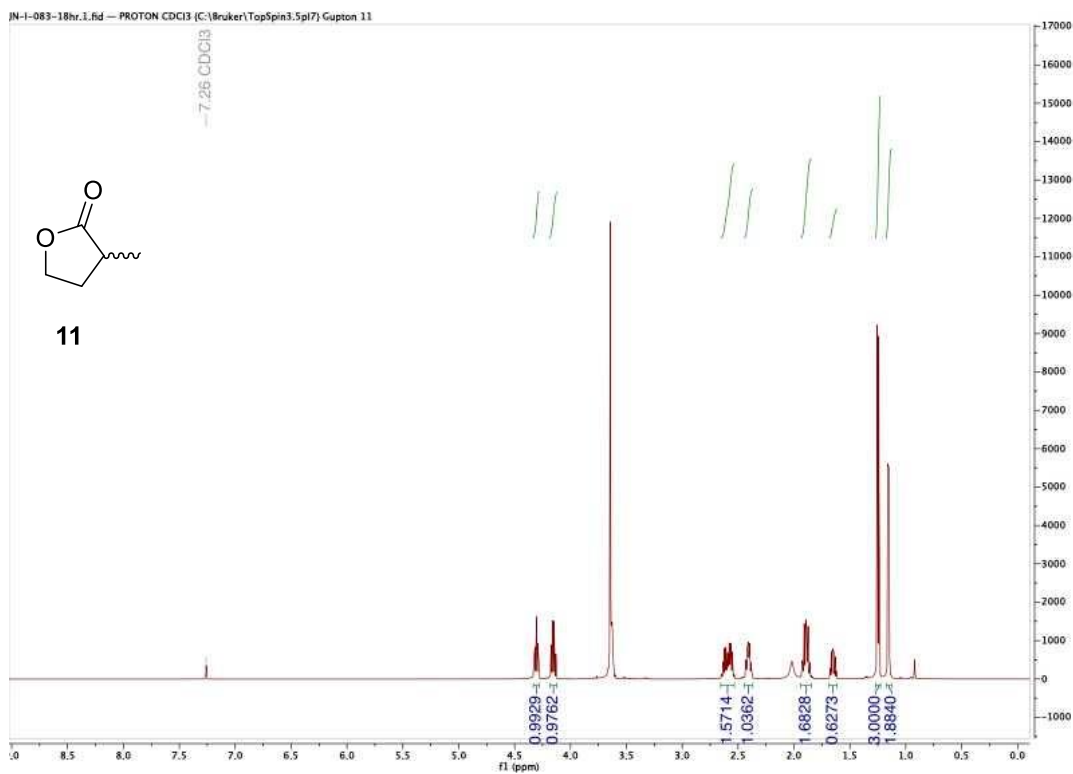




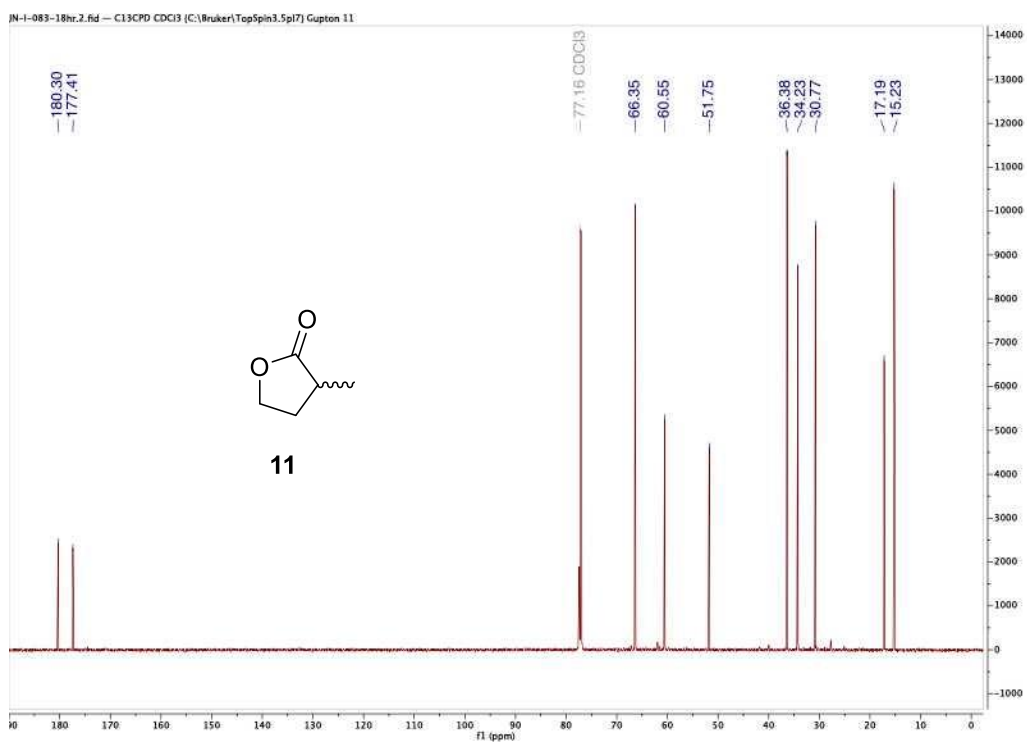
3-methyltetrahydro-2-furanone 11:  $\alpha$ -methylene- $\gamma$ -butyrolactone (**10**) (0.5 g, 5.1 mmol) was combined in a reactor vial with 0.1 equivalent of 10 wt% Pd/C catalyst (54 mg, 0.5 mmol) in methanol (8 mL). The vial was attached to an HEL hydrogenation unit where it was set to run at room temperature at a pressure of 35 bar and stirring at a rate of 250 RPM for 8 hours. After 8 hours, the reaction mixture was filtered to remove palladium on carbon and then the methanol was removed. The crude reaction was used without further purification.

$^1\text{H}$  NMR (600 MHz, Chloroform-*d*)  $\delta$  4.31 (td,  $J$ = 8.7, 2.7 Hz, 1H), 4.15 (td,  $J$ = 6.71, 6.56 Hz, 1H), 2.63-2.55 (m, 2H), 2.43-2.38 (m, 1H), 1.93-1.86 (m, 2H), 1.68-1.62 (m, 1H), 1.25 (d,  $J$ = 7.08 Hz, 3H), 1.15 (d,  $J$ = 7.08 Hz, 2H).

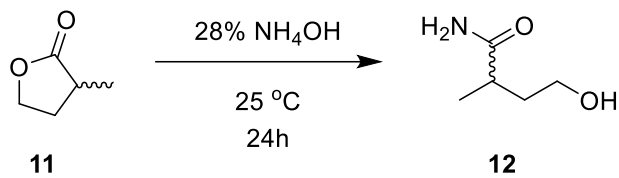
$^{13}\text{C}$  NMR (150 MHz, Chloroform-*d*)  $\delta$  180.3, 177.41, 66.35, 60.55, 51.75, 36.38, 34.23, 30.77, 17.19, 15.23. Spectra agrees with literature.<sup>60</sup>



NMR Spectra 3. <sup>1</sup>H NMR Spectra of 3-methyltetrahydro-2-furanone **11**

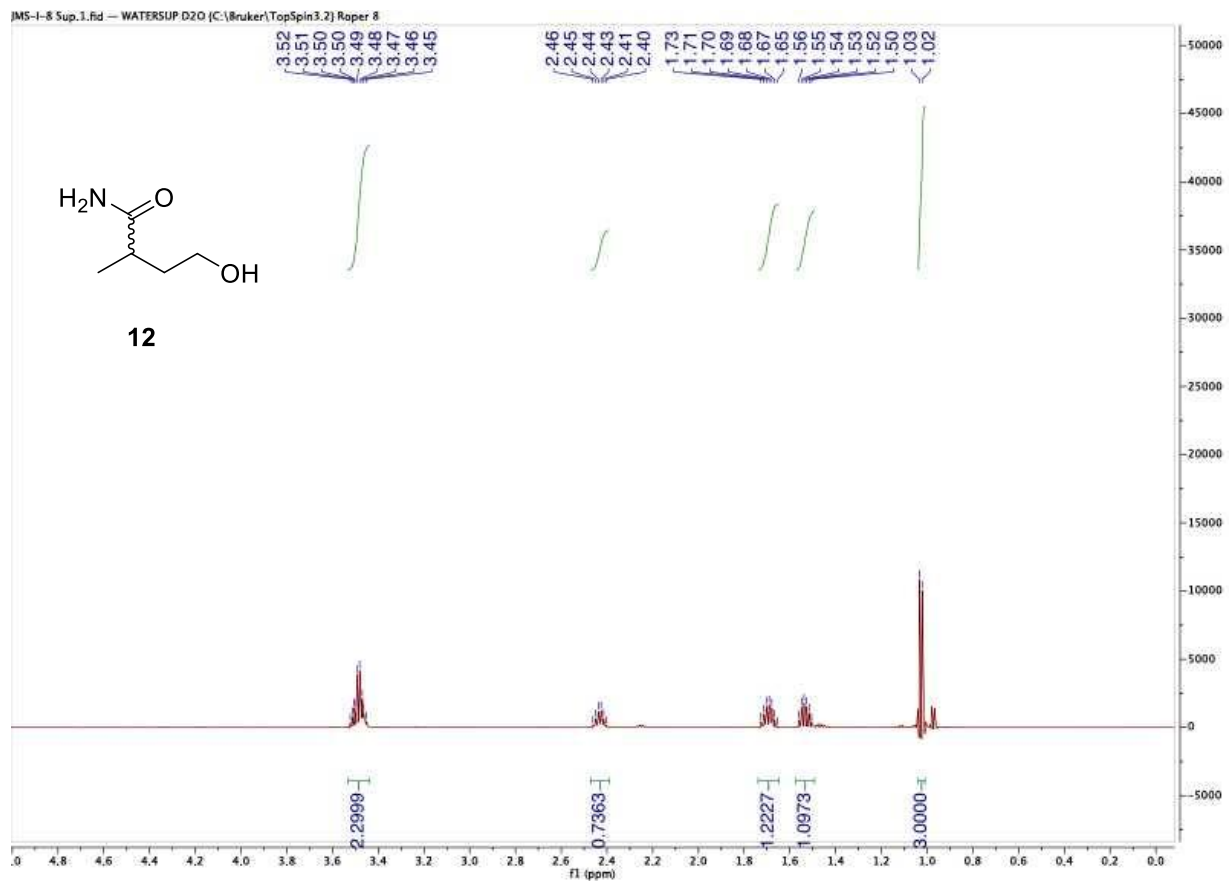


NMR Spectra 4. <sup>13</sup>C NMR Spectra of 3-methyltetrahydro-2-furanone **11**

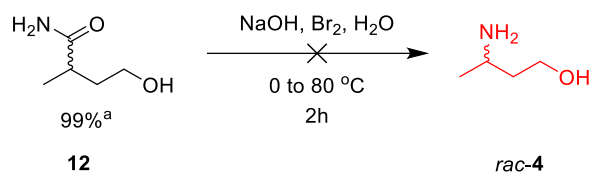


4-hydroxy-2-methylbutanamide **12**: To a 50 mL flask was added **11** (4.25 mL, 44.9 mmol, 1 eq), followed by 16 mL of 28%  $\text{NH}_4\text{OH}$  (112.3 mmol, 2.5 eq). After the mixture had stirred for 24h at 25 °C, the mixture was passed through an ion-exchange column (100 g, Dowex 5-WX8) to remove the remaining  $\text{NH}_4\text{OH}$ . The material was used in the next step without further purification. The structure of **12** was confirmed by  $^1\text{H-NMR}$  and purity was found to be 99.3% via LC/MS ( $M/Z = 118.2$ )

$^1\text{H NMR}$  (600 MHz,  $\text{D}_2\text{O}$ )  $\delta$  3.49 (m, 2H), 2.43 (m, 1H), 1.69 (m, 1H), 1.54 (m, 1H), 1.02 (d,  $J=6.93$  Hz, 3H).



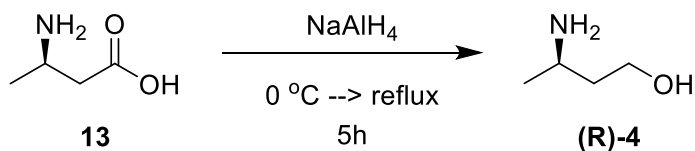
NMR Spectra 5. <sup>1</sup>H NMR Spectra of 4-hydroxy-2-methylbutanamide **12**.



Rac-3-aminobutanol 4: NaOH (11.2 g, 280 mmol, 6.2 eq) was dissolved in 86 mL of DI H<sub>2</sub>O and stirred in an ice-water/NaCl bath. Once the internal temperature of the NaOH solution reached 0 °C, Br<sub>2</sub> (2.76 mL, 53.9 mmol, 1.2 eq) was added dropwise via syringe. The mixture was stirred at 0 °C for 30 min. **12** (5.22 g, 44.9 mmol, 1 eq) was added via an addition funnel. After addition, the reaction was heated at 80 °C to an internal temperature of 76.5 °C for 2h.

Unfortunately, **4** was unable to be isolated for analysis. We performed initial explorations into purification using ion-exchange chromatography, salting out, enzymatic isolation, Schotten-Baumann, and solvent exchange. However, these routes were unsuccessful in providing clean material and we switched to our route using the amino acid before any optimization was performed.

#### 1.7.2.2. Amino Acid Route



(R)-3-Aminobutanol 4: To a 1000 mL 3-neck round bottom flask was fitted a temperature probe, reflux condenser, and stir bar. The flask was flushed with N<sub>2</sub>. Anhydrous THF (200 mL) was then added. The flask was placed in an ice/NaCl bath and cooled to an internal temperature of -10 °C. Sodium Aluminum Hydride (26.1g, 484 mmol, 2.0 eq.) was added using a solid addition funnel and the mixture was allowed to stir. (R)-3-aminobutanoic acid (**13**) was added slowly so as to

maintain an internal temperature below 5.2 °C. After stirring for 1 hour, the flask was removed from the ice bath and allowed to warm to room temperature. After 1 hour at room temperature, the reaction was heated to reflux (internal temperature: 67 °C) with continued stirring. After 4 hours at reflux, the reaction was cooled back to < 0 °C. 10% NaOH in water (50mL) was added dropwise to quench excess NAH. Addition of NaOH solution was done slowly so as to keep internal temperature below 10 °C. Additional NaOH solution (200 mL) was then added to dissolve remaining aluminum salts and the mixture was stirred for 30 min. The reaction mixture was transferred to a separatory funnel and the organic and aqueous layers were separated. The basic aqueous layer (pH ~11) was extracted twice more with recycled THF (200 mL each, 400 mL total).

Following combination of the organic layers, the material was distilled through either a Pope Scientific Thin Film Evaporator (70% yield, 84 wt% purity), or through traditional short-path distillation (66% yield, 99 wt% purity) (Figure 6.). Purity was determined by quantitative <sup>1</sup>H NMR (QNMR) spectroscopy using mesitylene as an internal standard.

<sup>1</sup>H NMR (600 MHz, DMSO-*d*<sub>6</sub>) δ 3.47 (m, 2H), 2.86 (m, 1H), 1.38 (m, 2H), 0.96 (d, J= 6.42, 3H)

<sup>13</sup>C NMR (150 MHz, DMSO-*d*<sub>6</sub>) δ 59.01, 44.45, 42.13, 24.56.

Chiral Analysis was performed using a carboxybenzyl (CBZ) protecting group to better differentiate the enantiomers and provide a chromophore for chiral supercritical fluid (SFC) instrument:

Derivatization procedure: (*R*)-3-aminobutanol (500 mg, 1 eq.), sodium carbonate (1.78 g, 3 eq.), and 20 mL of a 1:1 dioxane:H<sub>2</sub>O mixture were stirred at 25 °C. Benzyl chloroformate

(881  $\mu\text{L}$ , 1.1 eq.) was added and the reaction stirred for 12 h. The reaction mixture was concentrated and then partitioned between  $\text{H}_2\text{O}$  (50 mL) and ethyl acetate (50 mL). The aqueous layer was extracted twice with ethyl acetate (50 mL each, 100 mL total). The organics were dried over sodium sulfate, filtered and concentrated. Upon concentration the viscous oil solidified into white crystals.

The CBZ-derivatized (*R*)-3-aminobutan-1-ol sample was dissolved in ethanol and analyzed by chiral SFC. A ChiralPak IB-N5 column (4.6 X 100mm; 5 $\mu\text{M}$ , Chiral Technologies, Inc.) was used with a 10% isopropanol (90%  $\text{CO}_2$ ) mobile phase at 3 mL/min. Under these conditions the desired (*R*) enantiomer elutes at 3.1 minutes while the undesired enantiomer elutes at 3.6 minutes (Figure 21).

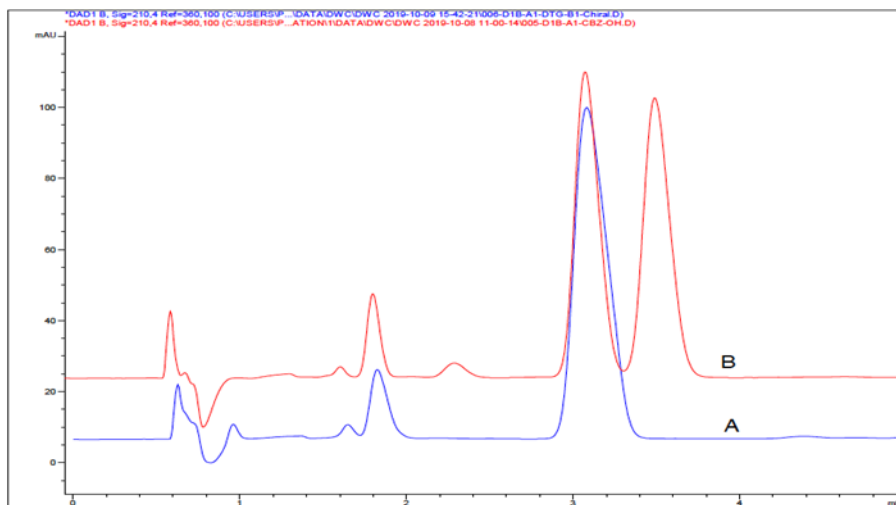
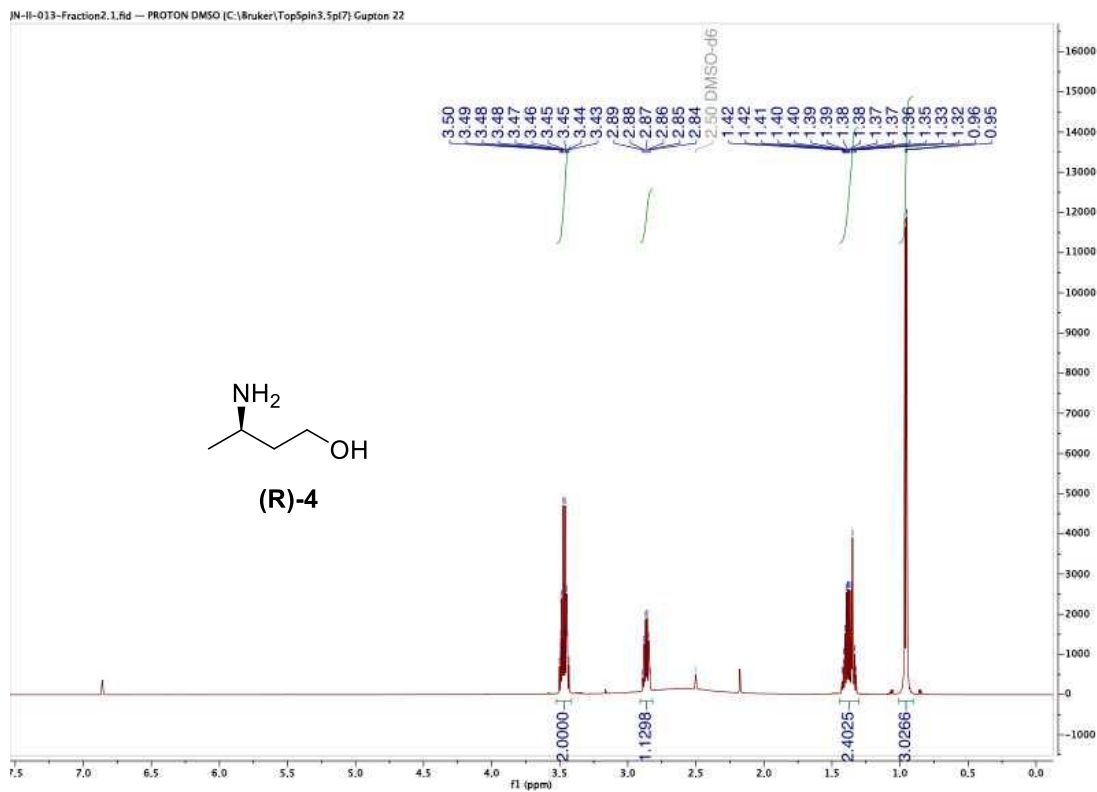
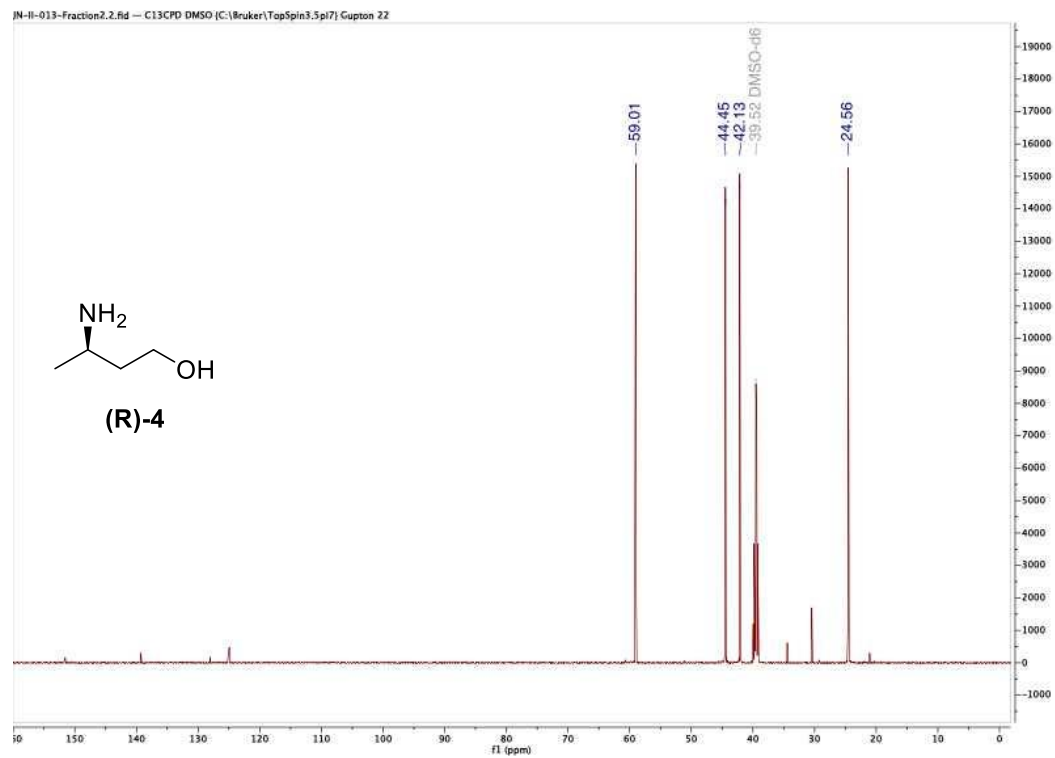


**Figure 21.** Chromatograms of the desired Aminoalcohol enantiomer (A) and the racemic mixture (B).



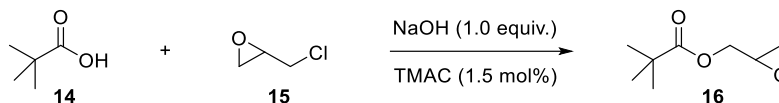
NMR Spectra 6. <sup>1</sup>H NMR Spectra of (R)-3-aminobutanol 4.



NMR Spectra 7. <sup>13</sup>C NMR Spectra of (R)-3-aminobutanol 4.



### 1.7.3. Procedures and Data Towards (*S*)-Glycidyl Pivalate



**(*S*)-glycidyl pivalate 16:** To a solution of pivalic acid **1** (20 g, 196 mmol, 1 equiv) in (*R*)-epichlorohydrin **2** (54.4 g, 587 mmol, 46.1 mL, 3 equiv) were added NaOH (7.8 g, 196 mmol, 1 equiv, pellets) and tetramethyl ammonium chloride (TMAC) (430 mg, 4 mmol, 0.02 equiv) in one portion at room temperature. The suspension was then stirred at 50 °C until the reaction was complete as monitored by quantitative <sup>1</sup>H NMR spectroscopy. 1,3,5-trimethoxybenzene was used as an internal standard. Once complete, the reaction suspension was filtered and washed with ~30 mL of DCM. The DCM was then removed by rotary evaporation and the reaction mixture was purified by vacuum distillation.

**Vacuum Distillation Procedure:** After removal of the majority of the DCM, a short path distillation apparatus was attached to the RBF containing the reaction. The excess epichlorohydrin was removed first at vacuum pressures < 10 torr and at a temperature of ~40-50 °C. After epichlorohydrin was completely distilled, the bottoms of the distillation were transferred to a smaller volume RBF and once again connected to the short path distillation apparatus. (*S*)-Glycidyl Pivalate **16** was then distilled with high purity (>95 wt %) and moderate yield (63%).

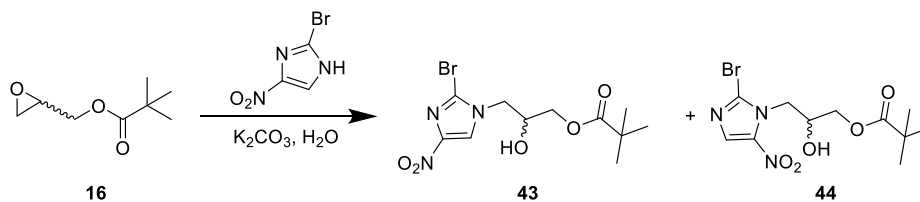
<sup>1</sup>H NMR (600 MHz, DMSO-*d*<sub>6</sub>) δ 4.38 (dd, *J* = 2.26, 12.46 Hz, 1H), 3.85 (dd, *J* = 5.92, 12.50 Hz, 1H), 3.17 (m, 1H), 2.77 (t, *J* = 4.42 Hz, 1H), 2.62 (dd, *J* = 2.38, 4.86, 1H), 1.17 (s, 9H)

<sup>13</sup>C NMR (151 MHz, DMSO-*d*<sub>6</sub>) δ 177.11, 64.41, 48.94, 43.54, 38.22, 26.79

$[\alpha]_D +19.1$  (c 1.8,  $\text{CHCl}_3$ , 25 °C)

Continuous Distillation of Epichlorohydrin in Toluene: To a three-neck round bottom flask containing glycidyl pivalate (~62 g) and excess racemic epichlorohydrin (~62 mL) was added 120 mL of toluene. The outer two necks were fitted with rubber stoppers and a short path distillation apparatus was connected to the center neck. The flask was then heated and the reaction mixture was distilled under vacuum (67-94 torr). Periodically throughout the distillation process, additional toluene was added via syringe to the round bottom flask in an attempt to maintain the reaction volume in the flask. Using 1,3,5-Trimethoxy benzene as an internal standard, the presence of epichlorohydrin was observed to decrease over the course of the distillation with minimal decomposition of the target glycidyl pivalate material (Figure 10).

Determination of Enantiomeric Ratio by HPLC:



**Scheme 7.** Derivatization of Glycidyl Pivalate for Analysis of Enantiomeric Purity.

Derivatization procedure (Scheme 7): Water (5 mL) and potassium carbonate (720 mg, 5.2 mmol, 1 eq.) were combined in a vial and stirred at RT for 5-10 minutes until the solution was clear. 4-nitro-2-bromo-imidazole (1.0 g, 5.2 mmol, 1 eq.) was then added to the vial followed by glycidyl pivalate (1.15 g, 7.3 mmol, 1.4 eq.). The reaction was then stirred for another 5-10 min at RT. The vials were then warmed to 65 °C and the solution allowed to react until complete (monitored by LCMS).

Enantiomeric ratio determination: Upon completion of the above reaction as monitored by LCMS, the samples were analyzed using SFC. This data showed an enantiomeric ratio of 97:3 of our desired product **43** as well as a small amount of **44** which also exhibited an enantiomeric ratio of 97:3. (**S**)-**43**: 8.423 min, 83.37%; (**R**)-**43**: 6.720 min, 2.8%; **44**: 7.94 min, 13.4%; *ent*-**44**: 7.64 min, 0.4%. Our desired enantiomer was confirmed by following the same synthesis shown in Scheme 7, but using (*S*)-glycidyl pivalate from a known<sup>32</sup> route starting from glycidol and pivaloyl chloride.

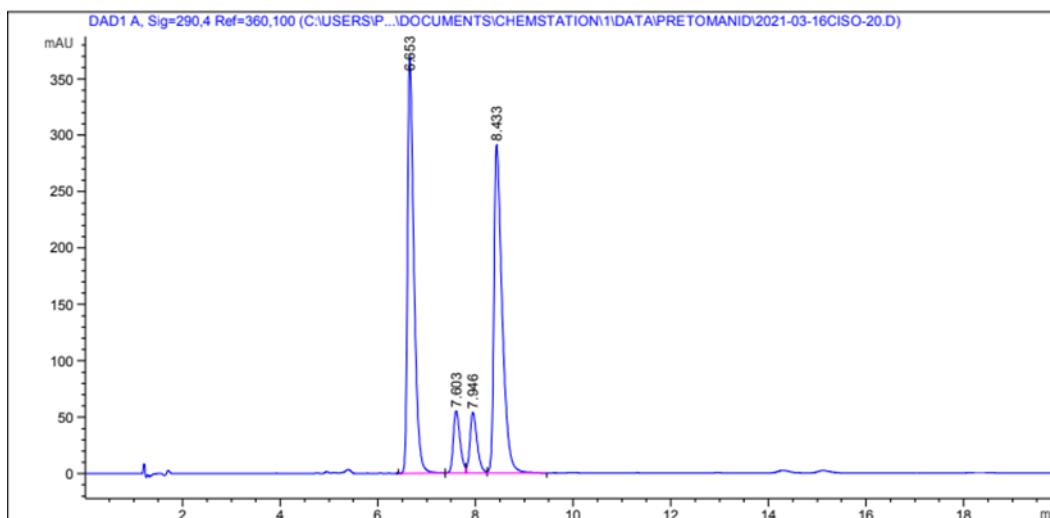


Figure 23. Chromatogram for Derivatized products **43** and **44** from Racemic Glycidyl Pivalate

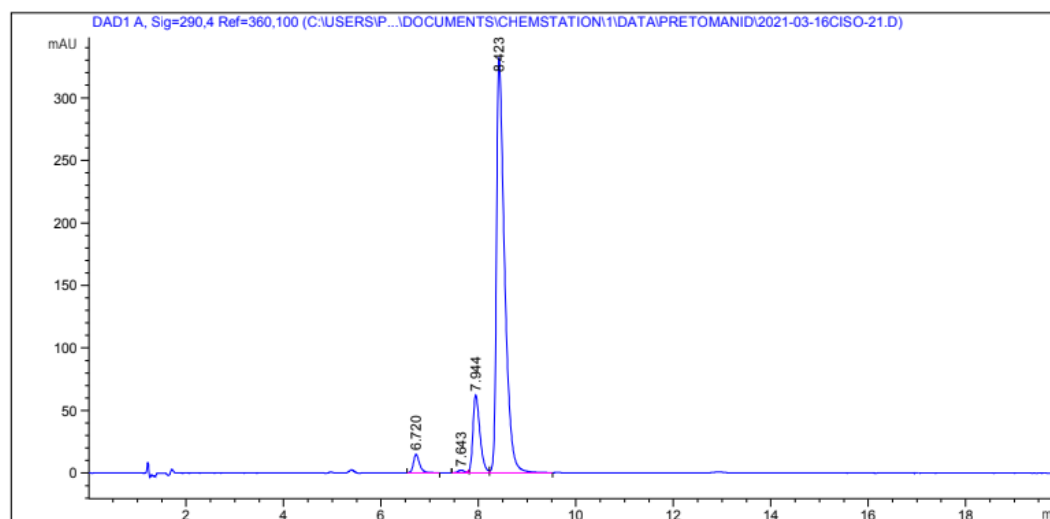
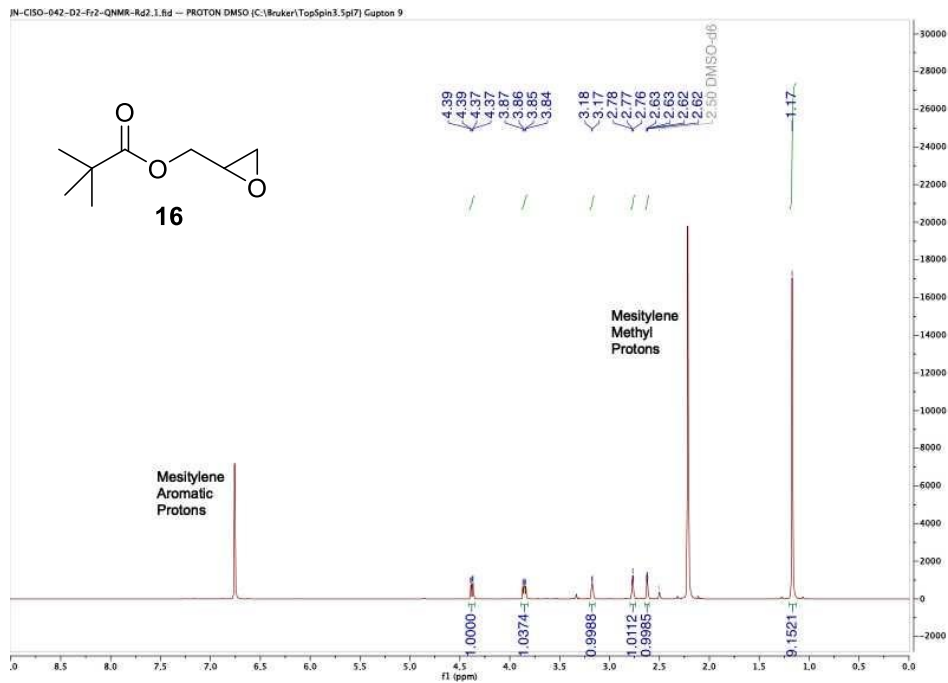


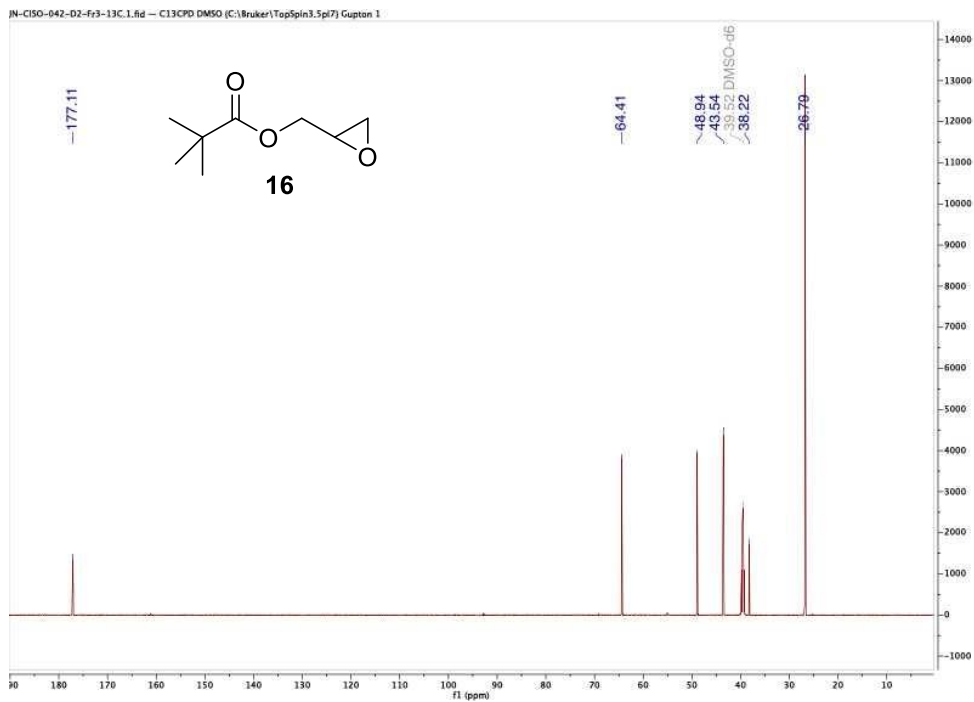
Figure 22. Chromatogram for Derivatized products **43** and **44** from Enantioenriched Glycidyl Pivalate

Table 6. Retention times, Area % and Assigned Compounds for the Chromatograms.

Entry	RT (min)	Area % at 290 nm	Compounds
From Racemic glycidyl pivalate	6.653	43.2%	( <i>R</i> )- <b>43</b>
	7.603	6.7%	Regioisomer <i>ent</i> - <b>44</b>
	7.946	6.9%	Regioisomer <b>44</b>
	8.433	43.2%	( <i>S</i> )- <b>43</b>
From enantioenriched ( <i>S</i> )-glycidyl pivalate	6.720	2.8%	( <i>R</i> )- <b>43</b>
	7.643	0.4%	Regioisomer <i>ent</i> - <b>44</b>
	7.944	13.4%	Regioisomer <b>44</b>
	8.423	83.4%	( <i>S</i> )- <b>43</b>



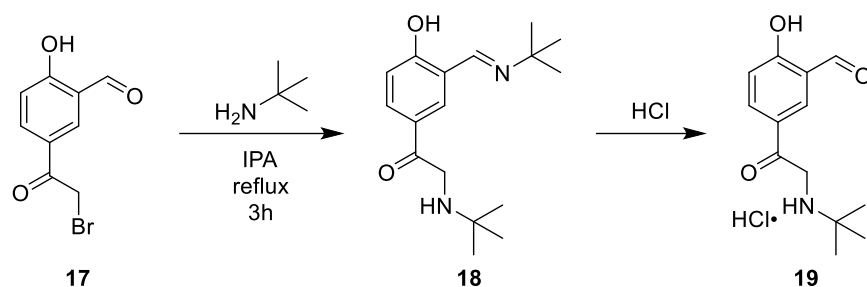
NMR Spectra 8. <sup>1</sup>H NMR of Glycidyl Pivalate 16.



NMR Spectra 9. <sup>13</sup>C NMR of Glycidyl Pivalate 16.

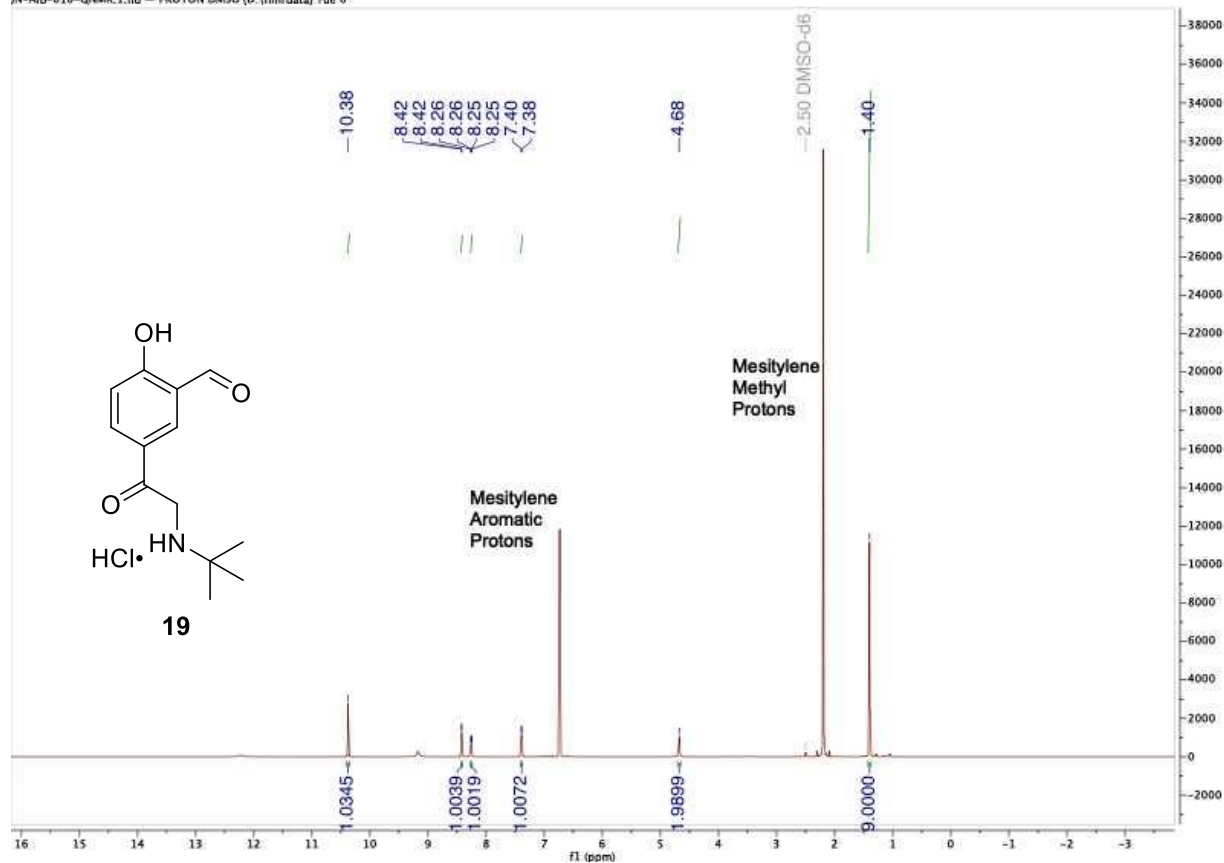
## 1.7.4. Procedures and Data Towards Albuterol

### 1.7.4.1. Traditional Route

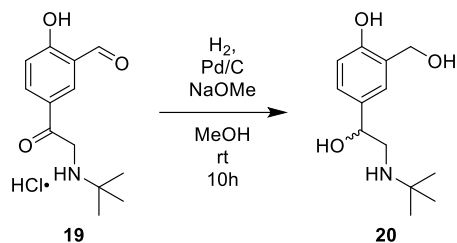


Amino-keto-aldehyde salt **19**: To a suspension of **17** (500mg, 2.06 mmol) in isopropanol (5 mL) was added tert-butyl amine (865  $\mu$ L, 8.23 mmol). The reaction was then stirred and heated to reflux for 18 hours. The reaction was cooled to room temperature and then 12M HCl (1 mL) was added slowly to the reaction mixture. After addition of HCl, the mixture is cooled to  $\sim$ -10  $^{\circ}$ C and a white precipitate is formed. The precipitate is filtered, washed with 5 mL of cold isopropanol and **19** is given in high purity (54% yield, 99 wt% purity by QNMR).

<sup>1</sup>H NMR (600 MHz, DMSO-d<sub>6</sub>)  $\delta$  10.38 (s, 1H), 8.42 (d, J= 2.33, 1H), 8.25 (dd, J= 2.33, 8.73 Hz, 1H), 7.39 (d, J= 8.77, 1H), 4.68 (s, 2H), 1.40 (s, 9H). Spectra agrees with prior literature.<sup>56</sup>

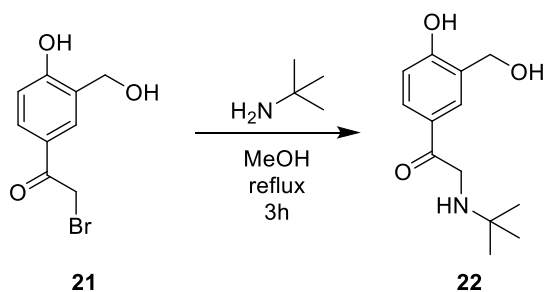


NMR Spectra 10. <sup>1</sup>H NMR Spectra of Amino-keto-aldehyde salt **19**.



**Albuterol 20:** To a suspension of HCl salt **19** (500 mg, 1.85 mmol) in methanol was added sodium methoxide (NaOMe) (100 mg, 1.85 mmol) at room temperature. The reaction mixture was allowed to stir for 5 minutes. After 5 minutes, 10 wt% palladium on carbon (197 mg, 185  $\mu$ mol) was added to the reaction mixture. The reaction mixture was transferred to a steel vessel for use on an HEL Chemscan instrument. The instrument was programmed to supply 80 psi of H<sub>2</sub> pressure and stir at 750 rpm for 10 hours. After completion of the reaction, the mixture was analyzed by LCMS (24% (Area %)).

#### 1.7.4.2. Modified Route



#### Amino-keto-diol 22:

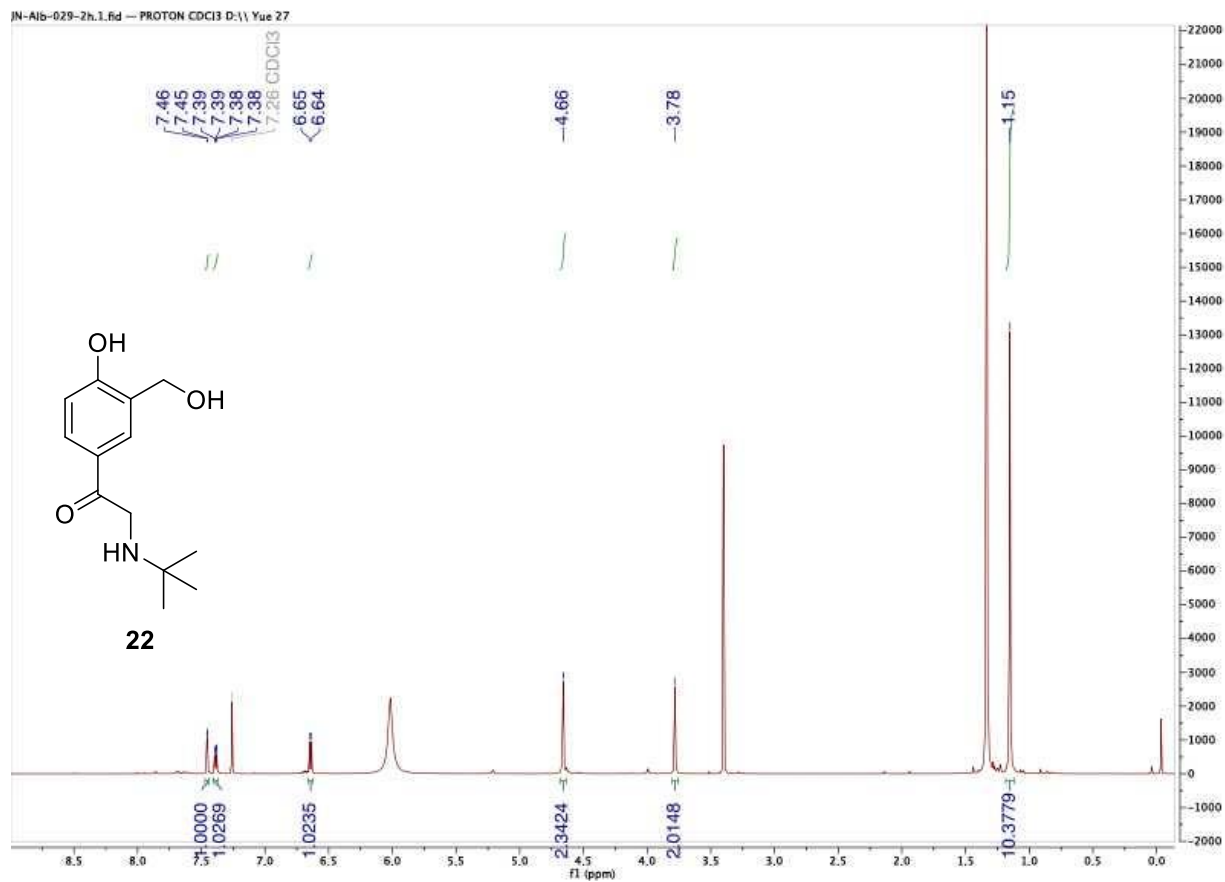
**Batch:** To a solution of bromo-keto-diol **21** (500 mg, 2.04 mmol) in methanol (5 mL) was added *tert*-butyl amine (858  $\mu$ L, 8.16 mmol). The reaction mixture was stirred and heated to reflux



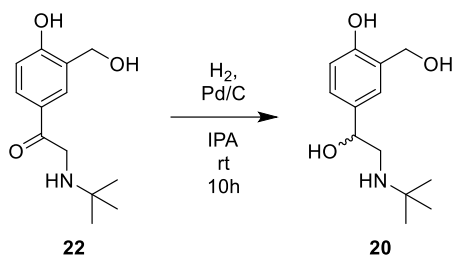
for 3 hours. After 3 hours, the reaction mixture was allowed to cool and a sample of **22** in solution was taken for LCMS analysis (75% (area %)), no residual starting material).

Continuous Flow: In separate Erlenmeyer flasks were prepared solutions of bromo-keto-diol **21** (500 mg, 2.04 mmol) in methanol (25 mL) and *tert*-butylamine (858  $\mu$ L, 8.16 mmol) in methanol (25 mL). The two solutions were drawn through tubing at a rate of 1.6 mL/min and mixed using a Y-connector which led to the reaction tubing and resulted in an estimated flow rate of 3.2 mL/min. The reaction tubing had an inner volume of 100 mL, resulting in a residence time of ~30 min. After passing through the reactor, a sample of **22** in solution was taken for LCMS analysis (54% AY (area %), 28% (area %) residual starting material).

$^1\text{H}$  NMR (600 MHz, Chloroform-*d*)  $\delta$  7.45 (d, *J* = 1.79 Hz, 1H), 7.39 (dd, *J* = 1.85, 8.51 Hz, 1H), 6.64 (d, *J* = 8.47 Hz, 1H), 4.66 (s, 2H) 3.78 (s, 2H), 1.15 (s, 9H).



NMR Spectra 11. <sup>1</sup>H NMR Spectra for Amino-keto-diol **22**.



#### Albuterol Free Base **20**:

Batch: To an HEL Chemsan reactor vial was added amino-keto-diol **22** (500mg, 2.11 mmol) and 10 wt% palladium on carbon (224 mg, 0.211 mmol). The HEL instrument was programmed to heat to 40 °C, pressurize to 80 psi H<sub>2</sub> gas, and stir at 750 rpm for 10 hours. After 10 hours, the reaction was removed from the instrument and a sample was taken for LCMS (area %) analysis (46%, 18% unknown impurity (168 m/z)).

ThalesNano H-Cube Mini: A reaction mixture from the synthesis of **22** was diluted from ~5 mL to ~25 mL. The solution was then passed through the H-Cube Mini at a rate of 0.3 mL/min. The instrument was programmed to have a H<sub>2</sub> pressure of 30 bar and a temperature of 60 °C. After passing through the H-cube, the material was cycled through the system 3 more times and LCMS (area %) analysis was performed (9.9% AY, 18% **22**, 47% unknown impurity (168 m/z)).

H-Cube with Prior Work-up: After completion of amination reaction to form **22**, the solvent was removed under vacuum by rotary evaporator and the crude oil reconstituted in 10 mL of ethyl acetate. The ethyl acetate was then washed 3 times with DI water (3 X 10 mL) and brine (1 x 10 mL). The organic layer was collected and anhydrous sodium sulfate (~1g) and activated charcoal (~1g) were added. The mixture was filtered and washed with additional ethyl acetate (10 mL). The ethyl acetate was then removed under vacuum by rotary evaporator, and the crude oil was reconstituted in methanol (25mL). The solution was then run through the H-Cube under the

same conditions as above. LCMS analysis was performed and starting material was no longer observed after 2 cycles through the H-Cube. The LCMS did show high amounts of the undesired 168 m/z impurity which is believe to be an undesired reaction between **22** and water. This method gave 20 in solution (25% (area %), 0% **22**, 47% unknown impurity (168 m/z).

## **2. Applying the Principles of Process Intensification to Fluoroquinolone Antibiotics**

### **2.1. Background**

#### 2.1.1. Process Intensification

Process intensification (PI) can be broadly defined as a method with the goal of making chemical processes cheaper, smaller, safer, and less energy intensive.<sup>61</sup> This definition is one of many, but it is congruent with the way we approach process intensification and has the eventual goal of applying this method to manufacturing. PI is closely related to the techniques I discussed in Chapter 1.1. and is generally the overarching method with which those techniques are applied to a chemical synthesis.

Previously, our primary aim was in the cost-reduction of pharmaceutical ingredients, which was achieved through modifications of synthetic routes, optimization of reactions, and use of safer or more available starting materials. This chapter will explore how the synthesis of fluoroquinolones can be improved using process intensification with the goal of forming a new, convergent synthesis. In addition to performing optimization of the current route, it is also important to identify alternate routes towards API synthesis to improve its robustness against economic factors and supply chain vulnerabilities. Reagents are typically chosen as a result of their efficacy in a reaction as well as their cost compared to other similar reagents. For example, in our work on DTG, we transitioned from lithium aluminum hydride to the less expensive sodium aluminum hydride and were able to obtain similar yields of the reaction. Due to market uncertainty and strong dependencies on changes in volume and synthesis costs, the identification of alternate reagents and synthetic routes is crucial to maintaining low API costs.

In order to maintain consistent prices for API manufacturing, it can be helpful to perform exploration into alternate routes with different starting materials and reagents to determine the best available route. Although this technique would result in additional operation costs to address regulatory issues, the long term offset of identifying cheaper starting materials and reactions can be beneficial. It is additionally helpful for the “back-up” synthesis to share a common intermediate with the standard synthesis so that the final step(s) can continue to be performed in the same way, including purification and formulation of the final compound. This also is beneficial to API synthesis as the analytical methods and impurity profiles of the new synthesis will be closer to the standard route, allowing for easier transition.

Process intensification has the capability of greatly improving manufacturing towards cheaper and more accessible APIs. By applying techniques of PI, synthetic routes can be made to be more efficient, safer, and more robust, all aspects which can help to lower the costs of essential medicines.

### 2.1.2. Fluoroquinolone Antibiotics

Fluoroquinolones (Figure 24), based on the 4-quinolone substructure, have been studied for almost sixty years with regard to their bioactivity as an antibiotic.<sup>62,63</sup> In 1962, nalidixic acid (Figure 25) was first developed as part of a group of naphthyridones screened at the Sterling-Winthrop Research Institute.<sup>64</sup> Initial uses for nalidixic acid were limited to fighting Gram-negative bacteria responsible for urinary tract infections (UTIs). However, due to its narrow spectrum of use and associated adverse side effects, the development of an improved antibiotic was necessary.<sup>65</sup>

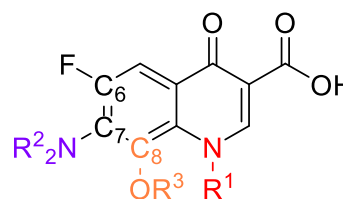


**Figure 24.** General Structure of Fluoroquinolones

Although nalidixic acid is technically a naphthyridone in structure, its development resulted in further screens which identified the bioactivity of quinolones and led to further studies on this new class of drugs.

During the 1970s and 1980s, the study of quinolone-based antibiotics began to develop and a number of improvements were made to increase the activity of the drugs. Flumequine, first patented in 1973, incorporated a fluorine substitution on the C6 position. This development greatly increased the spectrum of activity of quinolones and the vast majority of subsequent drugs include the same fluorine substitution.<sup>66</sup> Other fluoroquinolones in the second generation continued to improve on the Gram-negative activity through the addition of a piperazine ring at the C7 position.<sup>67</sup> The second-generation also introduced ciprofloxacin, which, through the addition of a cyclopropyl moiety on the amine of the quinolone, increased the overall activity of the compound.<sup>68</sup> Ciprofloxacin remains an effective and widely used antibiotic for the treatment of UTIs, respiratory tract infections (RTIs), and gastrointestinal infections.<sup>65,69-73</sup> Due to its efficacy and wide range of uses, ciprofloxacin is listed on the World Health Organization's (WHO) list of Essential Medicines.<sup>55</sup>

Further research resulted in the fluoroquinolone ofloxacin which added a methyl substituent to the second nitrogen of the piperazine ring resulting in increased activity against Gram-positive bacteria.<sup>74</sup> This was further developed by the addition of an ether group at the C8

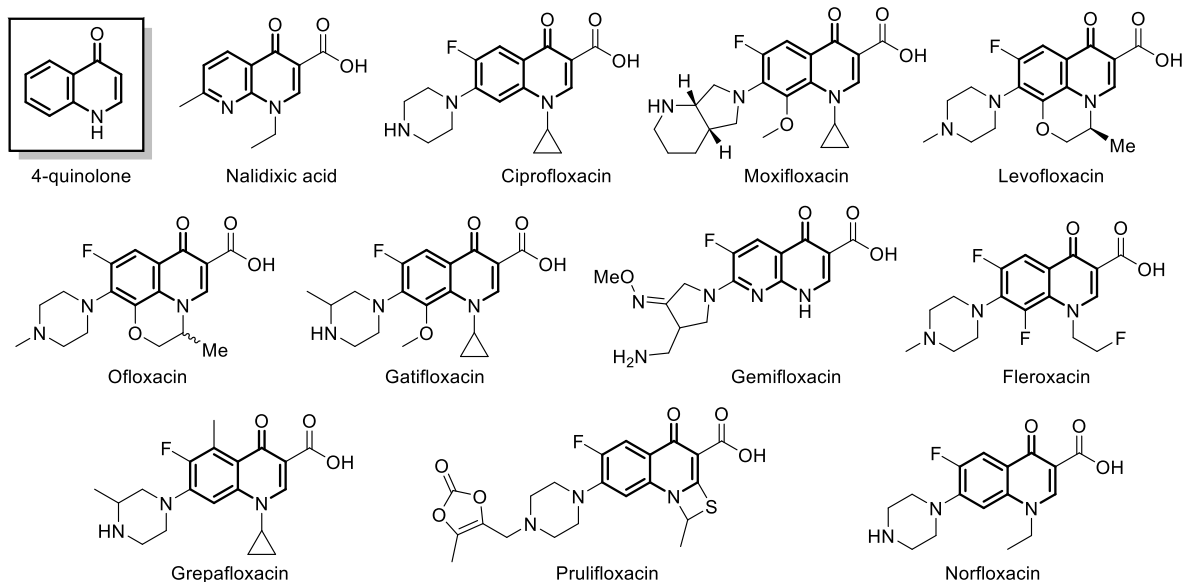


**Figure 25.** Select Collection of Fluoroquinolone Antibiotics

carbon.<sup>75</sup> In the case of ofloxacin, a morpholine ring is incorporated as the ether component (R3) in a fused ring system through the quinolone nitrogen. Ofloxacin contains a single chiral center, of which the L-isomer is the only biologically active one. This has resulted in the isolation of this enantiomer as its own, more potent drug, levofloxacin.<sup>76,77</sup> Both ofloxacin and levofloxacin are listed as WHO Essential Medicines.

As the development of quinolone antibiotics makes its way into the third generation, further substitutions to the quinolone backbone such as amino, methyl, and alcohol groups on C5 as well as replacing the *N*-methyl piperazine seen in ofloxacin with other alkylated piperazines and pyrrolidiny rings, have been performed, greatly increasing the available library of biologically active FQAs. Modifications to alternate sites of the benzene such as halogenation of C8 with chlorine or fluorine resulted in some improvement against Gram-positive bacteria.<sup>75</sup>



The fourth generation provided a large leap in efficacy as compared to the third.<sup>78</sup> While retaining the ability to remain active against both Gram-positive and Gram-negative bacteria, the fourth generation also improved their ability to inhibit anaerobic organisms. This was

**Table 7.** MIC<sub>90</sub> Values of Selected Fluoroquinolone Antibiotics.

MIC <sub>90</sub> (mg L <sup>-1</sup> )	Gram-negative pathogens		Gram-positive pathogens	
	<i>E. Coli</i>	<i>P. aeruginosa</i>	<i>S. aureus</i>	<i>S. pneumoniae</i>
	Nalidixic acid	8	>64	>64
Ciprofloxacin	0.03	1	1	2
Ofloxacin	0.12	4	0.5	2
Moxifloxacin	0.06	8	0.06	0.12
Gatifloxacin	0.06	4	0.25	0.25

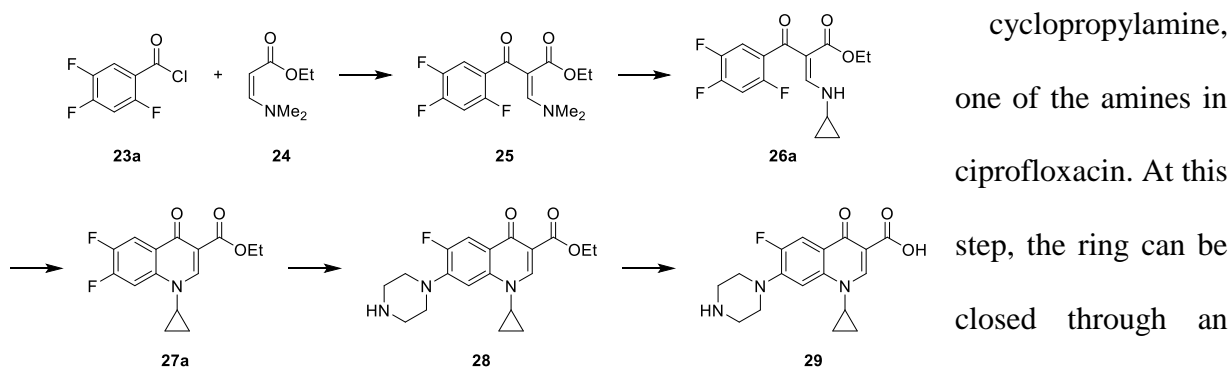
accomplished by returning to the naphthyridone core structure as observed in compounds such as gemifloxacin.<sup>79</sup> Moxifloxacin, currently listed as a WHO Essential Medicine,

incorporates an azabicyclic group at C7. This replaces previously used heterocyclic amines such as piperazine and its presence was found to greatly improve the Gram-positive activity.<sup>68</sup> This effect can be observed by comparing the enhanced activity of moxifloxacin which contains the azabicyclic group and gatifloxacin which is identical except for the presence of an alkylated piperazine instead (Table 7)<sup>80</sup>.

Over time, small changes to the substituents of 4-quinolone have revealed a wide array of bioactive antibiotics. In order to continue development and expedite the transition from bioactivity testing to drug synthesis, a streamlined synthesis of quinolones which tolerates the installation of multiple interchangeable functional groups at the three major substitution locations is desirable. A convergent synthetic route to multiple fluoroquinolones will help in decreasing their respective costs and broaden access to them around the world.

## 2.2. Prior Art

The synthesis of fluoroquinolone antibiotics (FQAs) has been explored significantly over the last 60 years, with many synthetic routes developed for a single antibiotic as well as general routes to multiple fluoroquinolones.<sup>81</sup> In 2017, in a paper focusing on the synthesis of the FQA ciprofloxacin, the Jamison group identified a route to ciprofloxacin (Scheme 8) through a C-acylation reaction of trifluorobenzoyl chloride **23a** (\$179/kg<sup>v</sup>) to vinylogous carbamate **24** which provided the  $\beta$ -ketoester **25**.<sup>82</sup> The dimethylamine moiety could then be replaced with



**Scheme 8.** Chemical Transformations in the Synthesis towards Ciprofloxacin

nucleophilic aromatic substitution ( $S_NAr$ ), displacing a fluorine. An intermolecular  $S_NAr$  reaction can then be performed to install the piperazine ring at the C<sub>7</sub> position. Hydrolysis of the ester to the carboxylic acid forms the final product ciprofloxacin. This route, although relatively streamlined, does contain a few problems that lead to high cost of the API. First, the major cost driver of the reaction is the starting material, trifluorobenzoyl chloride which is expensive and drives up the cost of the API accordingly. The trifluoro-substituted aromatic ring is costly, that provides an opportunity for alternate starting materials having fewer fluorine substituents to decrease costs. Second, the use of the dimethylamine as a leaving group could be replaced with a more direct addition of the cyclopropylamine moiety to help decrease costs.

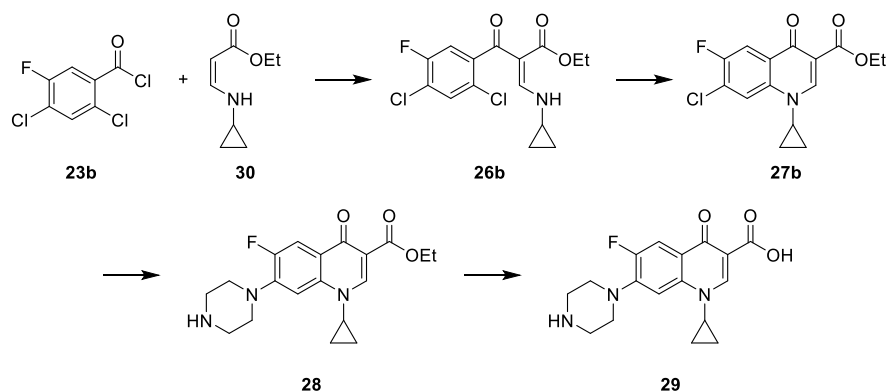
<sup>v</sup> Costing from Indian Import/Export databases Zauba and Datamyne

After reviewing this synthetic route, the Gupton group believed they could optimize the reactions and modify the starting materials and the steps to decrease the cost of the API.

### 2.3. Early Gupton Work<sup>83</sup>

The first action that was taken towards improving the synthesis of ciprofloxacin was identifying an alternative starting material, the current cost-driver for the route. The prior route used trifluorobenzoyl chloride **23a** which is helpful as it establishes the fluorine substituent very early on in the synthesis, negating the need for harsh fluorination conditions at a later step.

However, only a single fluorine is present in the final molecule, and the two additional ones in the starting material are simply present to



facilitate the two  $S_NAr$

reactions during the synthesis. In order to address the cost, the Gupton group proposed the idea of using a lower cost trihalogenated benzoyl chloride, 2,4-dichloro-5-fluorobenzoyl chloride **23b** (\$9.78/kg<sup>vi</sup>) for the synthesis. In  $S_NAr$  reactions, fluorine is the most reactive halogen, followed by chlorine.<sup>84</sup> This is due to fluorine's higher electronegativity and the greater dipole moment that exists between fluorine and the benzene. Since chlorine is also a reactive halogen, the use of dichlorofluorobenzoyl chloride (DCFBC) **23b** was expected to provide adequate reactivity to perform the desired substitutions.

<sup>vi</sup> Costing from Indian Import/Export databases

The second change to the proposed chemistry was the direct addition of the required amine moiety prior to the acylation step between the benzoyl chloride and vinylogous carbamate. The established route utilized a vinylogous carbamate bearing a dimethylamine group. Due to the lack of a free proton on the nitrogen, the formation of the undesired *N*-acylation side product is not possible and results in exclusive formation of the desired *C*-acylation to give the  $\beta$ -ketoester (**25**).

However, if the goal is to install the cyclopropylamine during the formation of the vinylogous carbamate, there would be an

available free proton on the nitrogen

that could result in undesired *N*-

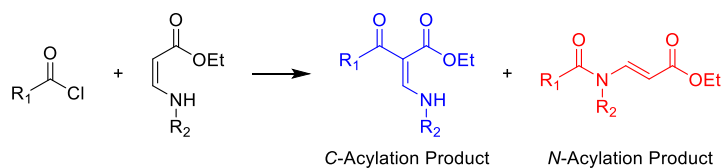


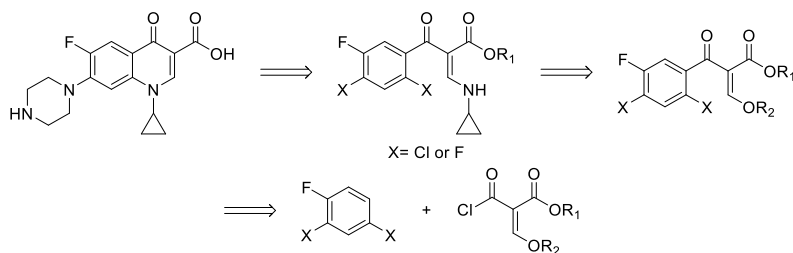
**Figure 26.** C-acylation and N-acylation Products

acylation. During initial screens of this reaction, following the conditions outlined in the published route, it was observed that there was a preference for the undesired *N*-acylation reaction compared to the desired *C*-acylation reaction (10:1). Through a series of base screens, it was determined that lithium bases provided high specificity for the *C*-acylation (>100:1). LiHMDS showed the most promising result with high conversion and isolated yield prompting the continuation of the work using LiHMDS. Beginning with DCFBC, ciprofloxacin could be synthesized in 4 chemical steps (Scheme 9), and an additional step to form the API as an HCl salt. The group demonstrated this route through transfer into a continuous flow process with an overall yield of 83% compared to the prior literature route of 60%. The decrease in cost from switching to DCFBC made up for the cost of the LiHMDS used for the acylation step. However, in the years since this work was performed, lithium prices have increased drastically in large part due to its use in the batteries for electric vehicles (EVs). This increase in the cost of a vital reagent has prompted us to take another look at the synthesis of ciprofloxacin to determine if there are ways to decrease the cost further and utilize more available and cost-effective starting materials.

## 2.4. Friedel-Crafts Acylation for the Synthesis of Fluoroquinolone Antibiotics

### 2.4.1. Introduction

Initially, one of the steps that was studied to decrease the cost of the synthesis towards

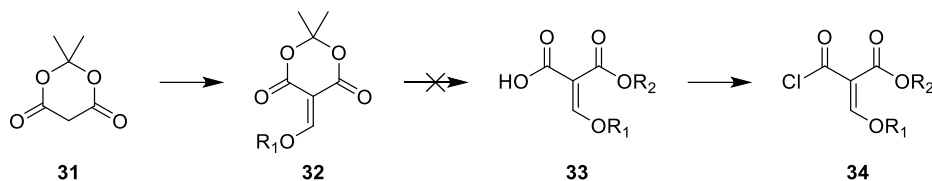


**Scheme 10.** Initial Retrosynthetic Strategy to Ciprofloxacin

ciprofloxacin was to switch from a trifluorinated starting material to a dichlorofluoro equivalent. In response to this change, we also wanted to

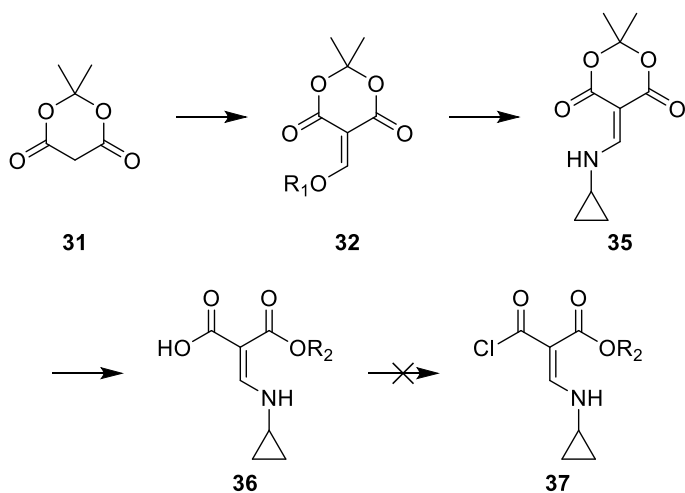
explore the use of 2,4-dichlorofluorobenzene (**38**, Scheme 13) in ciprofloxacin synthesis instead of the benzoyl chlorides that were being used in the literature. Although the cost difference was not drastic between the chlorinated benzene and benzoyl chloride, it did allow for a different approach. Our first idea (Scheme 10) was to generate the  $\beta$ -ketoester with vinylogous ether separately and perform a Friedel-Crafts acylation (FCA) onto the halogenated benzene to form the backbone of our product. From this point, the synthesis would be similar to other developed syntheses where the ether is replaced with the desired amine moiety and then an  $S_NAr$  is performed to close the ring. In order to form the desired vinylogous ether, we looked for a route that utilized widely available starting materials and reagents.

## 2.4.2. Meldrum's Acid



**Scheme 11.** Proposed Synthesis Towards Vinyl Ether from Meldrum's Acid

In our search for a cost-effective synthesis, we identified Meldrum's Acid (MA) (\$18.5/kg<sup>vii</sup>) as a viable starting material. This material could be reacted with trialkyl orthoformates to form a vinyl ether at the  $\alpha$ -carbon between the two carbonyl groups. Subsequently, we planned to perform a ring opening using an alcohol solvent, forming the general backbone of our keto-ester **33**. From there, we projected the carboxylic acid could be chlorinated to give the acid chloride **34** and then proceed forward with the Friedel-Crafts acylation with a halogenated benzene. Unfortunately, although the initial reaction performed well, the standard ring opening conditions resulted in no reaction on the vinyl ether using an alcohol solvent<sup>85</sup> or resulted in hydrolysis of the ether to form the alcohol under acidic conditions<sup>86</sup>. In order to facilitate the ring opening, we changed the sequence of reactions and install the cyclopropylamine earlier in the synthesis (Scheme 12). Previously, the installation of cyclopropylamine was planned to take place



**Scheme 12.** Reassessed Meldrum's Acid Route

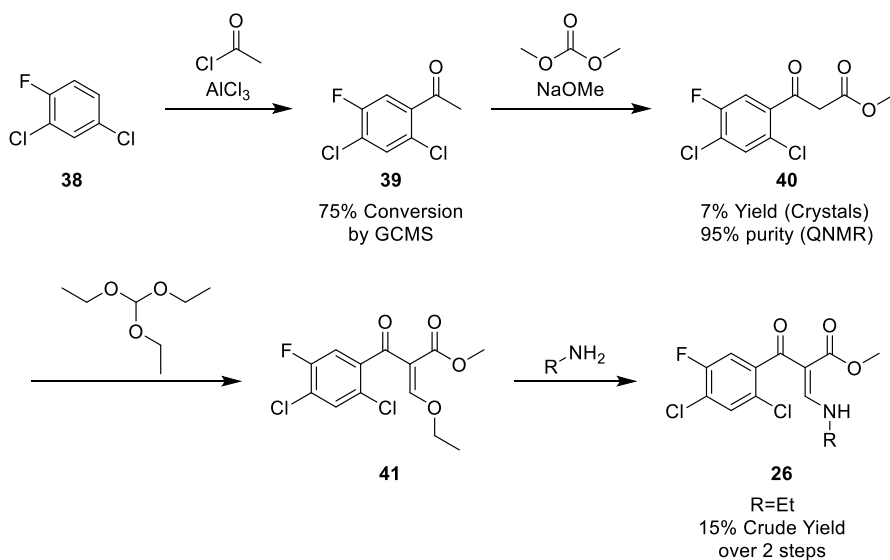
after the Friedel-Crafts reaction, but our inability to open the Meldrum's acid ether led us to identify literature report which suggested the presence of an amine group would allow for the ring opening.<sup>87</sup> The amination of the vinyl ether went smoothly to **35** and

<sup>vii</sup> Costing Determined from Indian Import/Export Databases Zauba and Datamyne

we were able to open the MA ring to form **36** (85% crude yield).<sup>88</sup> However, attempts at chlorination and subsequent Friedel-Crafts were unsuccessful, most likely due to competing, undesired chlorination of the amine. We decided against protection of the amine to prevent chlorination as it was not economically efficient. Once again, we found ourselves returning to the drawing board to explore additional alternate routes.

### 2.4.3. Step by Step Formation of the Backbone

In lieu of our attempts to form the vinylogous ether or vinylogous carbamate backbone and install it directly on a halogenated benzene, we decided we would start directly from the halogenated benzene and build out the backbone of our FQA from simple aromatic compounds (Scheme 13). This route could be accomplished by the Friedel-Crafts acylation of 2,4-dichlorofluorobenzene (DCFB) with acetyl chloride. Subsequent reaction with dimethyl carbonate and sodium methoxide



**Scheme 13.** Friedel-Crafts Acylation Route Towards Stepwise Formation of the Fluoroquinolone Backbone

the other syntheses of ciprofloxacin and other FQAs. The formation of this common intermediate provides the first opportunity for the generation of a broad range of FQAs. During the amination

reaction, any desired amine moieties present in other FQAs can be installed, with minimal expected changes in the chemical procedure. This route also provides us with the opportunity to make ciprofloxacin without the use of an expensive benzoyl chloride and without installing the dimethylamine group as the leaving group.

#### 2.4.3.1. Friedel-Crafts Optimization

The key step is the Friedel-Crafts acylation of our desired halogenated benzene. To keep our work in line with the earlier work performed in our group, we decided to use a similarly substituted 2,4-dichloro-5-fluorobenzene **38** as its corresponding benzoyl chloride **23b** was used previously. Initial experiments that were performed following literature conditions utilized dichloromethane<sup>89</sup> (DCM) or nitrobenzene<sup>90</sup> as a solvent with slight excesses of aluminum chloride as Lewis acid catalyst, which functions by activating the acylating agent. These experiments were unsuccessful and showed low consumption of the starting material. We attempted the reaction in alternative conditions utilizing neat acetyl chloride as the reaction solvent in lieu of any traditional solvents to increase interactions between the reagents.<sup>91</sup> Our initial explorations into this reaction yielded low conversion of starting material (~10-15%) which we attributed to the high reaction temperature. The reaction was performed at 110 °C, well above the boiling point of acetyl chloride (52 °C). As a result, even with a condenser to reduce loss through evaporation, there was a significant loss of reagent from the flask which resulted in high viscosity of the reaction mixture and poor stirring. We concluded the lack of reagent was a major factor causing reaction failure, and therefore performed the reaction with large excess (10 eq.) of acetyl chloride to facilitate the stirring of the reaction mixture. This adaptation did not show any improvements.



Stepping back from the specific chemistry, we viewed the reaction set-up under the lens of large-scale manufacturing and what equipment they would utilize under these conditions. We realized that the most effective way to prevent reactant loss through evaporation was to run the reaction in a sealed reaction vessel. The main issue with this setup is the generation of pressure within the reactor during the course of the reaction.

At large-scale, this experiment would be performed in steel reaction vessels with glass linings capable of withstanding high pressures. However, generation of HCl during the reaction prevented the use of the available steel vessels in our labs. The vessels are made with Hastelloy C276, a nickel-chromium-molybdenum alloy, which has resistance to corrosion and would most likely be unaffected by the HCl generated. However, the tubing and fittings that are connected to the vessel manifold are not corrosive resistant and would be rendered inoperable through continuous use for this reaction.

Thus, the best course, though not ideal, was to run the experiments in glass reaction vessels rated for high pressures (150 psi @ 120 °C). As an additional safety precaution, the reactions were run behind a blast-shield in case of a rupture.

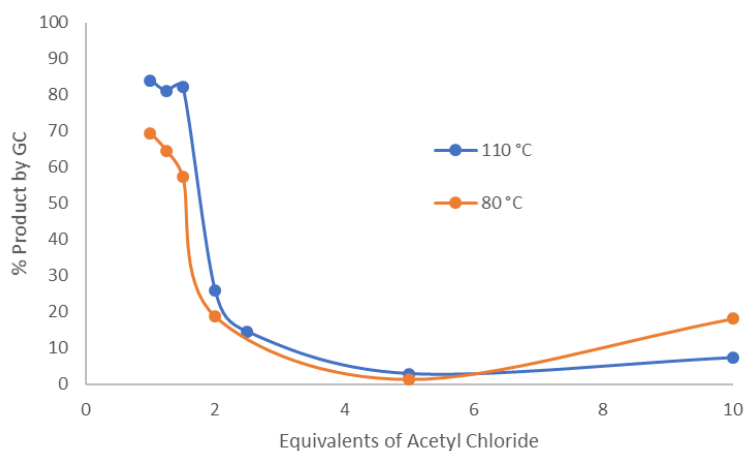


**Figure 27.** Friedel-Crafts Acylation of DCFB Performed in a Sealed Tube

Initially, using 10 equivalents of acetyl chloride resulted in low conversion at both 80 °C (18%) and 110 °C (8%). We observed that the transfer of reactions in a sealed tube reactor worked as expected and observed improved stirring compared to our reactions using a condenser. With improved stirring, we decided to explore conditions with fewer equivalents of acetyl chloride.

Curiously, we observed that as we decreased the equivalents of acetyl chloride, the conversion of starting material (DCFB) to product (dichlorofluoro acetophenone) increased (Figure 27).

A closer look at the proposed mechanism for Friedel-Crafts acylation<sup>92-99</sup> revealed that the reaction proceeds through an initial coordination between the Lewis acid (LA) and the acylating

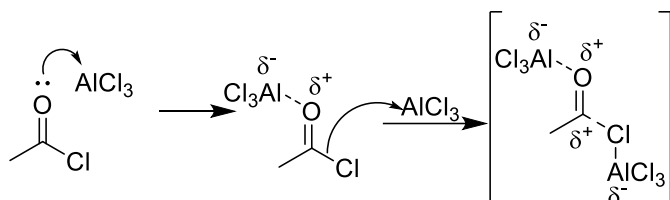


**Figure 28.** Initial Coordination of AlCl<sub>3</sub> with Acetyl Chloride in a Friedel-Crafts Acylation Mechanism

agent, in our case acetyl chloride. This is followed by the coordination of a second equivalent of the LA with the chloride of acetyl chloride (Figure 28).

This results in dissociation of the acetyl chloride chlorine from the molecule, forming a second donor-acceptor complex. This partial positive charge ( $\delta^+$ ) allows for a typical electrophilic aromatic substitution reaction ( $S_{EAr}$ ) which gives rise to an aromatic ketone-Lewis acid complex and at which point, there is only a single LA coordinating with the molecule. The LA complex can be hydrolyzed to form the desired acetophenone. Prior to hydrolysis, only one of the aluminum (III) chloride molecules remains coordinated to the oxygen, while the other is regenerated during the  $S_{EAr}$  and continues to react with additional acylating agent.

The main takeaway in regards to our neat reaction is that large excess of the acetyl chloride resulted in coordination with only a single equivalent of the aluminum chloride instead of two. Therefore, dissociation of the chlorine, which creates the partial positive charge ( $\delta^+$ ) at the carbonyl, is less likely to occur, resulting in low reaction conversion. This is supported by our results which showed a large increase in conversion to product when the equivalents of acetyl chloride were near or below the equivalents of aluminum chloride. Using this information, we continued further FCA reactions using only one equivalent of acylating agent and running at 110 °C.

### 2.4.3.1.1. Alternate Halogenated Benzenes

In addition to DCFB, we wanted to determine whether we could perform Friedel-Crafts acylations on alternatively halogenated benzenes. The most desired was 1,2,4-trifluorobenzene as the cost difference between trifluorobenzene and DCFB is nominal unlike the difference between

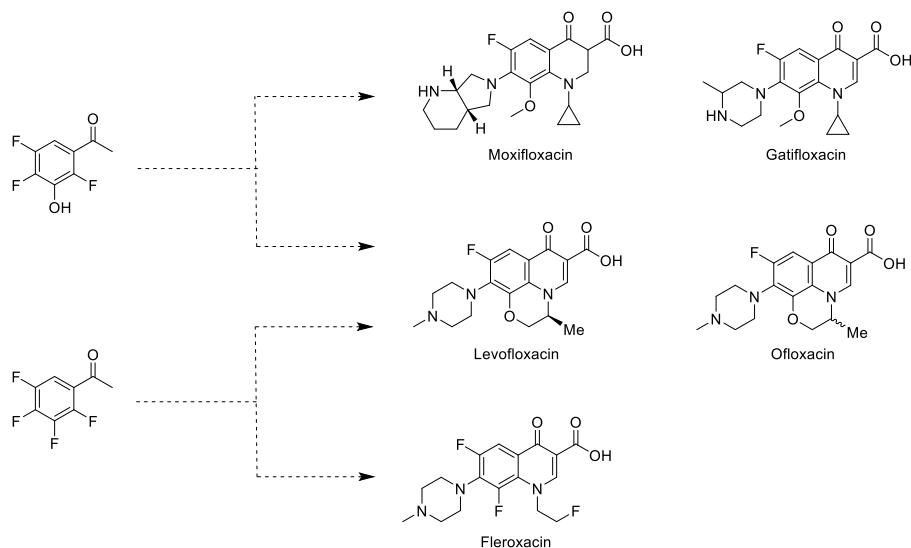


**Figure 29.** Proposed FQAs from Different Halogenated Acetophenones

present in ciprofloxacin. Acylation of other halogenated benzenes to form additional acetophenones could also be used in the synthesis of a wider variety of FQAs (Figure 29). Two such examples of this were 2,3,6-trifluorophenol and 1,2,3,4-tetrafluorobenzene.

Initial reactions focused on the trifluorobenzene **43** and trifluorophenol **44** and followed the same reaction conditions as our DCFB acylation. These reactions showed no conversion to

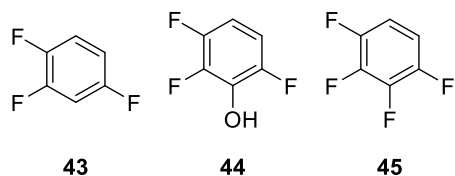


**Figure 30.** Alternate Halobenzenes for Friedel-Crafts Acylation

starting material. We believed that the lack of reaction was a result of these benzenes being electron deficient as a result of the three fluorines on the ring which prevented the reaction with acetyl chloride. Due to these initial

results, we did not explore this reaction with tetrafluorophenol **45**. Instead, we looked to our

acylating reagent to see if we could improve its reactivity and therefore account for decreased activity of the aromatic ring.

We performed the FCA following the same conditions as we had established, but with the replacement of acetyl chloride with acetyl bromide, which has an improved reactivity.<sup>100</sup> An additional benefit of the switch to acetyl bromide was also its higher boiling point (77 °C).

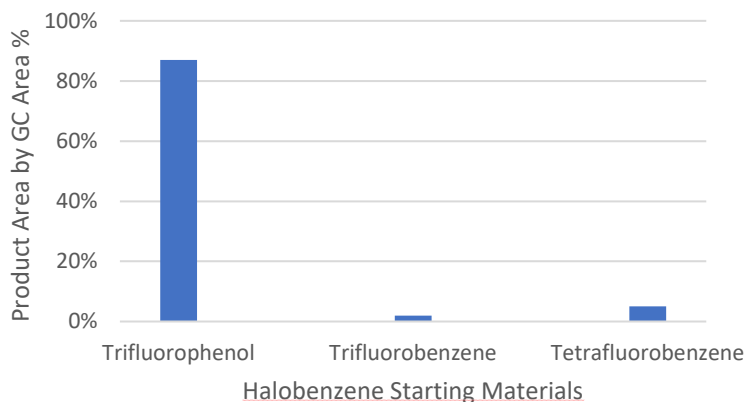


**Figure 31.** Acylation of Halobenzenes Using Acetyl Bromide

Although the boiling point is still below the reaction temperature, it results in less pressure build-up and safer operation. Due to the decreased pressure build-up, this reaction would also be less dangerous on large scale compared to the reaction with acetyl chloride. The reaction was performed using acetyl bromide on the three alternative halogenated benzenes which gave improved results (Figure 31). Trifluorophenol **44** showed the highest conversion (87%) to product, but unfortunately, trifluorobenzene **43** and tetrafluorobenzene **45** each showed less than 10% conversion. This opened up the opportunity for possible routes to FQAs such as moxifloxacin, gatifloxacin, levofloxacin, and ofloxacin. Due to its better activity as a leaving group, we hypothesized that the use of acetyl iodide could improve the conversion of trifluorobenzene **43** and tetrafluorobenzene **45**, but due to its cost we chose not to explore those reactions.<sup>100</sup> Due to the high conversion of our trifluorophenol reaction, we explored the use of acetyl bromide for our DCFB starting material. This reaction showed high conversion, but large amounts of regioisomer was observed which led to dismissal of those conditions.

Further investigations into the acetyl bromide reaction with trifluorophenol **44** were disappointing, as the spectroscopic data suggested that instead of synthesizing the desired acetophenol **46a**, we synthesized its regioisomer **46b** (Figure 33). This was determined using the splitting pattern of the remaining aromatic proton that is observed when performing  $^1\text{H}$  NMR spectroscopy. First, to better understand this, the splitting observed in our trifluorophenol starting material **44** must be observed. The splitting patterns of  $\text{H}_a$  and  $\text{H}_b$  are dependent on their coupling with neighboring protons as well as coupling with each of the three fluorines on the aromatic ring. Assuming the splitting effect from each of the fluorines was different, we would see a total of 12 peaks for each proton. This is a result of splitting from 3 distinct fluorines and from the other

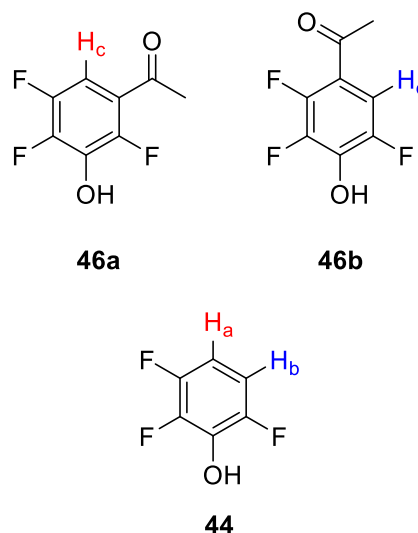


**Figure 33.** Possible Products of FCA of Trifluorophenol **44** with Acetyl Bromide.

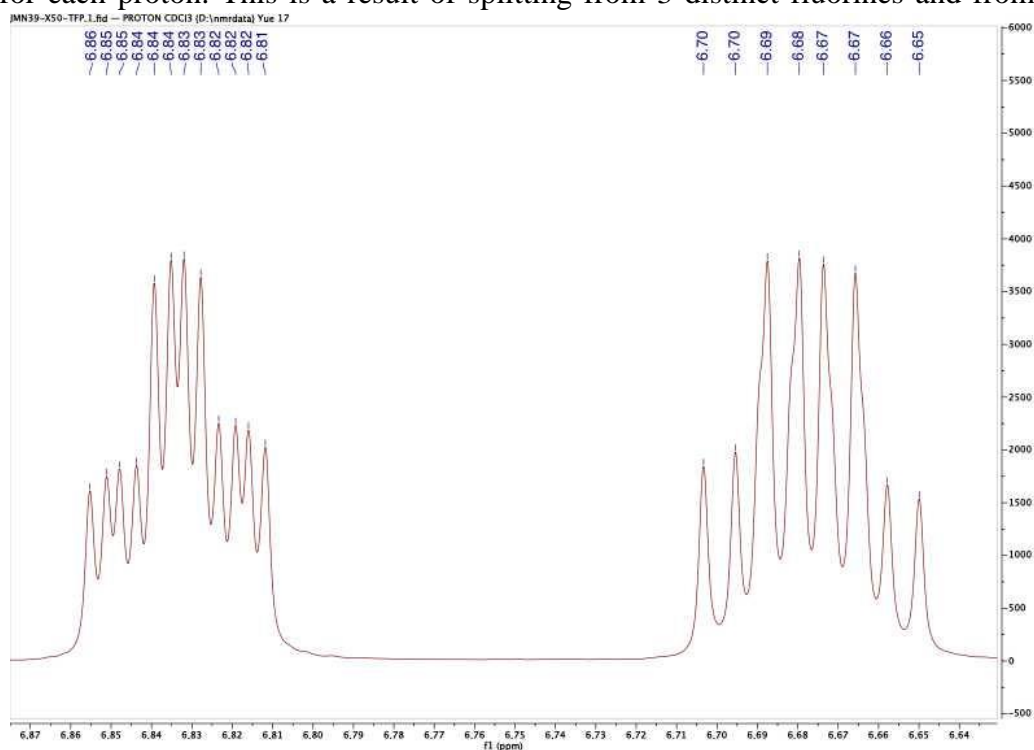


**Figure 32.**  $^1\text{H}$  NMR Spectra Zoom (6.63-6.88 ppm) for the Aromatic Protons of 2,3,6-trifluorophenol **44**.

hydrogen (1→2→4→8→12). However, when we look at the NMR spectra for **44**, we see one set of aromatic peaks with 12 distinct peaks (6.83 ppm), and one set of aromatic peaks with 8 distinct peaks (6.67 ppm) (Figure 32). Closer inspection of the set with 8 peaks shows that the four central peaks each have a small shoulder which is not separate enough to form its own peak. This can be attributed to the splitting caused by the fluorine para to H<sub>b</sub>. The proton para to fluorine on an unsubstituted benzene ring presents with a coupling constant of 0.2 Hz and a range from 0-4 Hz in substituted benzenes, which would result in the shoulders of the central peaks in the peaks centered at 6.68 ppm.<sup>101</sup> Therefore, the peaks centered at 6.83 ppm with 12 distinct peaks are most likely attributed to H<sub>a</sub>, and the peaks centered at 6.67 ppm with 8 distinct peaks are most likely attributed to H<sub>b</sub>.

Based on the spectra of **44**, close inspection of the NMR spectra of the reaction between acetyl bromide and trifluorophenol **44** should show a splitting pattern with 8 distinct peaks if the desired product **46a** is produced. This is because there is no longer splitting from a neighboring proton in addition to the fluorines, so we no longer observe the 12 distinct peaks from the starting material. The 8 distinct peaks are present in the NMR, leading to the initial conclusion that the proton is H<sub>c</sub> and the desired product has been made.

However, closer inspection of the coupling constants (Figure 34) of the outer peaks to be 2.28 Hz. This small of a coupling constant is only possible if the proton is coupling with a fluorine

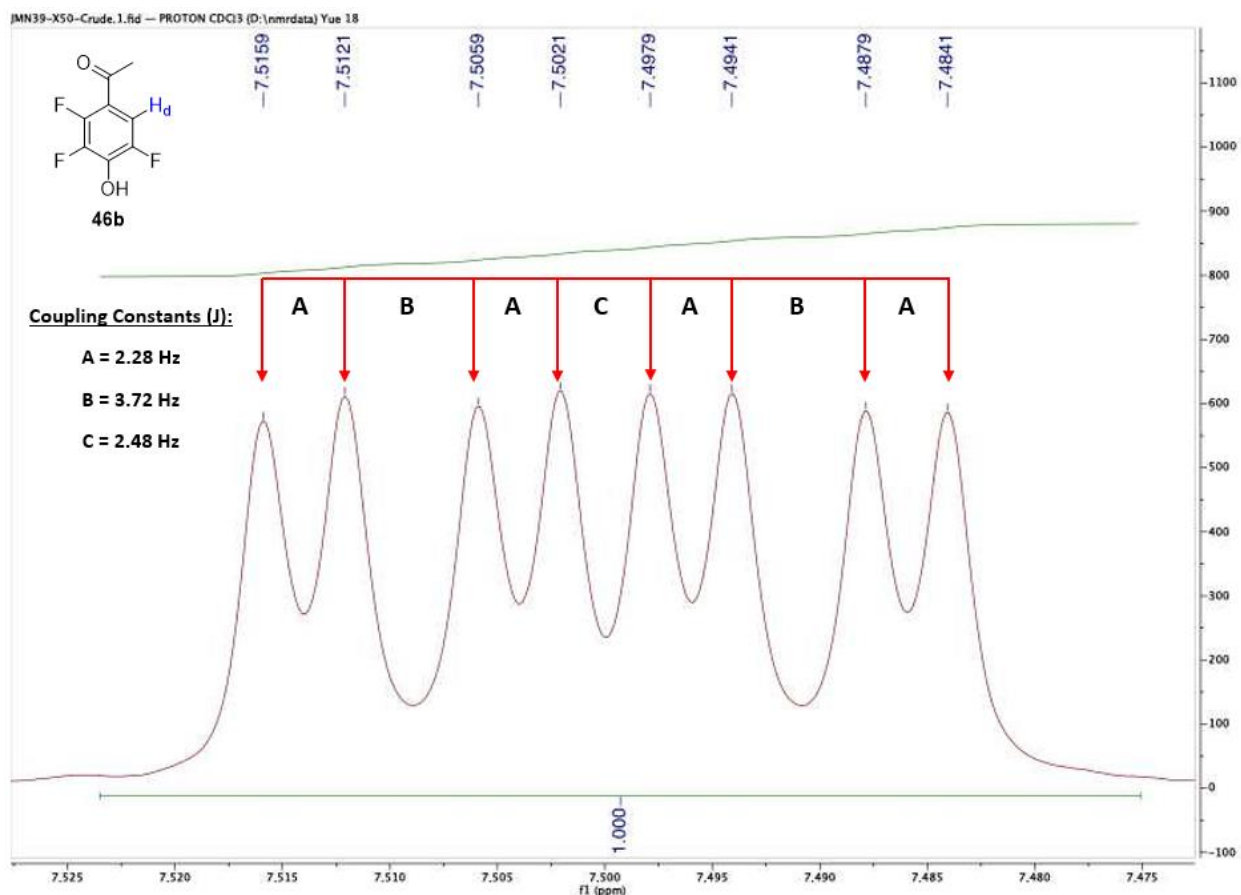


**Figure 34.**  $^1\text{H}$  NMR Spectra Zoom (7.47-7.53 ppm) for the Aromatic Proton of Crude Reaction Mixture Believed to Contain **46b**.

in the para position, as is the case for  $H_b$  where we observe indistinct shoulders on the central four peaks (Figure 32). Although we saw extremely low coupling from the fluorine para to  $H_b$  in the starting material, the acetyl substituent on the reaction product must be causing a change in the para-fluorine's splitting effect and resulting in a higher coupling constant for  $H_d$ . As mentioned before, the range of coupling for a proton with a para fluorine is 0-4 Hz. As a result, the corrected conclusion is that the observed proton is  $H_d$  and the reaction formed the undesired regioisomer **46b**.

Although this is an unfortunate result, it is by no means an end to the exploration that can be done on this reaction process. Alcohol substituents are strong para directors for FCA which is most likely causing the undesired regioisomer.<sup>102</sup> The effects of this electron configuration can be

mitigated by the use of alternately substituted benzenes, perhaps those with ethers instead of alcohols, which are less electron withdrawing due to the alkyl group providing electron density to the oxygen. In addition, the use of *meta*-directing groups such as carboxylic acids, esters, nitro groups, or a nitrile could be used to promote acylation at the desired site. Unfortunately, these groups are innately electron withdrawing and will further decrease the activity of the aromatic ring for the purposes of the reaction. Therefore, if the use of any *meta*-directing groups should be balanced out with the use of a dichloro-substituted benzene instead of the trifluoro and acetyl bromide will most likely still be required to improve reactivity.

One positive from our formation of **46b**, was also derived from the NMR spectra. When looking at the data, we observed that the signal for the methyl group of the acetophenone presented as a doublet.<sup>103</sup> Further investigation of this led us to literature which suggested that the protons in the  $\alpha$ -position of an acetophenone, where there is a fluorine on the neighboring benzene site, shows splitting. This through-space coupling that we observe in our spectra of **46b** helps to confirm that we have formed the acetophenone, but the lack of splitting supports that in our other synthesis of DCFA **39**, the acylation occurred at the desired site. If the acylation had occurred at the undesired site *ortho* to the single fluorine substituent, we would have observed splitting in the <sup>1</sup>H NMR spectra of **39**.

#### 2.4.3.2. $\beta$ -Ketoester Backbone Formation

After successful formation of the desired acetophenone, it was reacted with a dialkyl carbonate and base to form a  $\beta$ -ketoester (Scheme 13, Step 2) which will act as part of the backbone of our final FQA product. The final structure of FQAs includes a carboxylic acid, not an ester, but the ester can be easily hydrolyzed to the acid at a later stage as is demonstrated in other syntheses.<sup>82</sup> For our experiments, we determined that sodium methoxide (NaOMe) acted as a strong enough



base to deprotonate at the beta carbon of the acetophenone which can then react with alkyl carbonates.

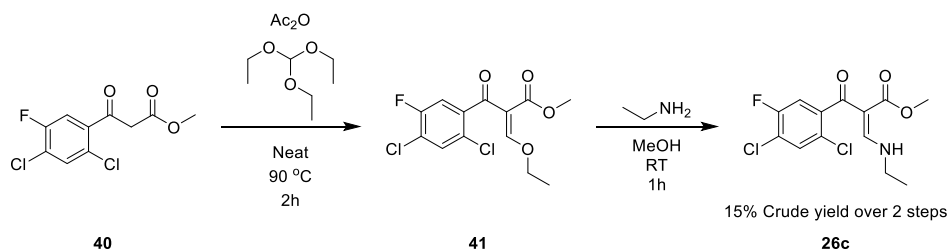


**Figure 35.** Crystal formation of  $\beta$ -ketoester **40** after Column Chromatography

This step currently shows low isolated yield (IY) (7% IY, 95% purity) and due to generation of side products, requires purification using column chromatography to purify the reaction mixture. However, fractions collected after column chromatography have the potential to spontaneously form crystals (Figure 35). As a result we hypothesize that a crystallization method for the crude reaction mixture could be developed as a more economical purification technique. In addition, further exploration into

reaction optimization as well as alkyl carbonate selection could improve the results.

#### 2.4.3.3. Continuation to a Convergent Synthesis



**Scheme 14.** Synthesis of Common Intermediate **26c** towards Norfloxacin over Two Steps

The main purpose of this synthetic route is to obtain the acyclic intermediate (**26**). This intermediate is present in a wide variety of fluoroquinolone antibiotic syntheses and can proceed to the final API through three well-known steps: cyclization,  $S_NAr$ , and hydrolysis of the ester to

the carboxylic acid. In the case of ciprofloxacin, the API is most often formulated as an HCl salt, which can be formed at the end of the synthesis. In order to bring our  $\beta$ -ketoester forward to the intermediate, we must first install the vinyl ether and then replace the ether with our desired amine group. This can be achieved using triethyl orthoformate followed by installation of the desired amine group. Following amination, the material converges with other FQA syntheses and can be carried forward to the desired antibiotic. The application of these steps to the synthesis of norfloxacin, in particular, is amenable as the vinylogous carbamate **26c** has low solubility in methanol and crashes out from solution. Using these two steps in sequence, we were able to produce **26c** in 15% yield over 2 steps from **40**.

## 2.5. $S_NAr$ of Fluoroquinolone Antibiotic Intermediates

Fluoroquinolone antibiotics all share a cyclic amine ring substituent off of C<sub>7</sub> which helps to promote their bioactivity. For FQAs such as ciprofloxacin and norfloxacin, this

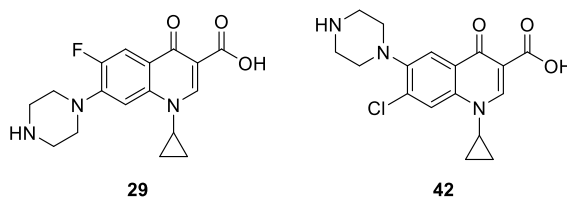


**Figure 36.** Ciprofloxacin (**29**) and the Undesired Side-product of  $S_NAr$  (**42**)

cyclic amine is piperazine. Substituted piperazines are also seen in other FQAs like levofloxacin, gatifloxacin, and fleroxacin among others. Therefore, the installation of this substituent is an important step in the synthesis of FQAs and it also provides an opportunity for expanding the scope of our synthesis to a wider range of antibiotics.

During the initial work performed by the Gupton group towards ciprofloxacin, it was realized that an undesired side product occurred during the course of the final  $S_NAr$  reaction when the piperazine reacted at the fluorine substituent instead of at the intended chlorine substituent.

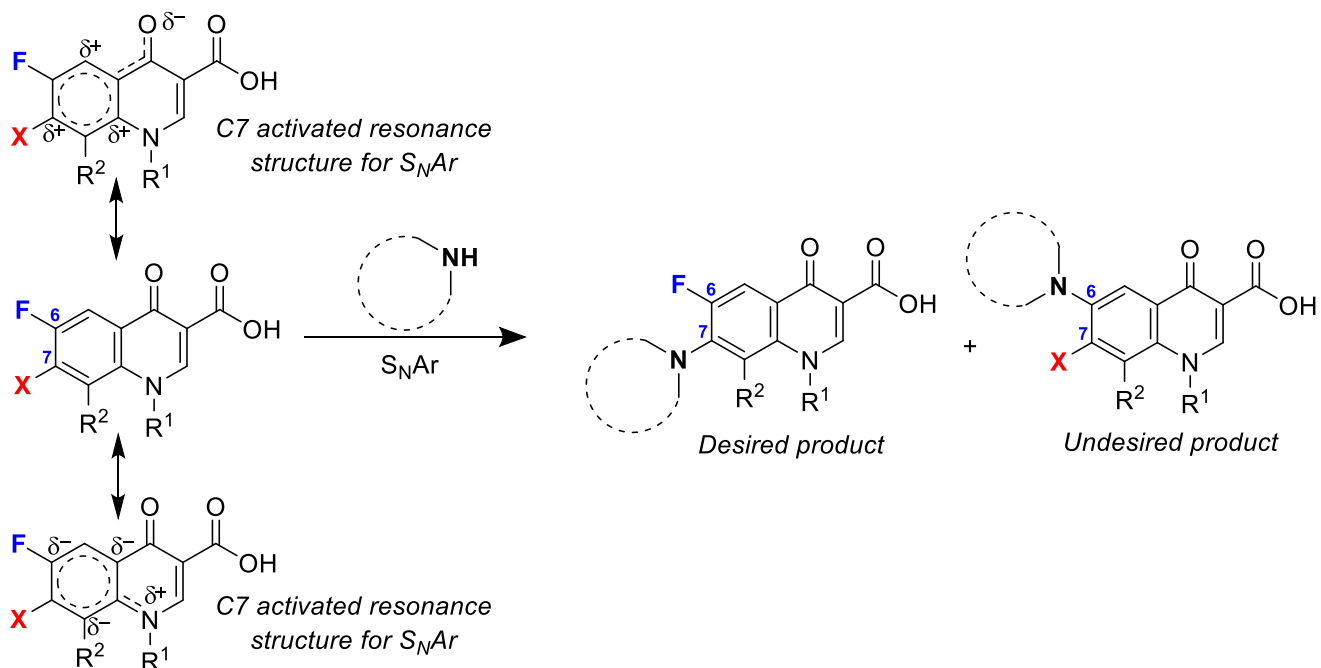


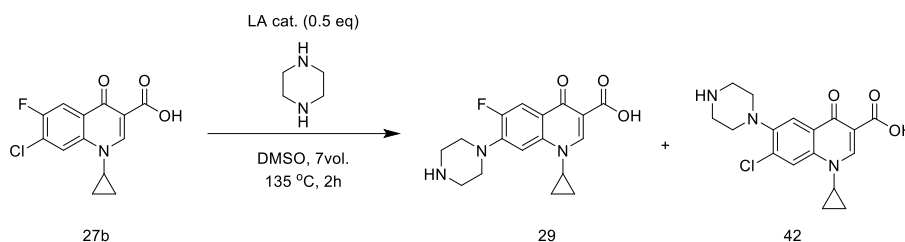
**Figure 37.** Resonance Structures Showing Activation of C7 and C6 Sites of Fluoroquinolone Precursor

Under our standard reaction conditions, this impurity was about 9-10% compared to the desired product. We believe this is due to higher reactivity of fluorine in  $S_NAr$  than chlorine.<sup>84</sup> Since the new synthesis through Friedel-Crafts acylation also requires a chlorine substituent, we decided to look into possible improvements on this  $S_NAr$  reaction.

As shown in Figure 37, the halogen at C7 is more activated as a result of the electron withdrawing and donating properties of the ketone and amine substituents. The C7 site is activated by resonance with the electronic withdrawing effect of the ketone, there is also a relatively minor activation of the C6 site by the fluorine substituent due to the more polarized C-F bond. In addition, the C6 site is deactivated by the electron donating effect of the amine group.

As expected, when the reaction is performed with a fluorine at the C7 position as in prior syntheses, there is little to no generation of undesired substitution product since the C7 is activated by resonance and the

**Table 8.** LA Catalyst Screens in DMSO

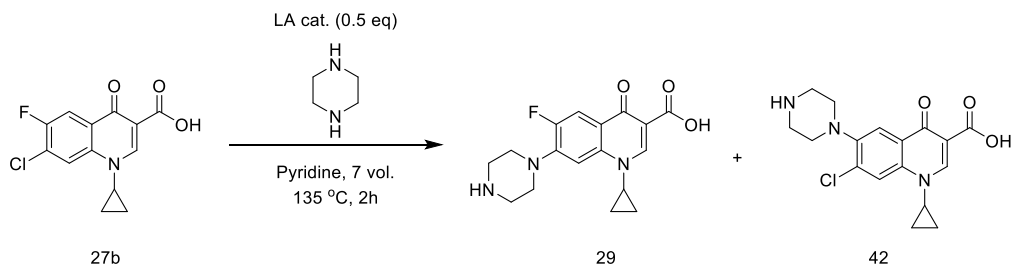


Catalyst Screen in DMSO					
Exp.	LA Catalyst	Area % <b>42</b> <sup>a</sup>	Exp.	LA Catalyst	Area % <b>42</b> <sup>a</sup>
1.0	--	9-10	1.12	FeCl <sub>3</sub>	4.2
1.1	AlCl <sub>3</sub>	3.1*	1.13	Er(OTf) <sub>3</sub>	4.9
1.2	ZnSO <sub>4</sub> *7H <sub>2</sub> O	22.9	1.14	ZrCl <sub>4</sub>	5.8
1.3	FeSO <sub>4</sub> *7H <sub>2</sub> O	16.5	1.15	TiCl <sub>4</sub>	7.3/3.3 <sup>b</sup>
1.4	Co(OAc) <sub>2</sub>	30.4	1.16	In(OTf) <sub>3</sub>	4.6
1.5	FeCl <sub>2</sub> *4H <sub>2</sub> O	14.1	1.17	ZnCl <sub>2</sub>	8.8
1.6	CoCl <sub>2</sub> *6H <sub>2</sub> O	6.8	1.18	TTIP	9.9/4.4 <sup>b</sup>
1.7	CuSO <sub>4</sub> *5H <sub>2</sub> O	9.0	1.19	MgCl <sub>2</sub>	7
1.8	CuCl	8.7	1.20	SnCl <sub>4</sub>	2.3
1.9	CuCl <sub>2</sub>	7.6	1.21	La(OTf) <sub>3</sub>	5.2
1.10	CeCl <sub>3</sub>	6.9	1.22	Fe(NO <sub>3</sub> ) <sub>3</sub> *9H <sub>2</sub> O	5.2
1.11	SnCl <sub>2</sub> *2H <sub>2</sub> O	5.3	--	--	--

<sup>a</sup>) Area % is measured at 210nm. <sup>b</sup>) LCMS peaks were poorly defined and integration of peak areas was difficult

polarized C-F bond. However, when the desired site for substitution is chlorinated, there is competition between the more electronically favorable position through resonance (C7) and the more electronically favorable site due to the polarized C-F bond, yielding a higher partial positive charge ( $\delta^+$ ) on C6 and resulting in nucleophilic substitution at C6. Although this is not a major product of the reaction, it does result in up to 10% loss of desired product which can be a significant loss. In order to address this issue, we explored the use of Lewis acids to improve the electron withdrawing of the ketone and increase the  $\delta^+$  at the C7 position (Table 8).

We explored a broad array of Lewis acids (Table 8) where we saw that some LA catalysts resulted in significant decrease of the undesired regioisomer, for example, tin (IV) chloride (entry 1.20) and aluminum (III) chloride (1.1). In order to fully explore this chemistry, we studied the

**Table 9.** LA catalyst Screens in Pyridine

Catalyst Screen in Pyridine							
Exp.	LA Catalyst	Area % <b>42</b> <sup>a</sup>	$\Delta$ Area % <sup>b</sup>	Exp.	LA Catalyst	Area % <b>42</b> <sup>a</sup>	$\Delta$ Area % <sup>b</sup>
2.1	AlCl <sub>3</sub>	1.2	-1.9	2.18	TTIP	2.8	-1.6
2.11	SnCl <sub>2</sub> *2H <sub>2</sub> O	5.50	0.20	2.20	SnCl <sub>4</sub>	1.6	-0.70
2.12	FeCl <sub>3</sub>	5.4	1.2	2.21	La(OTf) <sub>3</sub>	3.1	-2.1
2.13	Er(OTf) <sub>3</sub>	3.9	-1.0	2.22	Fe(NO <sub>3</sub> ) <sub>3</sub> *9H <sub>2</sub> O	7.6	2.4
2.15	TiCl <sub>4</sub>	NR	-	2.23	SnI <sub>4</sub>	1.1	--
2.16	In(OTf) <sub>3</sub>	4.0	-0.6	--	--	--	--

<sup>a</sup>) Area % is measured at 210 nm. <sup>b</sup>)  $\Delta$  Area % is the change in area % of **42** observed compared to the results in Table 8. NR means no reaction was observed

solvent effects from using DMSO and pyridine. In order to expedite results, we only performed this solvent experiment with the LA catalysts that showed promise in the DMSO reactions. As shown in Table 9, aluminum (III) chloride and tin (IV) chloride were among the best performing LAs. In light of the good results from tin (IV) chloride, we explored tin (IV) iodide as an alternative LA catalyst. Tin (IV) iodide also performed very well, even better than tin (IV) chloride and aluminum (III) chloride with the undesired side-product at only 1.1%.

During our studies using uncatalyzed S<sub>N</sub>Ar reactions, we observed that the final crystallization process yielded a 9-10% loss of desired product in addition to the purging of the regioisomeric impurity, resulting in only ~80% yield of product. Therefore, the decrease of the impurity to 1.1% is expected to result in a final yield of >95% after crystallization and purging of the impurity. This increase in yield would make significant impact into the final cost of the API. Due to these promising results, we continued our exploration into the reaction using SnCl<sub>4</sub> and SnI<sub>4</sub>.

**Table 10.** Equivalent screens of Tin (IV) LA Catalysts

LA Cat.	LA Cat.	Eq. of Cat.	Solvent	Area % <b>42</b> <sup>a</sup>
3.1	SnCl <sub>4</sub>	1	DMSO	2.1
3.2		0.5	DMSO	2.30
3.3		0.5	Pyridine	1.6
3.4		0.5	DMSO	2.8
3.5		0.5	Pyridine	1.1
3.6		0.25	Pyridine	2.5
3.7		0.25	DMSO	2.2
3.8		0.25	DMSO	2.0
3.9		0.1	Pyridine	18.2
4.0	SnI <sub>4</sub>	0.5	Pyridine	1.1
4.1		0.5	DMSO	1.5
4.2		0.25	Pyridine	5.7
4.3		0.25	DMSO	2.6
4.4		0.1	Pyridine	1.7

a) Area % is measured at 210 nm

regioisomer impurity **42** (1.1 %, entries 3.5 & 4.0). We have demonstrated an efficient method for final-step optimization towards ciprofloxacin. Although further studies with alternative benzene substitutions may be needed, we believe this technique will be effective for use in the syntheses of other FQAs. This is especially important since we have seen low activity of fluorine substituted benzenes for our Friedel-Crafts acylation reaction at the beginning of the synthesis. The use of chlorine substituted benzenes for FCA should provide more activity of the ring and allow for reaction to occur. Should the chlorine substituted benzenes be utilized, this S<sub>N</sub>Ar optimization should help in increasing the yield of the final FQA.

## 2.6. Conclusions and Next Steps

Our research group has developed an efficient, high yielding synthesis for ciprofloxacin, an important fluoroquinolone antibiotic. We have further expanded on this work to remove the major cost-driver of our own synthesis, the expensive lithium-based reagent, LiHMDS. Across

A study of the effect of LA loading was next examined (Table 10). From these studies, pyridine and 0.5 equivalents of either tin (IV) LA catalyst afforded the lowest amount of the

this work, we have demonstrated that FQAs can be achieved through an alternate synthesis which begins with a Friedel-Crafts acylation of a halogenated benzene. During the FCA, different halogenated benzenes can be utilized in order to synthesize multiple FQAs. Although the subsequent formation of the  $\beta$ -ketoester is currently low yielding, this reaction can most likely be optimized to obtain higher yield and avoid purification by column chromatography. Subsequent steps towards the common intermediate can also be improved through a wider range of screens (temperature, time, equivalents) and by using a design of experiment analysis. These steps will also require further exploration into the effect of different amine moieties on the reaction and purification through precipitation or crystallization. Once the common intermediate is synthesized, the ring closure and ester hydrolysis can be performed in the same manner as other fluoroquinolone syntheses.<sup>82</sup> Lastly, the  $S_NAr$  reaction to install the cyclic amine at the C7 position will require additional studies to determine the efficacy of the reaction with cyclic amines other than piperazine. Although the standard reaction without LA catalysts is effective in itself, the use of tin (IV) iodide, tin (IV) chloride, or aluminum (III) chloride can help to improve the overall yield and decrease loss of product during the crystallization of the API due to minimization of undesired regioisomers.

Our synthesis of fluoroquinolone antibiotics provides a convergent route which can be modified to manufacture multiple FQAs through modification of the amine and cyclic amine moieties at the time of their respective installations. In addition, the route provides an opportunity for broadening the scope to more fluoroquinolones through modification of the halogenated benzene to establish functional groups or reactive sites early in the synthesis. Currently, the biggest problem with this technique is working with multi-fluorinated benzenes which have electron-poor aromatic rings, and hence low acylation. Due to availability, cost, or both, we were unable to

explore as wide of a range of halogenated benzenes as we wanted to. However, as new techniques and supply volumes are constantly shifting, the exploration of those halobenzenes may be easier and more economically viable in the future.

In conclusion, a framework for alternative synthesis to fluoroquinolone antibiotics was established. This synthetic route can be developed to be integrated into large-scale manufacturing and with further exploration can be used in the synthesis of multiple fluoroquinolone antibiotics.

## **2.7. General Procedures and Experimental Data**

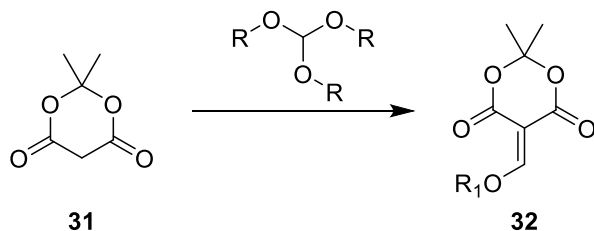
### **2.7.1. General Information**

All commercially available reagents were purchased from Acros Organics, Sigma-Aldrich, TCI, Alfa Aesar, Combi-Blocks, or Oakwood Chemical and used as received. Proton nuclear magnetic resonance ( $^1\text{H}$  NMR) spectra and carbon nuclear magnetic resonance ( $^{13}\text{C}$  NMR) were recorded on a Bruker Ascend-600MHz. Chemical shifts for protons are reported in parts per million (ppm) downfield from tetramethylsilane (TMS) or referenced to residual solvent. Chemical shifts for carbon are reported in ppm downfield from TMS or referenced to residual solvent. Data are represented as follows: chemical shift, multiplicity (br = broad, s = singlet, d = doublet, t = triplet, q = quartet, m = multiplet), coupling constant in hertz (Hz), integration.



## 2.7.2. Procedures and Data Towards the Synthesis of Fluoroquinolone Antibiotics

### 2.7.2.1. Meldrum's Acid Route



Meldrum's Acid Vinyl Ether 32: Meldrum's Acid **31** (7.5 g, 52 mmol) was added to a 50mL round bottom flask. To the flask was added trialkyl orthoformate (R=Me, 26 mL, 234 mmol) (R=Et, 39 mL, 234 mmol). The reaction mixture was heated to 95 °C and allowed to stir for 3 hours. After 3 hours, the reaction mixture was allowed to cool and the excess trialkyl orthoformate was removed by rotary evaporation. This material was used in the next step with no further purification.

R = Methyl: 92% Crude Yield

<sup>1</sup>H NMR (600 MHz, Chloroform-d) δ 8.16 (s, 1H), 4.28 (s, 3H), 1.73 (s, 6H).

<sup>13</sup>C NMR (151 MHz, Chloroform-d) δ 175.26, 163.17, 158.60, 104.65, 96.65, 66.16,

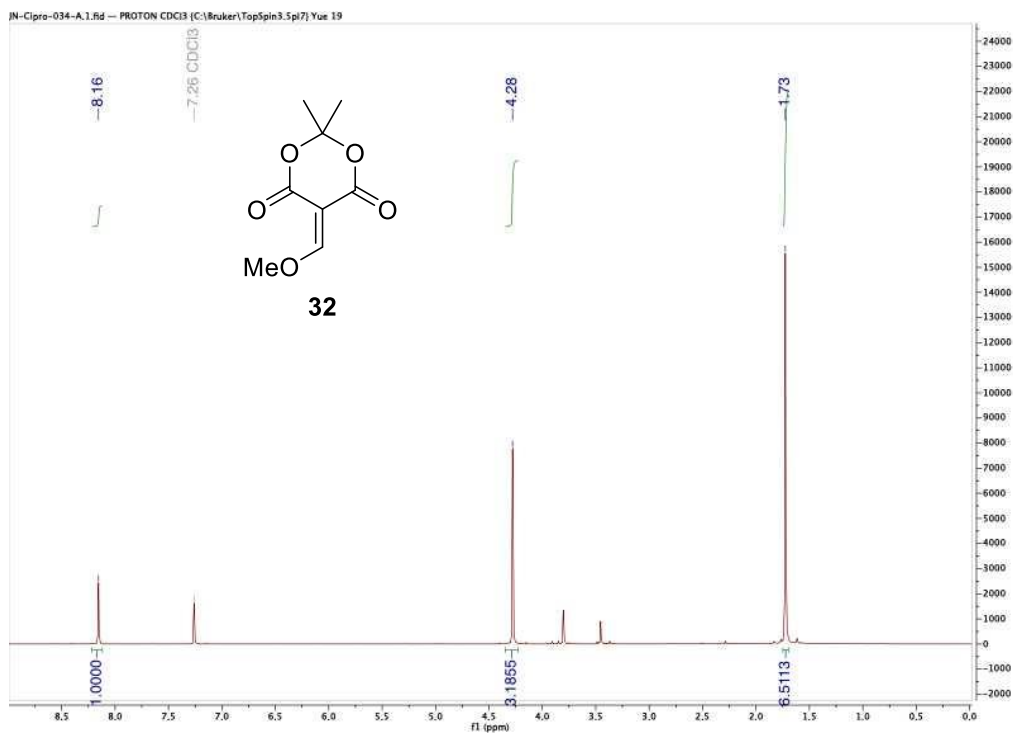
27.11

NMR agrees with literature spectra.<sup>104</sup>

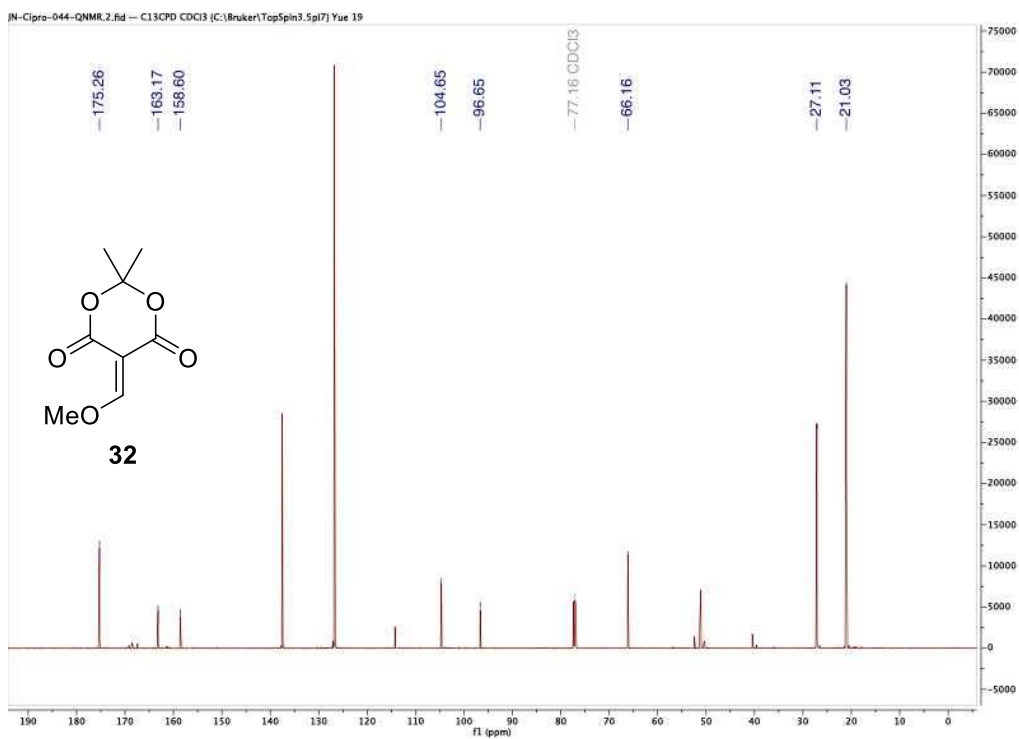
R = Ethyl: 86% Crude Yield

<sup>1</sup>H NMR (600 MHz, Chloroform-d) δ 8.23 (s, 1H), 4.51 (q, *J* = 7.1 Hz, 2H), 1.72 (s, 6H), 1.52 (t, *J* = 7.1 Hz, 3H).

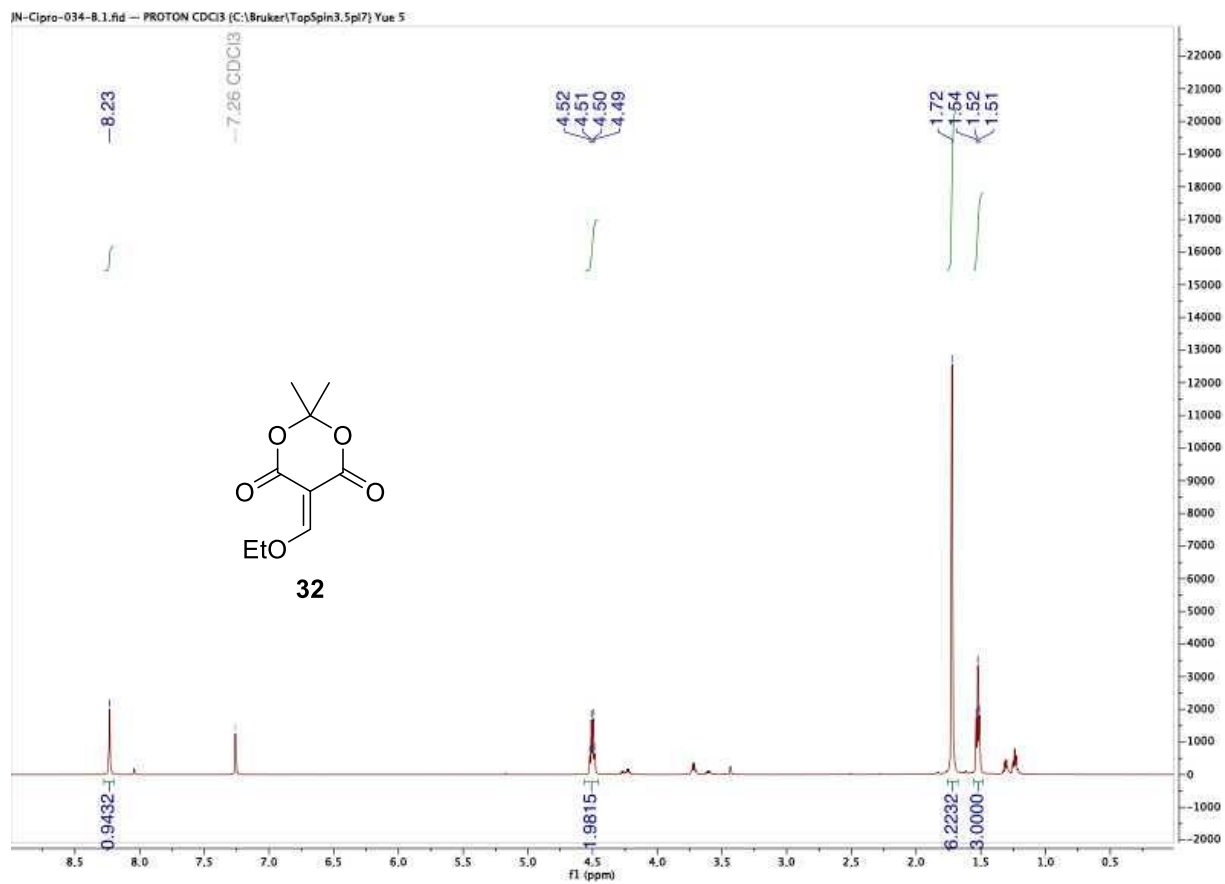
NMR agrees with literature spectra.<sup>105</sup>



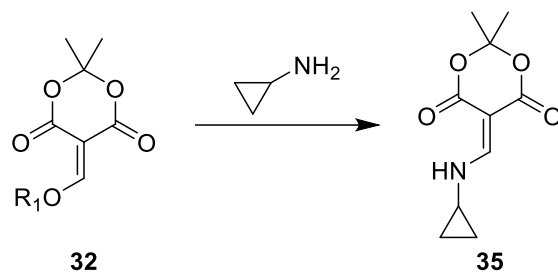
**NMR Spectra 12.**  $^1\text{H}$  NMR of Meldrum's Acid Vinyl Methyl Ether **32**



**NMR Spectra 13.**  $^{13}\text{C}$  NMR of Meldrum's Acid Vinyl Methyl Ether **32**

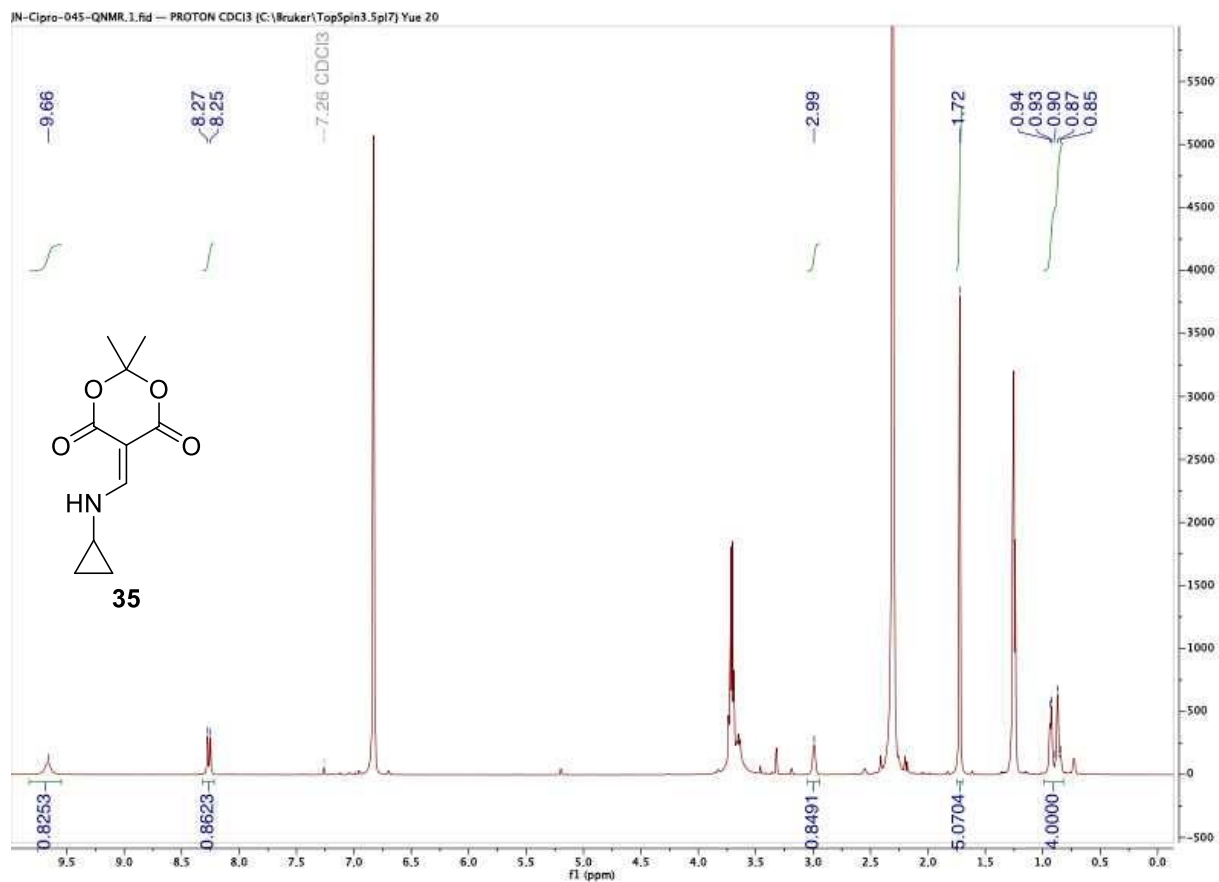


**NMR Spectra 14.**  $^1\text{H}$  NMR of Meldrum's Acid Vinyl Ether **32**

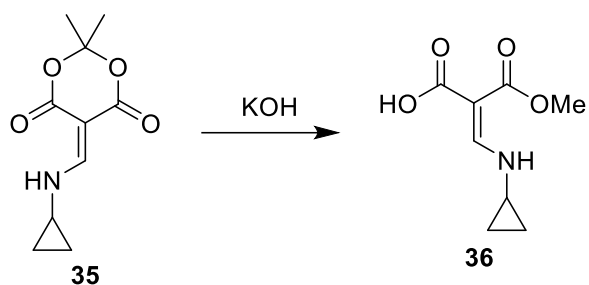


Meldrum's Acid Vinyl Cyclopropylamide 35: Meldrum's acid vinyl ether **32** (R = Methyl) (19.4g, 0.100 mol) was added to a 500 mL round bottom flask with ethanol (100 mL) and the mixture was allowed to stir. In a separate flask were combined cyclopropylamine (8.67 mL, 0.130 mol) and ethanol (100 mL). The cyclopropylamine solution was then added to the stirring mixture and the reaction was allowed to run for 1 hour at room temperature. After 1 hour, the solvent was removed by rotary evaporation. The product was used without any further purification (140% crude yield, 60% purity by QNMR).

$^1\text{H}$  NMR (600 MHz, Chloroform-d)  $\delta$  9.66 (br, 1H), 8.26 (d,  $J = 14.3$  Hz, 1H), 2.99 (s, 1H), 1.72 (s, 6H), 0.90 (m, 4H).



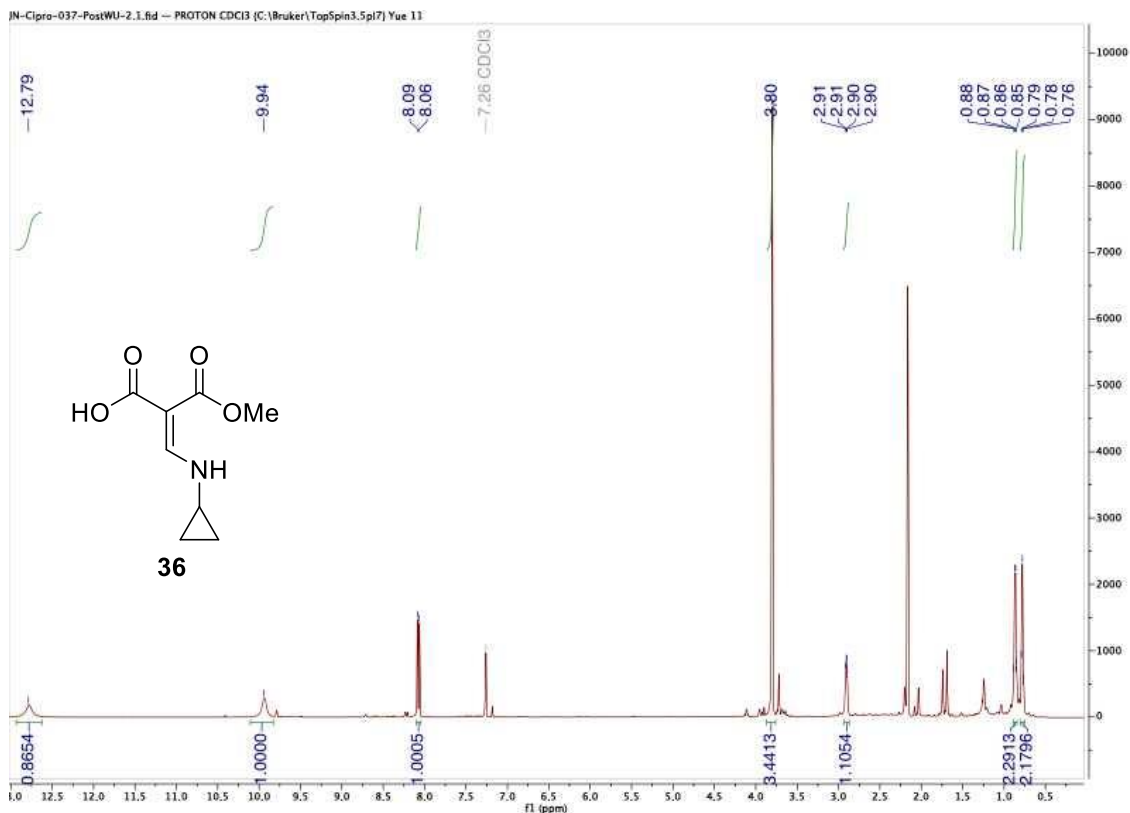
**NMR Spectra 15.**  $^1\text{H}$  of Meldrum's Acid Vinyl Cyclopropylamide **35**.



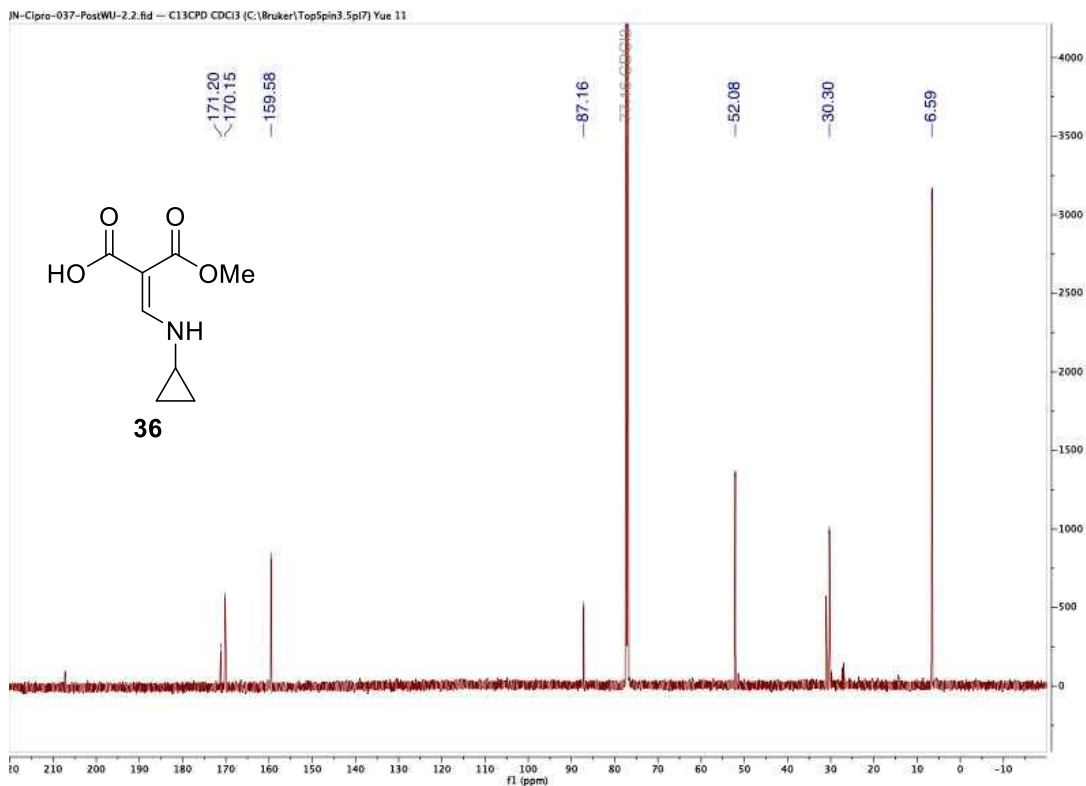
Cyclopropyl Vinylogous Carbamate 36: Meldrum's acid derivative **35** (500 mg, 2.4 mmol) was added to a 20 mL scintillation vial with methanol (15 mL). Potassium Hydroxide (133 mg, 2.4 mmol) was added to the vial and the reaction mixture was allowed to stir at room temperature overnight. After stirring overnight, the solvent was removed by rotary evaporation, reconstituted in ethyl acetate (10 mL), and washed 3x with DI water (5 mL). The organic layer was collected and solvent removed by rotary evaporation and the product was given in moderate yield (85% crude yield).

$^1\text{H}$  NMR (600 MHz, Chloroform-d)  $\delta$  12.79 (br, 1H), 9.94 (br, 1H), 8.07 (d,  $J = 13.93$  Hz, 1H), 3.8 (s, 3H), 2.90 (br, 1H), 0.88-0.76 (m, 4H).

$^{13}\text{C}$  NMR (151 MHz, Chloroform-d)  $\delta$  171.20, 170.15, 159.58, 87.16, 52.08, 30.30, 6.59.



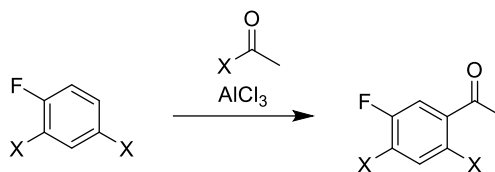
**NMR Spectra 16.**  $^1\text{H}$  of Cyclopropyl Vinylogous Carbamate **36**.



**NMR Spectra 17.**  $^{13}\text{C}$  of Cyclopropyl Vinylogous Carbamate **36**.

### 2.7.2.2. Friedel-Crafts Acylation Route

#### Halogenated Acetophenone General Method:

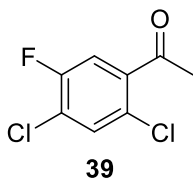


The synthetic method for Friedel-Crafts acylation of halobenzenes was the same for each of the halobenzenes and the acylating agents that was chosen. Aluminum chloride was used for all of our FCAs as well. This method was adapted from literature.<sup>91</sup>

To a sealed tube flask (rated for 150 psi @ 120 °C) with a stir bar was added aluminum chloride (1.5 equiv) and halogenated benzene or halogenated phenol (1.0 equiv). Acylating agent (acetyl chloride or acetyl bromide) (1.0 equiv) was then added to the flask and the flask was sealed. The flask was submerged in a silicone oil bath and allowed to stir. \*Note: In acetyl chloride reactions, stirring did not occur until reaction temperature was elevated to at least 70 °C. The reaction was slowly heated in stepwise fashion to make sure the flask was properly sealed and would not burst. The flask was heated to 110 °C and allowed to stir for 18 hours. After 18 hours, the reaction was allowed to cool to room temperature. Once the flask reached room temperature, it was opened slowly, taking care that expulsion of the generated HX gas remained in the fume hood. Once the flask was fully opened, a sample of the reaction mixture may be taken for analysis. Five volumes of 1M HCl was then added slowly to the reaction flask, the flask was resealed, and the reaction was heated to 80 °C with stirring for 2 hours. After 2 hours, the reaction was cooled to room temperature again. After cooling, 10 volumes of ethyl acetate (or isopropyl acetate) was added to the reaction mixture, followed by 10 volumes of DI water. The aqueous layer was washed



2 more times with ethyl acetate (or isopropyl acetate), the organic layers were collected, and the solvent was removed by rotary evaporation. The material could then be distilled using short-path distillation.



2,4-dichloro-5-fluoroacetophenone **39**:

Reaction performed starting from 2,4-dichlorofluorobenzene **38** (10g, 60 mmol) using acetyl chloride (4.3 mL, 60 mmol) as the acylating reagent. ~75% conversion from starting material (GCMS)

$^1\text{H}$  NMR (600 MHz, Chloroform- $d$ )  $\delta$  7.50 (d,  $J$  = 6.37 Hz, 1H), 7.41 (d,  $J$  = 8.79, 1H), 2.65 (s, 1H).

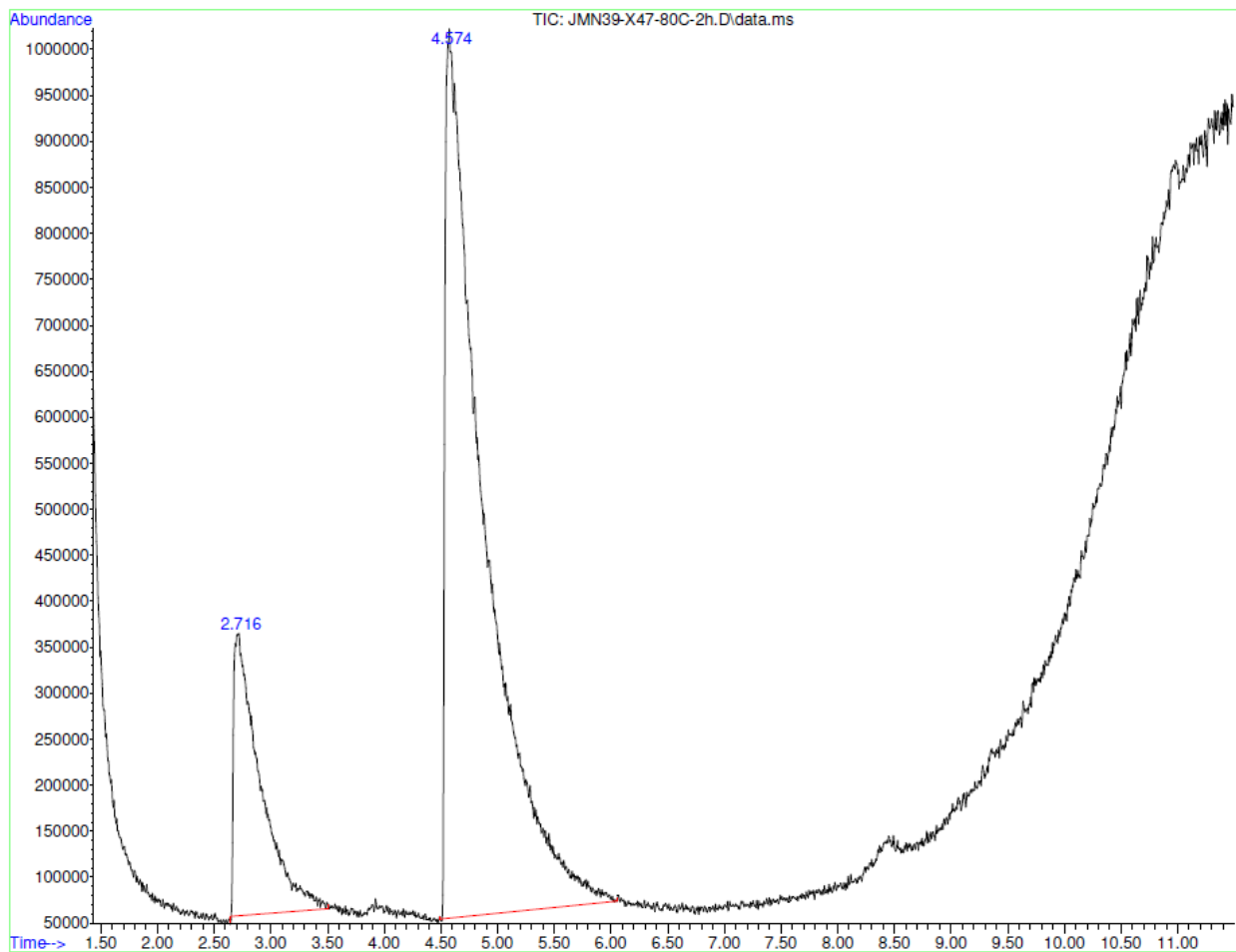
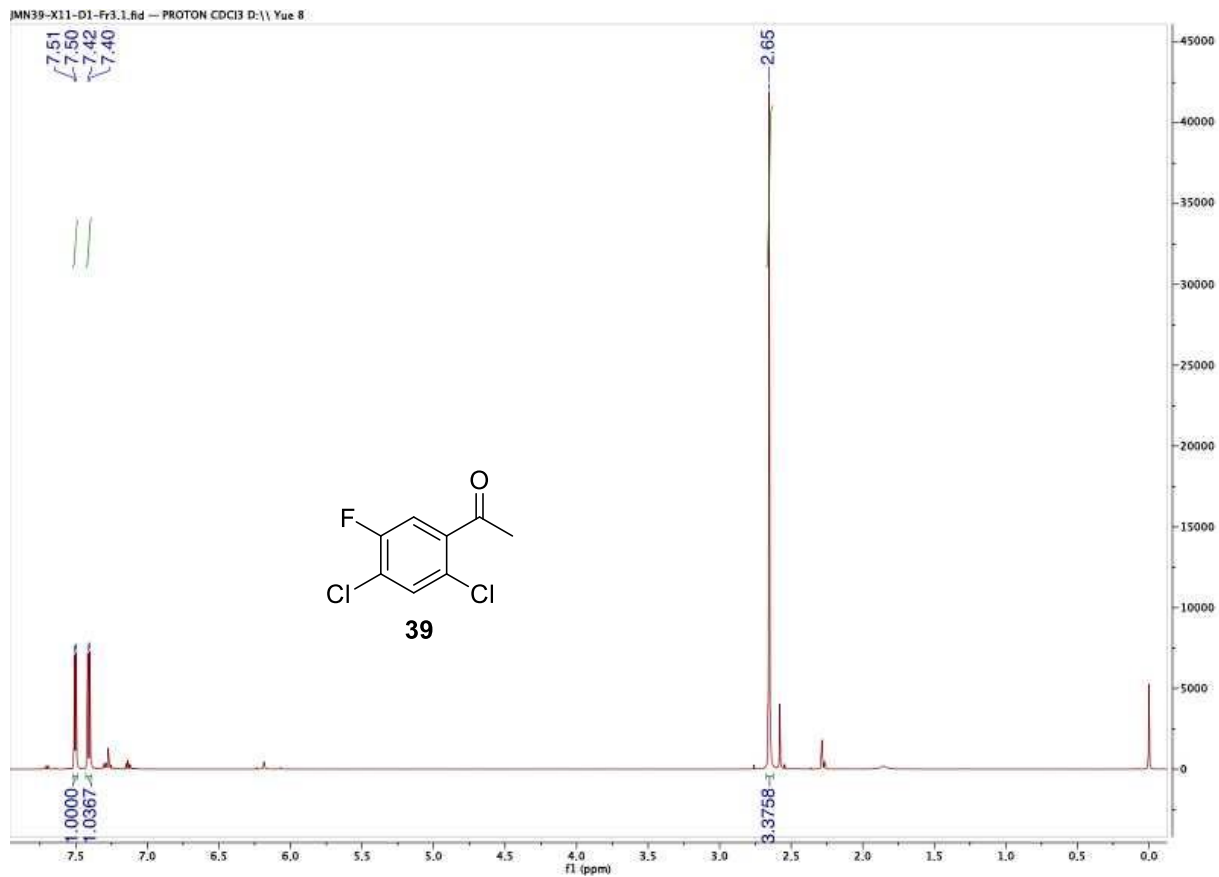
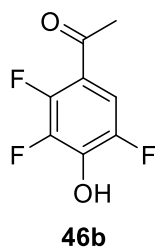


**Figure 38.** GCMS of Crude Reaction Mixture in the Synthesis of 2,4-dichloro-5-fluoroacetophenone **39**.



**NMR Spectra 18.** <sup>1</sup>H NMR of 2,4-dichloro-5-fluoroacetophenone **39**.



1-(2,3,5-trifluoro-4-hydroxyphenyl)ethan-1-one **46b**:

Reaction performed using 2,3,5-trifluorophenol **44** (10g, 67 mmol) and using acetyl bromide (5 mL, 67 mmol) as the acylating reagent.

$^1\text{H}$  NMR (600 MHz, Chloroform- $d$ )  $\delta$  7.50 (ddd,  $J = 2.28, 2.48, 3.72$  Hz, 1H), 2.64 (d,  $J = 5.28$  Hz, 3H)

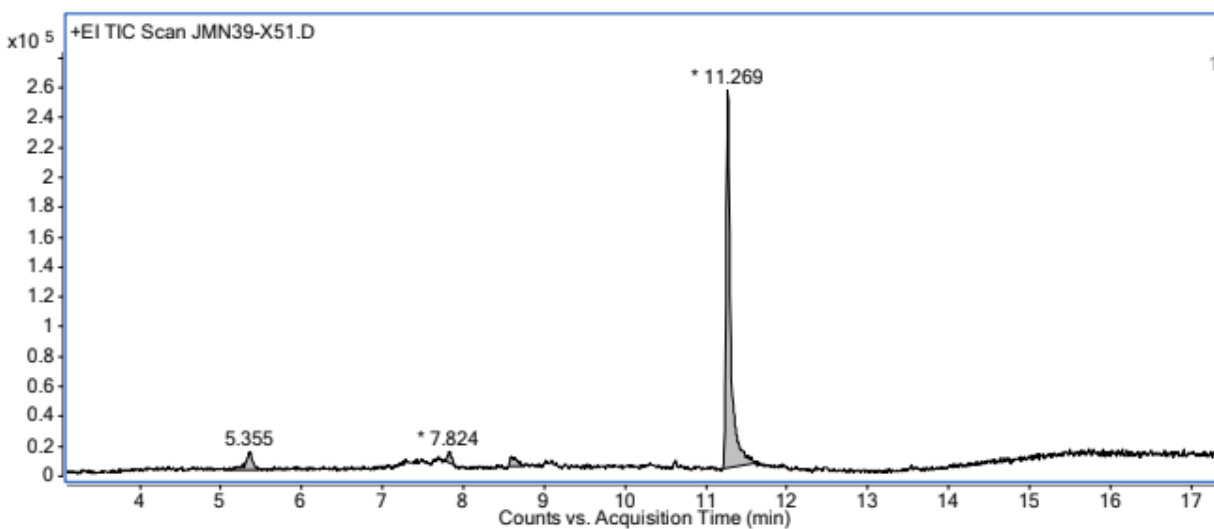
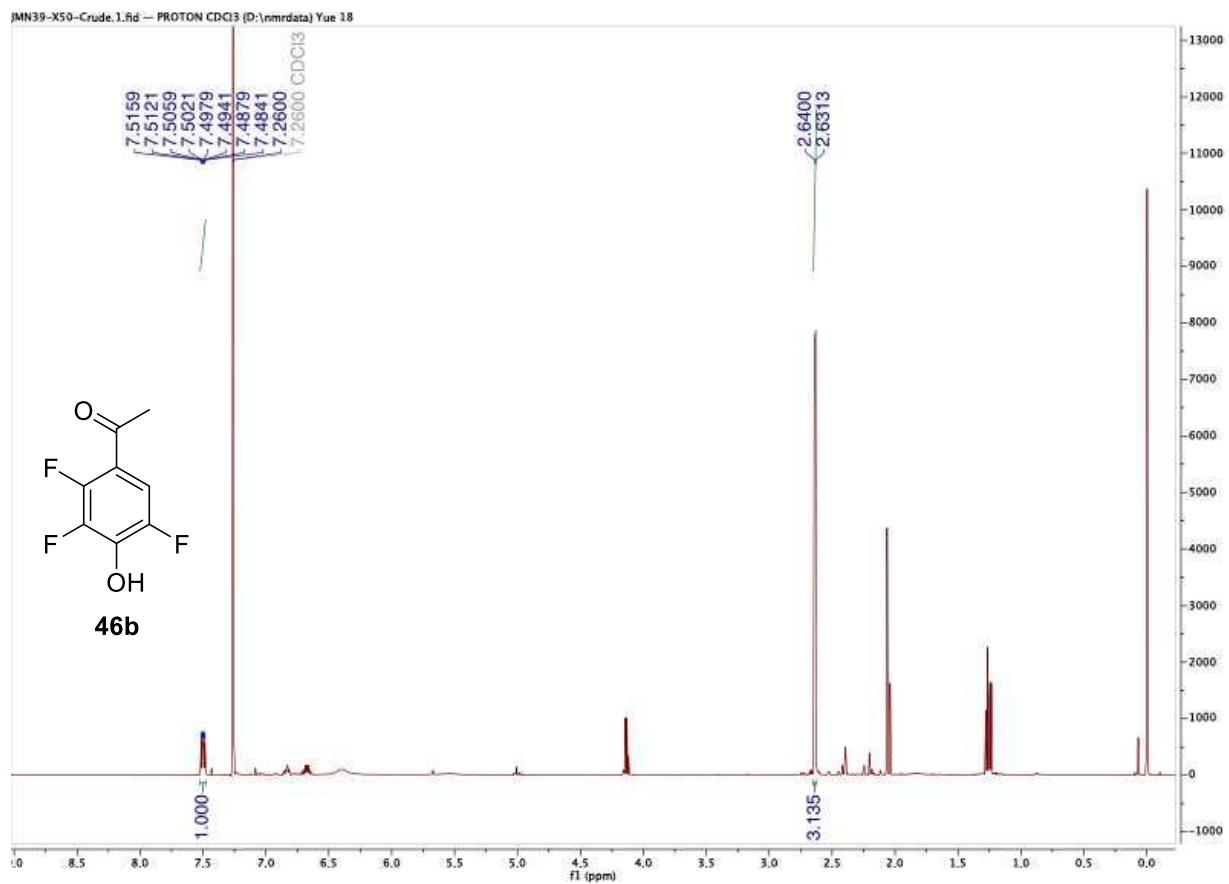
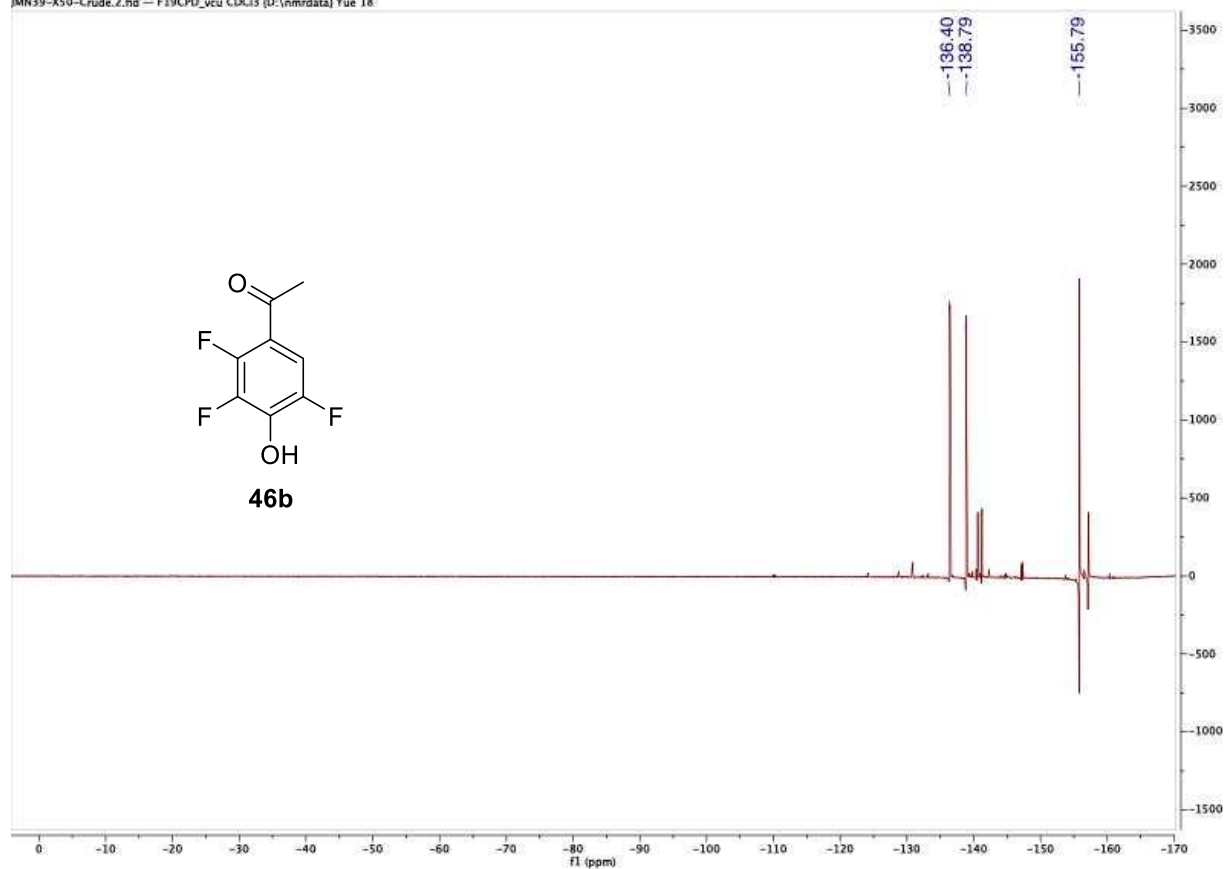


**Figure 39.** GCMS of Crude Reaction Mixture in the Attempted Synthesis of 1-(2,3,5-trifluoro-4-hydroxyphenyl)ethan-1-one **46b**.

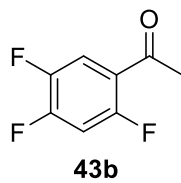


**NMR Spectra 19.**  $^1\text{H}$  NMR of 1-(2,3,5-trifluoro-4-hydroxyphenyl)ethan-1-one **46b**.

JMN39-X50-Crude.2.fid -- F19CPD\_vcu CDG3 (D:\nmrdata) Yue 18



**NMR Spectra 20.**  $^{19}\text{F}$  NMR of 1-(2,3,5-trifluoro-4-hydroxyphenyl)ethan-1-one **46b**.



1,3,4-trifluoroacetophenone **43b**:

Material was believed to be made in extremely low conversion (~2%) from starting material **43b** (2.0 g, 15 mmol) as determined by GCMS (174 m/z).

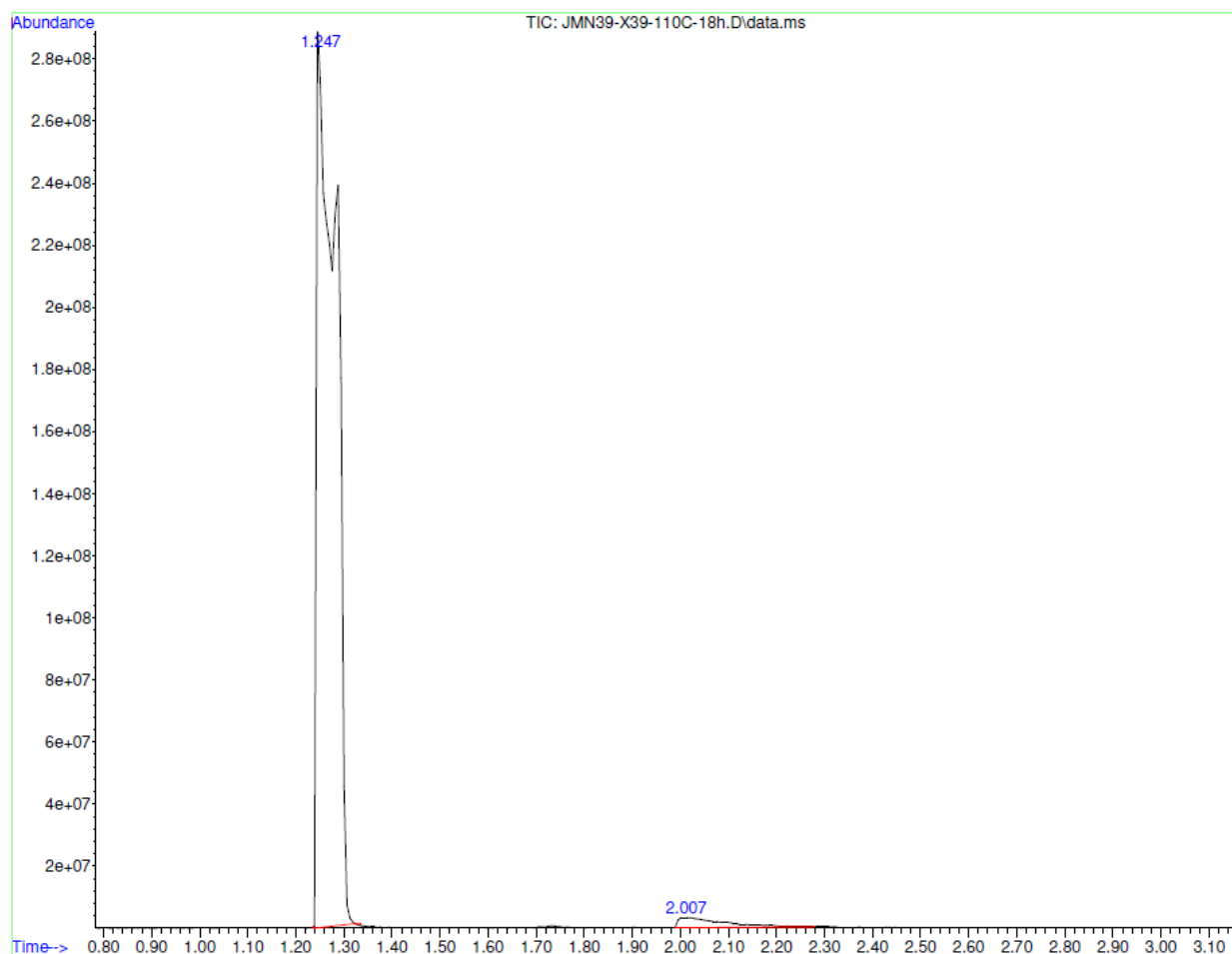
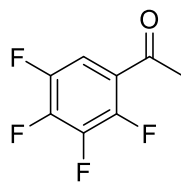


**Figure 40.** GCMS of Crude reaction mixture in the Attempted Synthesis of 1,3,4-Trifluoroacetophenone **43b**.



**45b**

1,2,3,4-tetrafluoroacetophenone **45b**:

Material was believed to be made (~5%) as determined by GCMS (192 m/z) from starting material **45b** (2.0 g, 13 mmol).

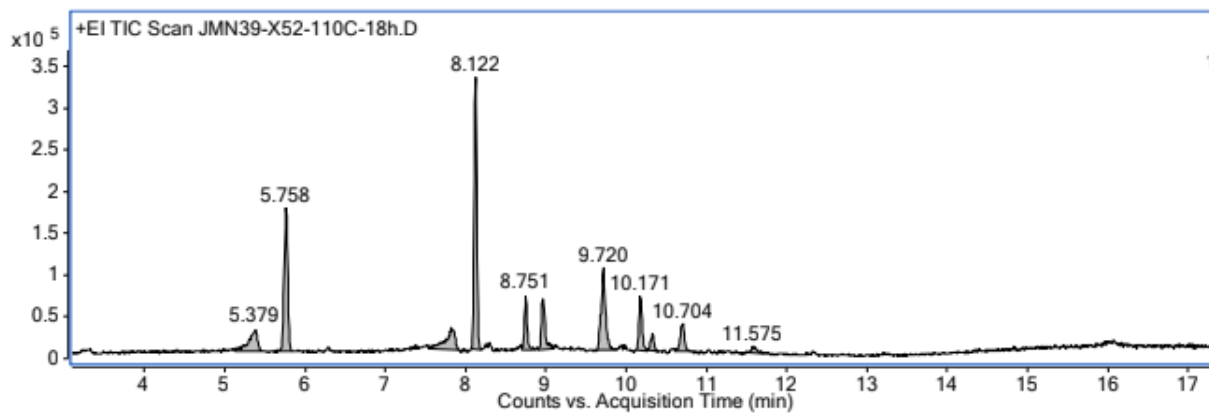
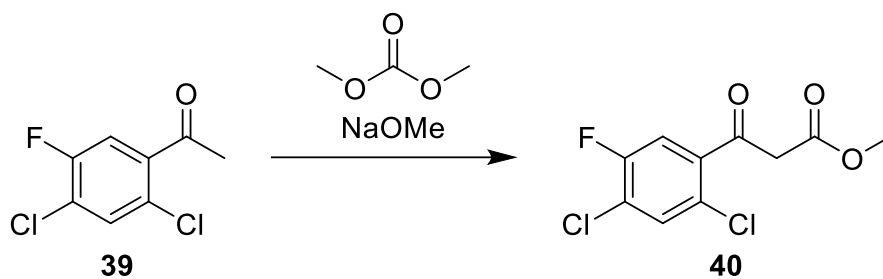


**Figure 41.** GCMS of Crude reaction mixture in the Attempted Synthesis of 1,2,3,4-Tetrafluoroacetophenone **45b**



2,4-dichloro-5-fluorobenzene-β-ketoester **40**.<sup>106</sup>

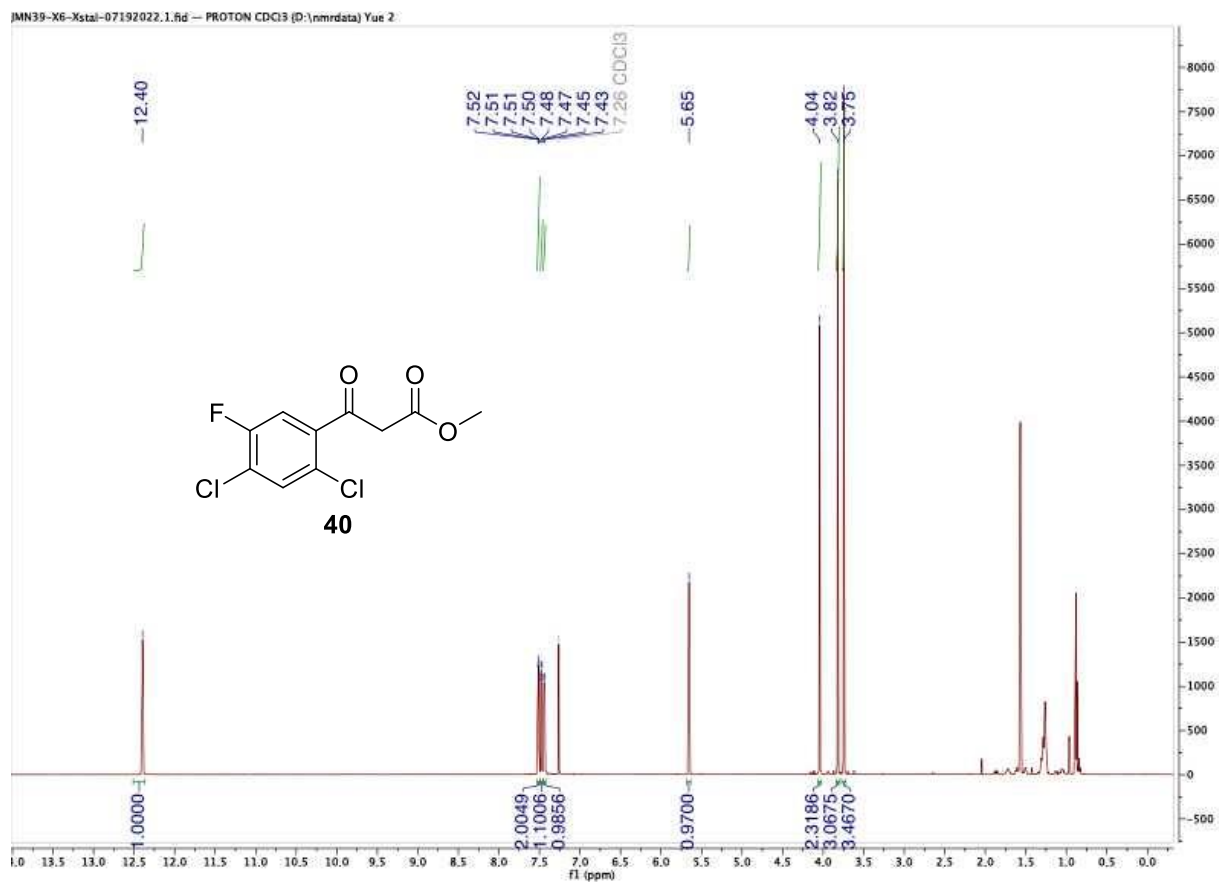
To a 50 mL round bottom flask containing toluene (10 mL) was added sodium methoxide (0.73g, 14 mmol), and dimethyl carbonate (0.81 mL, 9.7 mmol). The mixture was stirred and heated to 100 °C and allowed to stir for 5 min. Meanwhile, dichloro-fluoro-acetophenone **39** (DCFA) (1.0g, 4.8 mmol) was dissolved in toluene (10 mL). The DCFA and toluene solution was then added dropwise to the stirring mixture. After addition was complete, the reaction was stirred for 2 hours. After 2 hours, the reaction was cooled to room temperature and acetic acid (0.83 mL, 14 mmol) was added dropwise as a solid precipitated out of the solution. Ice water (~20 mL) was added to dissolve the solid. The mixture was then transferred to a separatory funnel. The toluene layer was collected and the aqueous layer was extracted with ethyl acetate (3 X 20 mL). The combined organic layers were washed with brine, dried using anhydrous sodium sulfate, and filtered. The solvents were then removed using a rotary evaporator. The residual crude oil was then purified using column chromatography. Upon collection from the column, spontaneous precipitation of crystals was observed. (90 mg, 7% yield, 95% purity)

<sup>1</sup>H NMR (600 MHz, Chloroform-d) δ 12.40 (s, 1H), 7.51 (dd, J = 6.34, 6.52 Hz, 2H), 7.47 (d, J = 8.65 Hz, 1H), 7.44 (d, J = 9.36 Hz, 1H), 5.65 (s, 1H), 4.04 (s, 2H), 3.82 (s, 3H) 3.75 (s, 3H)

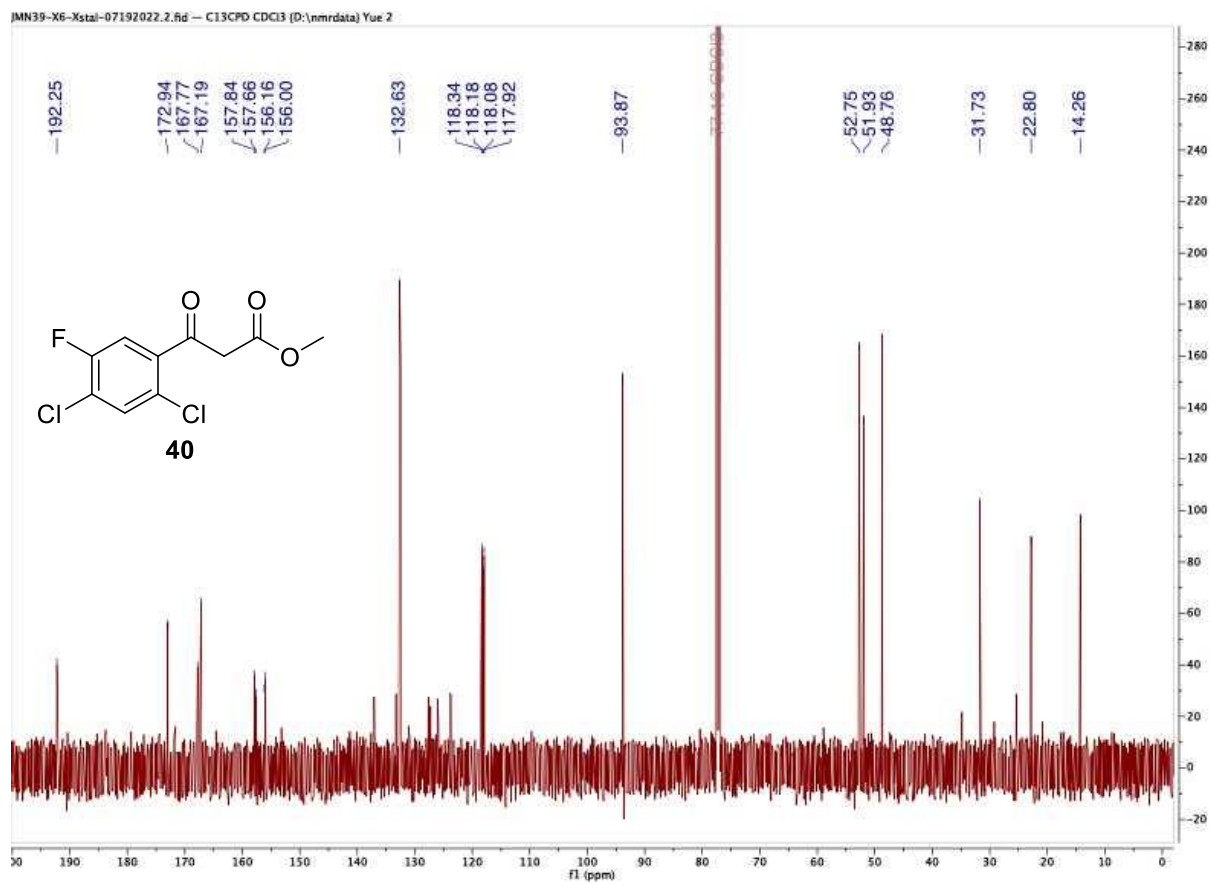
<sup>13</sup>C NMR (151 MHz, Chloroform-d) δ 192.25, 172.94, 167.77, 167.19, 157.84, 157.66, 156.16, 156.00, 132.63, 118.34, 118.18, 118.08, 117.92, 93.87, 52.75, 51.93, 48.76, 31.73, 22.80, 14.26.

<sup>1</sup>F NMR (565 MHz, Chloroform-d) δ -115.49, -116.53



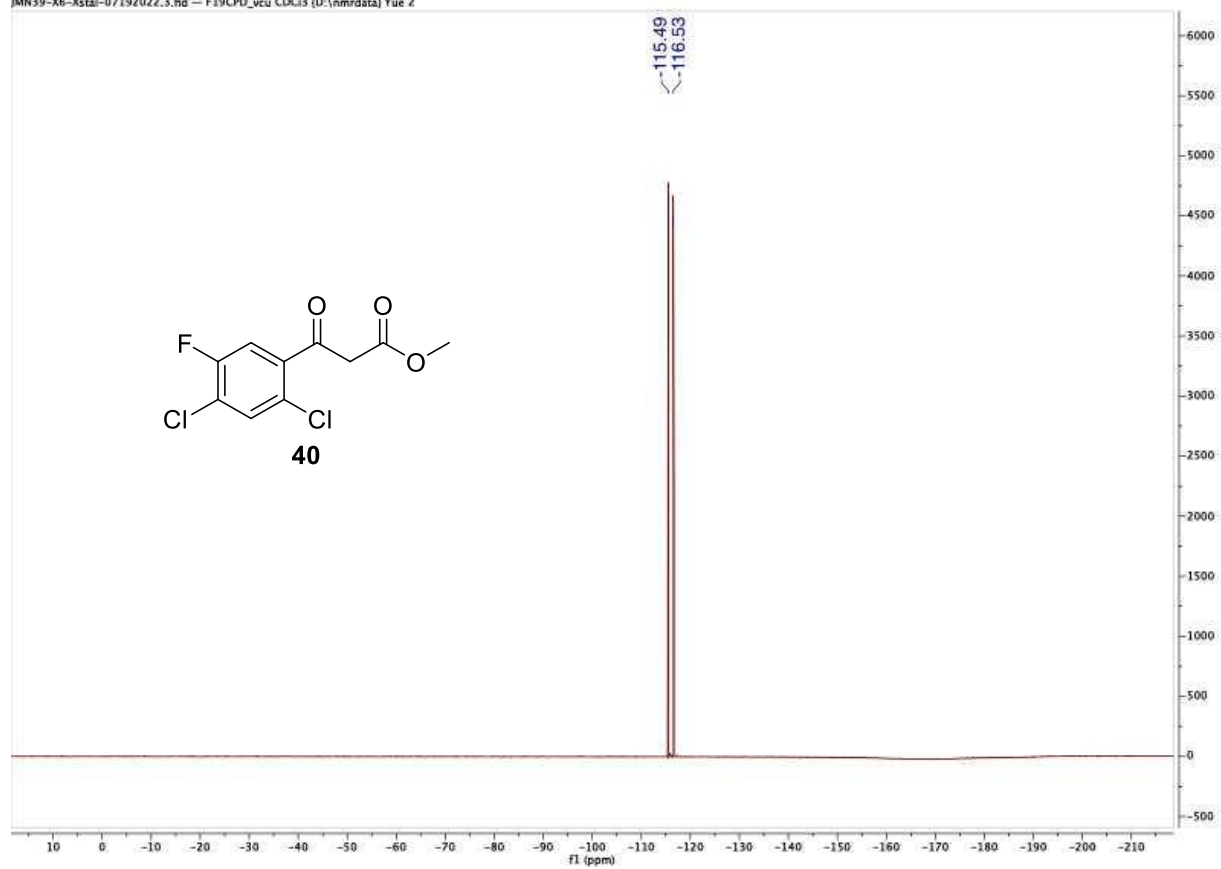


**NMR Spectra 21.**  $^1\text{H}$  NMR of 2,4-dichloro-5-fluorobenzene- $\beta$ -ketoester **40**.

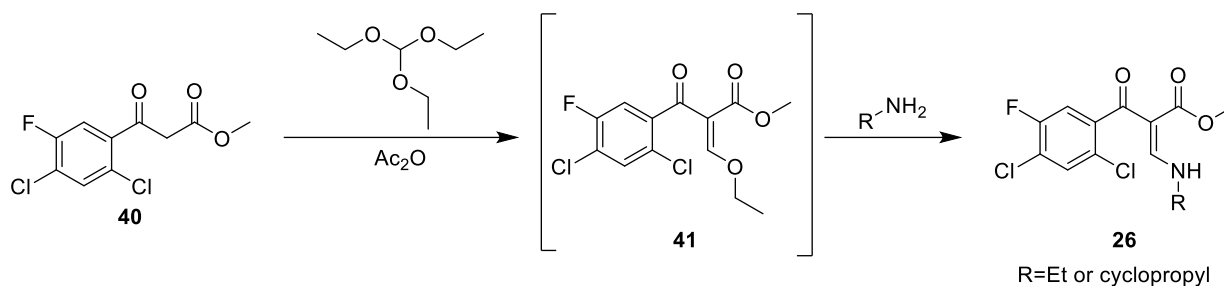


**NMR Spectra 22.**  $^{13}\text{C}$  NMR of 2,4-dichloro-5-fluorobenzene- $\beta$ -ketoester **40**.

JMN39-X6-Xsta1-07192022.3.fid -- F19CPD\_vcu CDCl3 (D:\nmrdata) Yue 2



**NMR Spectra 23.**  $^{19}\text{F}$  NMR of 2,4-dichloro-5-fluorobenzene- $\beta$ -ketoester **40**.

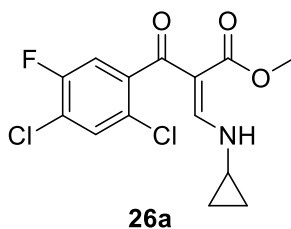


General Procedure for 2,4-Dichloro-5-fluorobenzene Vinyllogous Carbamate **26**:<sup>107</sup>

$\beta$ -ketoester **40** (1.0 equiv.) was added to a flask with triethyl orthoformate (1.5 equiv.). Acetic anhydride (2.5 equiv.) was then added. The reaction mixture was heated to 90 °C for 3 hours. After 3 hours, the reaction was cooled and the excess triethyl orthoformate and acetic anhydride were removed by rotary evaporation. The crude material **41** was then moved directly to the next step.

To the flask containing crude **41** was added methanol (2.5 volumes). In a separate flask, alkyl amine (ethylamine or cyclopropylamine) (1.0 equiv) was combined with methanol (2.5 volumes). The amine solution was added to the reaction flask and the mixture was stirred at room temperature for one hour. After one hour, the methanol was removed by rotary evaporation.

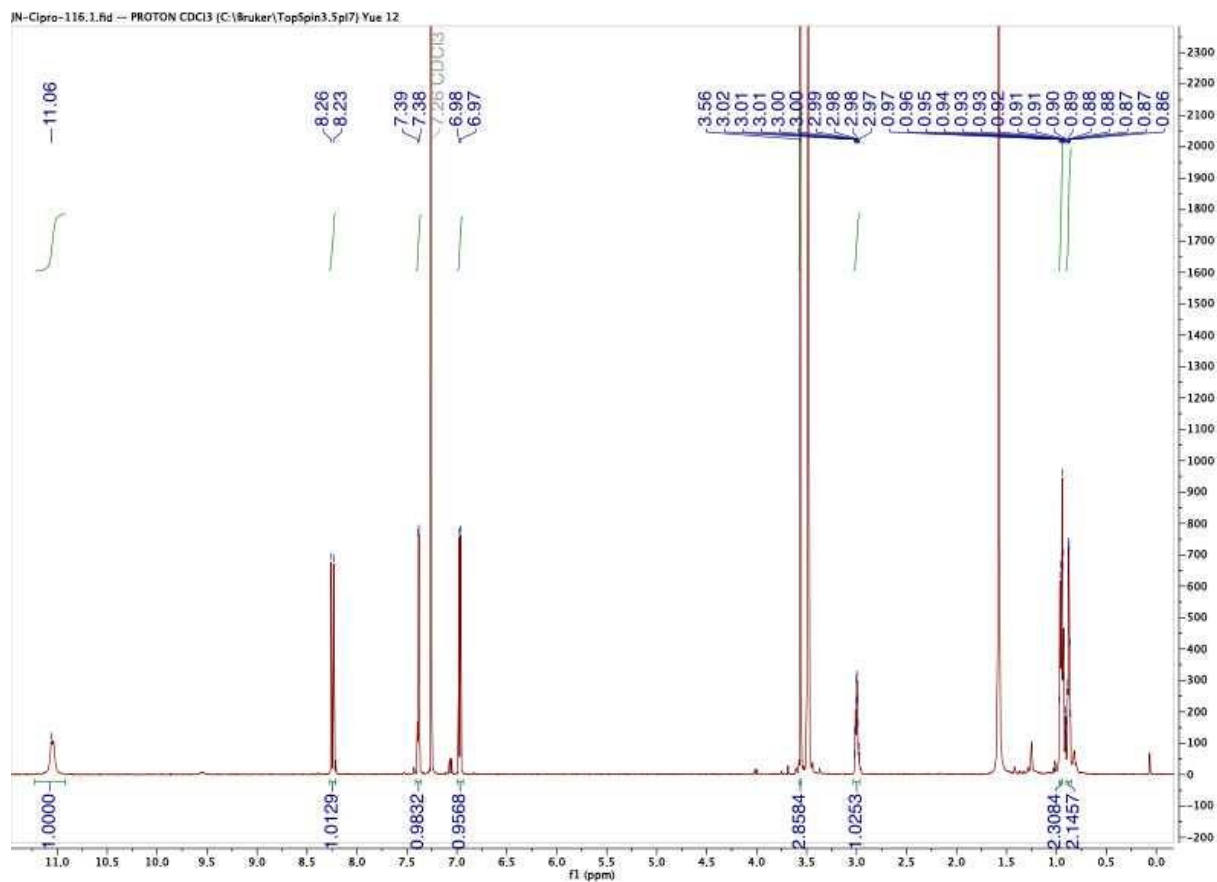
\*Note: In the case of using ethylamine, the product precipitated out of reaction and was collected by filtration instead.



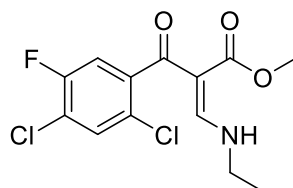
Cyclopropyl vinyllogous amide **26a**:

**26a** was made in crude yield of 16% over 2 steps from **40**.

$^1\text{H}$  NMR (600 MHz, Chloroform- $d$ )  $\delta$  11.06 (br, 1H), 8.25 (d,  $J = 13.8$  Hz, 1H), 7.39 (d,  $J = 6.46$  Hz, 1H), 6.97 (d,  $J = 8.61$  Hz, 1H), 3.56 (s, 3H), 3.00 (m, 1H), 0.97-0.93 (m, 2H), 0.90-0.86 (m, 2H).



**NMR Spectra 24.**  $^1\text{H}$  NMR of Cyclopropyl Vinylous Amide **26a**.

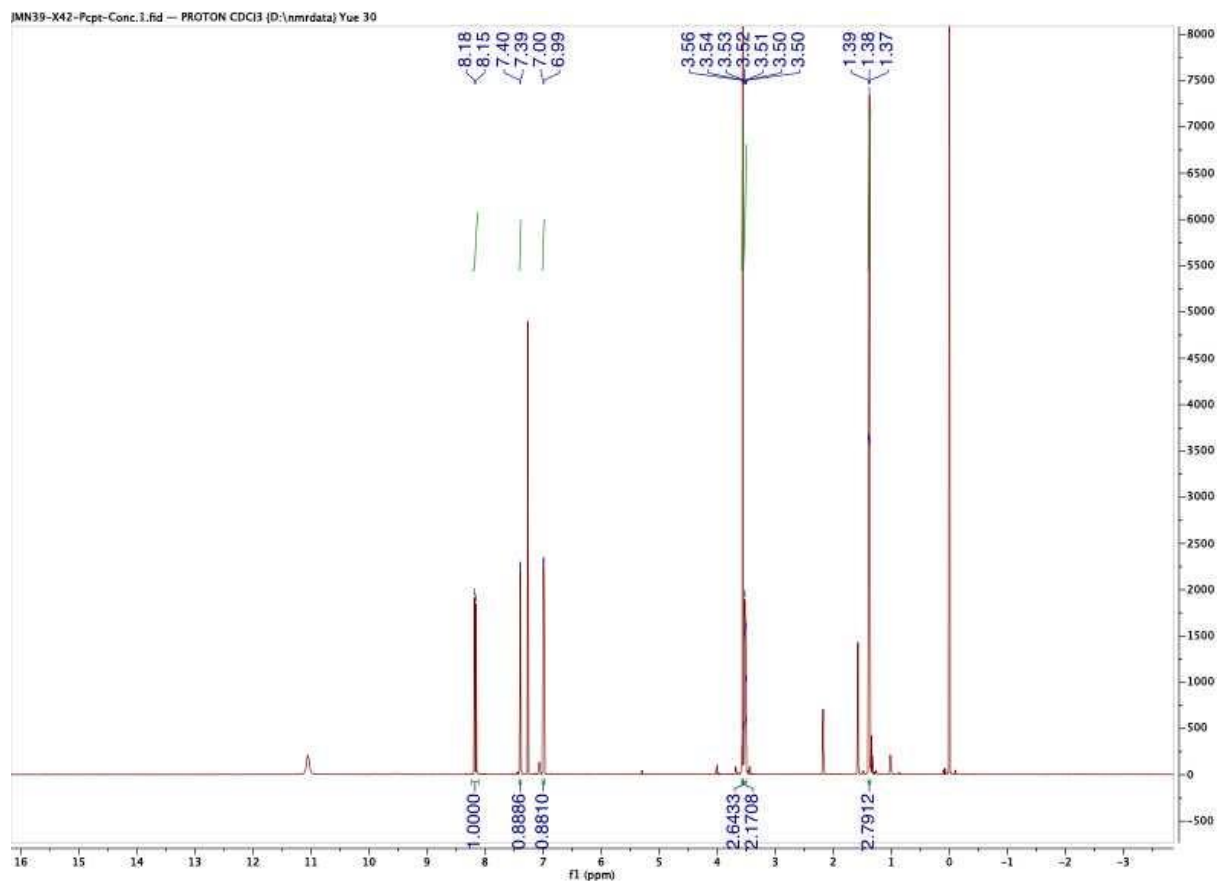


**26b**

Ethyl vinylogous amide **26b**:

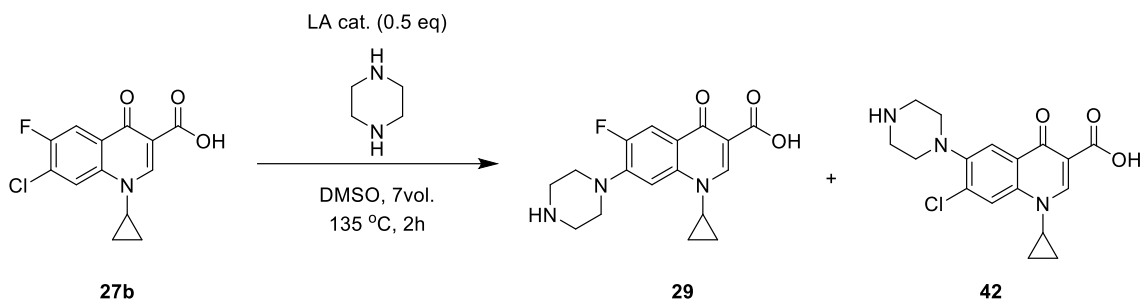
**26b** was made in crude yield of 15% (320 mg, 95% purity) over 2 steps from **40**.

$^1\text{H}$  NMR (600 MHz, Chloroform- $d$ )  $\delta$  11.05 (br, 1H), 8.15 (d,  $J = 14.7$  Hz, 1H), 7.39 (d,  $J = 6.4$  Hz, 1H), 6.99 (d,  $J = 8.53$  Hz, 1H), 3.56 (s, 3H), 3.52 (m, 2H), 1.38 (t,  $J = 7.3$  Hz, 3H).



**NMR Spectra 25.**  $^1\text{H}$  NMR of Ethyl Vinylogous Amide **26b**.

### 2.7.2.3. General Procedure for the S<sub>N</sub>Ar Reaction towards Ciprofloxacin (**29**):



All reactions were performed in glass reinforced sealed pressure tubes.

To a solution of 7-chloro-1-cyclopropyl-6-fluoro-4-oxo-1,4-dihydroquinoline-3-carboxylic acid (**27b**) (5.0 g, 0.018 mol) in DMSO (25 mL) was added piperazine (7.5 g, 0.09 mol). The contents were shaken at room temperature to mix, then Lewis acid catalyst (0.5 equiv.) was added. The reactor vessel was then sealed and placed in an oil bath to stir at 135 °C for 2 h. After stirring for 2 h, the reaction was allowed to cool to room temperature.

An equal volume of 1M aq. NaOH compared to the volume of solvent was added. The reaction mixture was filtered through a plug of celite and charcoal (10 g/10 g), washed twice with 2 plug volumes of water, and the filtrate was neutralized to a pH of 7 with 2M aqueous HCl. The product was collected by vacuum filtration and dried in a vacuum oven. **29** and **42** were identified by HPLC using a method developed from standards of the material.

## References

- (1) Dach, R.; Song, J. J.; Roschangar, F.; Samstag, W.; Senanayake, C. H. The Eight Criteria Defining a Good Chemical Manufacturing Process. *Org Process Res Dev* **2012**, *16* (11), 1697–1706. [https://doi.org/10.1021/OP300144G/ASSET/IMAGES/LARGE/OP-2012-00144G\\_0011.JPEG](https://doi.org/10.1021/OP300144G/ASSET/IMAGES/LARGE/OP-2012-00144G_0011.JPEG).
- (2) Food and Drug Administration. Food and Drug Administration Electronic Code of Federal Regulation (21CFR207.1)s. January 2023.
- (3) Wender, P. A.; Verma, V. A.; Paxton, T. J.; Pillow, T. H. Function-Oriented Synthesis, Step Economy, and Drug Design. *Acc Chem Res* **2008**, *41* (1), 40–49. [https://doi.org/10.1021/AR700155P/ASSET/IMAGES/LARGE/AR-2007-00155P\\_0016.JPEG](https://doi.org/10.1021/AR700155P/ASSET/IMAGES/LARGE/AR-2007-00155P_0016.JPEG).
- (4) Trost, B. M. On Inventing Reactions for Atom Economy. *Acc Chem Res* **2002**, *35* (9), 695–705. <https://doi.org/10.1021/AR010068Z/ASSET/IMAGES/LARGE/AR010068ZF34.JPEG>.
- (5) Anastas, P. T.; Warner, J. C. *Green Chemistry: Theory and Practice*; Oxford University Press: New York, 1998.
- (6) Katlama, C.; Murphy, R. Dolutegravir for the Treatment of HIV. *Expert Opin Investig Drugs* **2012**, *21* (4), 523–530. <https://doi.org/10.1517/13543784.2012.661713>.
- (7) Pommier, Y.; Johnson, A. A.; Marchand, C. Integrase Inhibitors to Treat HIV/Aids. *Nature Reviews Drug Discovery* **2005**, *4* (3), 236–248. <https://doi.org/10.1038/nrd1660>.
- (8) Aboud, M.; Orkin, C.; Podzamczar, D.; Bogner, J. R.; Baker, D.; Khuong-Josses, M. A.; Parks, D.; Angelis, K.; Kahl, L. P.; Blair, E. A.; Adkison, K.; Underwood, M.; Matthews, J. E.; Wynne, B.; Vandermeulen, K.; Gartland, M.; Smith, K. Efficacy and Safety of Dolutegravir–Rilpivirine for Maintenance of Virological Suppression in Adults with HIV-1: 100-Week Data from the Randomised, Open-Label, Phase 3 SWORD-1 and SWORD-2 Studies. *Lancet HIV* **2019**, *6* (9), e576–e587. [https://doi.org/10.1016/S2352-3018\(19\)30149-3](https://doi.org/10.1016/S2352-3018(19)30149-3).
- (9) Schreiner, E.; Richter, F.; Nerdinger, S. Development of Synthetic Routes to Dolutegravir. *Synthesis of Heterocycles in Contemporary Medicinal Chemistry* **2016**, 187–208. [https://doi.org/10.1007/7081\\_2016\\_200](https://doi.org/10.1007/7081_2016_200).
- (10) Ziegler, R. E.; Desai, B. K.; Jee, J. A.; Gupton, B. F.; Roper, T. D.; Jamison, T. F. 7-Step Flow Synthesis of the HIV Integrase Inhibitor Dolutegravir. *Angewandte Chemie International Edition* **2018**, *57* (24), 7181–7185. <https://doi.org/10.1002/ANIE.201802256>.
- (11) Hofmann, A. W. Ueber Die Einwirkung Des Broms in Alkalischer Lösung Auf Amide. *Berichte der deutschen chemischen Gesellschaft* **1881**, *14* (2), 2725–2736. <https://doi.org/10.1002/CBER.188101402242>.
- (12) Schotten, C. Ueber Die Oxydation Des Piperidins. *Berichte der deutschen chemischen Gesellschaft* **1884**, *17* (2), 2544–2547. <https://doi.org/10.1002/CBER.188401702178>.
- (13) Casiraghi, G.; Zanardi, F.; Rassa, G.; Spanu, P. Stereoselective Approaches to Bioactive Carbohydrates and Alkaloids-With a Focus on Recent Syntheses Drawing from the Chiral Pool. *Chem Rev* **1995**, *95* (6), 1677–1716. [https://doi.org/10.1021/CR00038A001/ASSET/CR00038A001.FP.PNG\\_V03](https://doi.org/10.1021/CR00038A001/ASSET/CR00038A001.FP.PNG_V03).



- (14) Brill, Z. G.; Condakes, M. L.; Ting, C. P.; Maimone, T. J. Navigating the Chiral Pool in the Total Synthesis of Complex Terpene Natural Products. *Chem Rev* **2017**, *117* (18), 11753–11795. [https://doi.org/10.1021/ACS.CHEMREV.6B00834/ASSET/IMAGES/LARGE/CR-2016-00834Z\\_0038.JPEG](https://doi.org/10.1021/ACS.CHEMREV.6B00834/ASSET/IMAGES/LARGE/CR-2016-00834Z_0038.JPEG).
- (15) Sivagurunathan, K.; Raja Mohamed Kamil, S.; Syed Shafi, S.; Liakth Ali Khan, F.; Ragavan, R. V. Efficient One-Pot Selective Reduction of Esters in  $\beta$ -Ketoesters Using LiHMDS and Lithium Aluminium Hydride. *Tetrahedron Lett* **2011**, *52* (11), 1205–1207. <https://doi.org/10.1016/J.TETLET.2011.01.030>.
- (16) Stover, C. K.; Warren, P.; VanDevanter, D. R.; Sherman, D. R.; Arain, T. M.; Langhorne, M. H.; Anderson, S. W.; Towell, J. A.; Yuan, Y.; McMurray, D. N.; Kreiswirth, B. N.; Barry, C. E.; Baker, W. R. A Small-Molecule Nitroimidazopyran Drug Candidate for the Treatment of Tuberculosis. *Nature* **2000**, *405* (6789), 962–966. <https://doi.org/10.1038/35016103>.
- (17) Conradie, F.; Diacon, A. H.; Ngubane, N.; Howell, P.; Everitt, D.; Crook, A. M.; Mendel, C. M.; Egizi, E.; Moreira, J.; Timm, J.; McHugh, T. D.; Wills, G. H.; Bateson, A.; Hunt, R.; Van Niekerk, C.; Li, M.; Olugbosi, M.; Spigelman, M. Treatment of Highly Drug-Resistant Pulmonary Tuberculosis. *New England Journal of Medicine* **2020**, *382* (10), 893–902. [https://doi.org/10.1056/NEJMOA1901814/SUPPL\\_FILE/NEJMOA1901814\\_DATA-SHARING.PDF](https://doi.org/10.1056/NEJMOA1901814/SUPPL_FILE/NEJMOA1901814_DATA-SHARING.PDF).
- (18) Keam, S. J. Pretomanid: First Approval. *Drugs* **2019**, *79* (16), 1797–1803. <https://doi.org/10.1007/S40265-019-01207-9/TABLES/3>.
- (19) Thompson, A. M.; Blaser, A.; Anderson, R. F.; Shinde, S. S.; Franzblau, S. G.; Ma, Z.; Denny, W. A.; Palmer, B. D. Synthesis, Reduction Potentials, and Antitubercular Activity of Ring A/B Analogues of the Bioreductive Drug (6S)-2-Nitro-6-[[4-(Trifluoromethoxy)Benzyl]Oxy]-6,7-Dihydro-5H-Imidazo[2,1-b][1,3]Oxazine (PA-824). *J Med Chem* **2009**, *52* (3), 637–645. [https://doi.org/10.1021/JM801087E/SUPPL\\_FILE/JM801087E\\_SI\\_001.PDF](https://doi.org/10.1021/JM801087E/SUPPL_FILE/JM801087E_SI_001.PDF).
- (20) Orita, A.; Miwa, K.; Uehara, G.; Otera, J. Integration of Solventless Reaction in a Multi-Step Process: Application to an Efficient Synthesis of PA-824. *Adv Synth Catal* **2007**, *349* (13), 2136–2144. <https://doi.org/10.1002/ADSC.200700119>.
- (21) Marsini, M. A.; Reider, P. J.; Sorensen, E. J. A Concise and Convergent Synthesis of PA-824. *Journal of Organic Chemistry* **2010**, *75* (21), 7479–7482. [https://doi.org/10.1021/JO1015807/SUPPL\\_FILE/JO1015807\\_SI\\_001.PDF](https://doi.org/10.1021/JO1015807/SUPPL_FILE/JO1015807_SI_001.PDF).
- (22) Thompson, A. M.; Sutherland, H. S.; Palmer, B. D.; Kmentova, I.; Blaser, A.; Franzblau, S. G.; Wan, B.; Wang, Y.; Ma, Z.; Denny, W. A. Synthesis and Structure-Activity Relationships of Varied Ether Linker Analogues of the Antitubercular Drug (6 S)-2-Nitro-6-[[4-(Trifluoromethoxy) Benzyl]Oxy]-6,7-Dihydro-5 H -Imidazo[2,1- b ][1,3]Oxazine (PA-824). *J Med Chem* **2011**, *54* (19), 6563–6585. [https://doi.org/10.1021/JM200377R/SUPPL\\_FILE/JM200377R\\_SI\\_001.PDF](https://doi.org/10.1021/JM200377R/SUPPL_FILE/JM200377R_SI_001.PDF).
- (23) CN104829584A - Synthesis Method of (R)-Glyceraldehyde Acetonide Compound, May 19, 2015.
- (24) CN101723920A - Process for Synthesizing (R)-Glycidyl Butyrate, November 2, 2010.
- (25) Yaegashi, K.; Furukawa, Y. US6946566B2 - Process for Preparation of Optically Active Halogeno Hydroxypropyl Compound and Glycidyl Compound - Google Patents, 2003.

- <https://patents.google.com/patent/US6946566B2/en?q=US6946566> (accessed 2023-03-28).
- (26) Chenyu, C.; Changming, C.; Chaoming, H.; Yi, L.; Yang, L.; Ling, W.; Ying, Z.; Lin, Z. WO2012037861, 2012.
- (27) June, R. K.; Rapean, J. C. US3075999, 1963.
- (28) Gouman, J.; Rens-van der Lee, S.; van't Sand, R. US8802872B2, June 2, 2014.
- (29) Leuschner, J.; Schäfer, H.; Leuschner, F. 3-(Acyloxy)Propanolamines: Agents with  $\beta$ -Adrenergic Blocking Activity. *Eur J Med Chem* **1994**, 29 (3), 241–243.  
[https://doi.org/10.1016/0223-5234\(94\)90042-6](https://doi.org/10.1016/0223-5234(94)90042-6).
- (30) Sung, J. U.; Seong, S. Y.; Kim, Y. S.; Park, J. H. US20200299247A1, 2020.
- (31) Kloos, N.; Drost, J. J. J. Epoxy Esters of Alpha, Alpha-Dialkyl Monocarboxylic Acids, 1965.
- (32) Ciblat, S.; Kim, J.; Stewart, C. A.; Wang, J.; Forgione, P.; Clyne, D.; Paquette, L. A. A Modular Approach to Marine Macrolide Construction. 4. Assembly of C36 - C51 and C29 - C44 Building Blocks and Evaluation of Key Coupling Reactions Targeting Spongistatin 1 (Altohyrtin A). *Org Lett* **2007**, 9 (4), 719–722.  
[https://doi.org/10.1021/OL063083I/SUPPL\\_FILE/OL063083ISI20070110\\_030235.PDF](https://doi.org/10.1021/OL063083I/SUPPL_FILE/OL063083ISI20070110_030235.PDF).
- (33) Xu, F.; Murry, J. A.; Simmons, B.; Corley, E.; Fitch, K.; Karady, S.; Tschäen, D. Stereocontrolled Synthesis of Trisubstituted Cyclopropanes: Expedient, Atom-Economical, Asymmetric Syntheses of (+)-Bicifadine and DOV21947. *Org Lett* **2006**, 8 (17), 3885–3888.  
[https://doi.org/10.1021/OL061650W/SUPPL\\_FILE/OL061650WSI20060707\\_052859.PDF](https://doi.org/10.1021/OL061650W/SUPPL_FILE/OL061650WSI20060707_052859.PDF).
- (34) Brachman, A. E.; Fang, J. C. Preparation of 2-Isobutyl-2-Methyl-4-Trimethylacetoxymethyl-1,3-Dioxolane and Its Reaction with Phosphoric Acid. *Journal of Organic Chemistry* **1959**, 24 (9), 1369–1371.  
[https://doi.org/10.1021/JO01091A625/ASSET/JO01091A625.FP.PNG\\_V03](https://doi.org/10.1021/JO01091A625/ASSET/JO01091A625.FP.PNG_V03).
- (35) Plutschack, M. B.; Pieber, B.; Gilmore, K.; Seeberger, P. H. The Hitchhiker's Guide to Flow Chemistry. *Chem Rev* **2017**, 117 (18), 11796–11893.  
[https://doi.org/10.1021/ACS.CHEMREV.7B00183/ASSET/IMAGES/MEDIUM/CR-2017-00183Y\\_0046.GIF](https://doi.org/10.1021/ACS.CHEMREV.7B00183/ASSET/IMAGES/MEDIUM/CR-2017-00183Y_0046.GIF).
- (36) Kirschning, A. Chemistry in Flow Systems. *Beilstein Journal of Organic Chemistry* **2009**, 5 (1), 15. <https://doi.org/10.3762/BJOC.5.15>.
- (37) Cherkasov, N.; Adams, S. J.; Bainbridge, E. G. A.; Thornton, J. A. M. Continuous Stirred Tank Reactors in Fine Chemical Synthesis for Efficient Mixing, Solids-Handling, and Rapid Scale-Up. *React Chem Eng* **2023**, 8 (2), 266–277.  
<https://doi.org/10.1039/D2RE00232A>.
- (38) Hurtado, F. J.; Kaiser, A. S.; Zamora, B. Fluid Dynamic Analysis of a Continuous Stirred Tank Reactor for Technical Optimization of Wastewater Digestion. *Water Res* **2015**, 71, 282–293. <https://doi.org/10.1016/J.WATRES.2014.11.053>.
- (39) Nandiwale, K. Y.; Hart, T.; Zahrt, A. F.; Nambiar, A. M. K.; Mahesh, P. T.; Mo, Y.; Nieves-Remacha, M. J.; Johnson, M. D.; García-Losada, P.; Mateos, C.; Rincón, J. A.; Jensen, K. F. Continuous Stirred-Tank Reactor Cascade Platform for Self-Optimization of Reactions Involving Solids. *React Chem Eng* **2022**, 7 (6), 1315–1327.  
<https://doi.org/10.1039/D2RE00054G>.

- (40) Hartman, R. L. Managing Solids in Microreactors for the Upstream Continuous Processing of Fine Chemicals. *Org Process Res Dev* **2012**, *16* (5), 870–887. [https://doi.org/10.1021/OP200348T/ASSET/IMAGES/LARGE/OP-2011-00348T\\_0014.JPEG](https://doi.org/10.1021/OP200348T/ASSET/IMAGES/LARGE/OP-2011-00348T_0014.JPEG).
- (41) Queirós, S.; Morais, V.; Rodrigues, C. S. D.; Maldonado-Hódar, F. J.; Madeira, L. M. Heterogeneous Fenton's Oxidation Using Fe/ZSM-5 as Catalyst in a Continuous Stirred Tank Reactor. *Sep Purif Technol* **2015**, *141*, 235–245. <https://doi.org/10.1016/J.SEPPUR.2014.11.046>.
- (42) Kappe, C. O. Controlled Microwave Heating in Modern Organic Synthesis. *Angewandte Chemie International Edition* **2004**, *43* (46), 6250–6284. <https://doi.org/10.1002/ANIE.200400655>.
- (43) Glasnov, T. N.; Kappe, C. O. The Microwave-to-Flow Paradigm: Translating High-Temperature Batch Microwave Chemistry to Scalable Continuous-Flow Processes. *Chemistry – A European Journal* **2011**, *17* (43), 11956–11968. <https://doi.org/10.1002/CHEM.201102065>.
- (44) Hornung, C. H.; Nguyen, X.; Carafa, A.; Gardiner, J.; Urban, A.; Fraser, D.; Horne, M. D.; Gunasegaram, D. R.; Tsanaktsidis, J. Use of Catalytic Static Mixers for Continuous Flow Gas-Liquid and Transfer Hydrogenations in Organic Synthesis. *Org Process Res Dev* **2017**, *21* (9), 1311–1319. [https://doi.org/10.1021/ACS.OPRD.7B00180/ASSET/IMAGES/LARGE/OP-2017-00180X\\_0008.JPEG](https://doi.org/10.1021/ACS.OPRD.7B00180/ASSET/IMAGES/LARGE/OP-2017-00180X_0008.JPEG).
- (45) Kralik, D.; Kovářová, A.; Vobecká, L.; Hasal, P.; Slouka, Z.; Příbyl, M. Continuous Flow Synthesis and Separation of Mandelic Acid Enantiomers in a Modular Microfluidic System. *Sep Purif Technol* **2023**, *309*, 123009. <https://doi.org/10.1016/J.SEPPUR.2022.123009>.
- (46) Mallia, C. J.; Baxendale, I. R. The Use of Gases in Flow Synthesis. *Org Process Res Dev* **2016**, *20* (2), 327–360. [https://doi.org/10.1021/ACS.OPRD.5B00222/ASSET/IMAGES/LARGE/OP-2015-002222\\_0043.JPEG](https://doi.org/10.1021/ACS.OPRD.5B00222/ASSET/IMAGES/LARGE/OP-2015-002222_0043.JPEG).
- (47) Yoshida, J. I.; Takahashi, Y.; Nagaki, A. Flash Chemistry: Flow Chemistry That Cannot Be Done in Batch. *Chemical Communications* **2013**, *49* (85), 9896–9904. <https://doi.org/10.1039/C3CC44709J>.
- (48) Hsueh, N.; Clarkson, G. J.; Shipman, M. Generation and Ring Opening of Aziridines in Telescoped Continuous Flow Processes. *Org Lett* **2015**, *17* (14), 3632–3635. [https://doi.org/10.1021/ACS.ORGLETT.5B01777/SUPPL\\_FILE/OL5B01777\\_SI\\_005.CIF](https://doi.org/10.1021/ACS.ORGLETT.5B01777/SUPPL_FILE/OL5B01777_SI_005.CIF).
- (49) Holst, D. E.; Wang, D. J.; Kim, M. J.; Guzei, I. A.; Wickens, Z. K. Aziridine Synthesis by Coupling Amines and Alkenes via an Electrogenerated Dication. *Nature* **2021**, *596* (7870), 74–79. <https://doi.org/10.1038/s41586-021-03717-7>.
- (50) Donnelly, K.; Baumann, M. Continuous Flow Technology as an Enabler for Innovative Transformations Exploiting Carbenes, Nitrenes, and Benzyne. *Journal of Organic Chemistry* **2022**, *87* (13), 8279–8288. [https://doi.org/10.1021/ACS.JOC.2C00963/ASSET/IMAGES/LARGE/JO2C00963\\_0002.JPEG](https://doi.org/10.1021/ACS.JOC.2C00963/ASSET/IMAGES/LARGE/JO2C00963_0002.JPEG).
- (51) Hatridge, T. A.; Liu, W.; Yoo, C. J.; Davies, H. M. L.; Jones, C. W. Optimized Immobilization Strategy for Dirhodium(II) Carboxylate Catalysts for C–H

- Functionalization and Their Implementation in a Packed Bed Flow Reactor. *Angewandte Chemie International Edition* **2020**, 59 (44), 19525–19531.  
<https://doi.org/10.1002/ANIE.202005381>.
- (52) Ahmedna, M.; Marshall, W. E.; Husseiny, A. A.; Rao, R. M.; Goktepe, I. The Use of Nutshell Carbons in Drinking Water Filters for Removal of Trace Metals. *Water Res* **2004**, 38 (4), 1062–1068. <https://doi.org/10.1016/J.WATRES.2003.10.047>.
- (53) Bogdan, A. R.; Dombrowski, A. W. Emerging Trends in Flow Chemistry and Applications to the Pharmaceutical Industry. *J Med Chem* **2019**, 62 (14), 6422–6468. [https://doi.org/10.1021/ACS.JMEDCHEM.8B01760/ASSET/IMAGES/MEDIUM/JM-2018-01760T\\_0011.GIF](https://doi.org/10.1021/ACS.JMEDCHEM.8B01760/ASSET/IMAGES/MEDIUM/JM-2018-01760T_0011.GIF).
- (54) Jat, K. R.; Khairwa, A. Levalbuterol versus Albuterol for Acute Asthma: A Systematic Review and Meta-Analysis. *Pulm Pharmacol Ther* **2013**, 26 (2), 239–248. <https://doi.org/10.1016/J.PUPT.2012.11.003>.
- (55) World Health Organization. *WHO Electronic Essential Medicines List (EEML)*; 2022. <https://doi.org/Licence:CCBY3.0IGO>.
- (56) Babad, E. C. N. I. J. R. S. S. M. A Short Synthesis of Albuterol. *Synthesis (Stuttg)* **1988**, No. 12, 966–968.
- (57) Ameredes, B. T.; Calhoun, W. J. Albuterol Enantiomers: Pre-Clinical and Clinical Value? *Frontiers in Bioscience - Elite* **2010**, 2 E (3), 1081–1092. <https://doi.org/10.2741/E166/PDF>.
- (58) Un-Noor, F.; Padmanaban, S.; Mihet-Popa, L.; Mollah, M. N.; Hossain, E. A Comprehensive Study of Key Electric Vehicle (EV) Components, Technologies, Challenges, Impacts, and Future Direction of Development. *Energies* **2017**, Vol. 10, Page 1217 **2017**, 10 (8), 1217. <https://doi.org/10.3390/EN10081217>.
- (59) Ge, Y.; Ye, F.; Liu, J.; Yang, J.; Spannenberg, A.; Jiao, H.; Jackstell, R.; Beller, M. Ligand-Controlled Palladium-Catalyzed Carbonylation of Alkynols: Highly Selective Synthesis of  $\alpha$ -Methylene- $\beta$ -Lactones. *Angewandte Chemie International Edition* **2020**, 59 (48), 21585–21590. <https://doi.org/10.1002/ANIE.202006550>.
- (60) Richers, J.; Heilmann, M.; Drees, M.; Tiefenbacher, K. Synthesis of Lactones via C-H Functionalization of Nonactivated C(Sp<sup>3</sup>)-H Bonds. *Org Lett* **2016**, 18 (24), 6472–6475. [https://doi.org/10.1021/ACS.ORGLETT.6B03371/ASSET/IMAGES/MEDIUM/OL-2016-03371Z\\_0006.GIF](https://doi.org/10.1021/ACS.ORGLETT.6B03371/ASSET/IMAGES/MEDIUM/OL-2016-03371Z_0006.GIF).
- (61) Stankiewicz, A.; Moulijn, J. A. *Re-Engineering the Chemical Processing Plant*; CRC Press, 2003. <https://doi.org/10.1201/9780203913291/RE-ENGINEERING-CHEMICAL-PROCESSING-PLANT-ANDRZEJ-STANKIEWICZ-JACOB-MOULIJN>.
- (62) Bisacchi, G. S. Origins of the Quinolone Class of Antibacterials: An Expanded “Discovery Story.” *J Med Chem* **2015**, 58 (12), 4874–4882. [https://doi.org/10.1021/JM501881C/ASSET/IMAGES/LARGE/JM-2014-01881C\\_0008.JPEG](https://doi.org/10.1021/JM501881C/ASSET/IMAGES/LARGE/JM-2014-01881C_0008.JPEG).
- (63) Liu, H.; Mulholland, S. G. Appropriate Antibiotic Treatment of Genitourinary Infections in Hospitalized Patients. *American Journal of Medicine* **2005**, 118 (7 SUPPL.), 14–20. <https://doi.org/10.1016/j.amjmed.2005.05.009>.
- (64) Leshner, G. Y.; Froelich, E. J.; Gruett, M. D.; Bailey, J. H.; Brundage, R. P. 1,8-Naphthyridine Derivatives. A New Class of Chemotherapeutic Agents. *J Med Pharm Chem* **1962**, 5 (5), 1063–1065. [https://doi.org/10.1021/JM01240A021/ASSET/JM01240A021.FP.PNG\\_V03](https://doi.org/10.1021/JM01240A021/ASSET/JM01240A021.FP.PNG_V03).

- (65) Emmerson, A. M.; Jones, A. M. The Quinolones: Decades of Development and Use. *Journal of Antimicrobial Chemotherapy* **2003**, *51* (suppl\_1), 13–20. <https://doi.org/10.1093/JAC/DKG208>.
- (66) Sharma, P. C.; Jain, A.; Jain, S. Fluoroquinolone Antibacterials: A Review on Chemistry, Microbiology and Therapeutic Prospects. *Acta Pol. Pharm.* **2009**, No. 66, 587–604.
- (67) Van Caekenberghe, D. L.; Pattyn, S. R. In Vitro Activity of Ciprofloxacin Compared with Those of Other New Fluorinated Piperazinyl-Substituted Quinoline Derivatives. *Antimicrob Agents Chemother* **1984**, *25* (4), 518–521. <https://doi.org/10.1128/AAC.25.4.518>.
- (68) Peterson, L. R. Quinolone Molecular Structure-Activity Relationships: What We Have Learned about Improving Antimicrobial Activity. *Clinical Infectious Diseases* **2001**, *33* (Supplement\_3), S180–S186. <https://doi.org/10.1086/321846>.
- (69) Kong, C. J.; Fisher, D.; Desai, B. K.; Yang, Y.; Ahmad, S.; Belecki, K.; Gupton, B. F. High Throughput Photo-Oxidations in a Packed Bed Reactor System. *Bioorg Med Chem* **2017**, *25* (23), 6203–6208. <https://doi.org/10.1016/J.BMC.2017.07.004>.
- (70) Mitscher, L. A. Bacterial Topoisomerase Inhibitors: Quinolone and Pyridone Antibacterial Agents. *Chem Rev* **2005**, *105* (2), 559–592. <https://doi.org/10.1021/CR030101Q/ASSET/IMAGES/LARGE/CR030101QF00044.JPG> G.
- (71) Aldred, K. J.; Kerns, R. J.; Osheroff, N. Mechanism of Quinolone Action and Resistance. *Biochemistry* **2014**, *53* (10), 1565–1574. [https://doi.org/10.1021/BI5000564/ASSET/IMAGES/LARGE/BI-2014-000564\\_0007.JPEG](https://doi.org/10.1021/BI5000564/ASSET/IMAGES/LARGE/BI-2014-000564_0007.JPEG).
- (72) Linder, J. A.; Huang, E. S.; Steinman, M. A.; Gonzales, R.; Stafford, R. S. Fluoroquinolone Prescribing in the United States: 1995 to 2002. *American Journal of Medicine* **2005**, *118* (3), 259–268. <https://doi.org/10.1016/j.amjmed.2004.09.015>.
- (73) Andriole, V. T. The Quinolones: Past, Present, and Future. *Clinical Infectious Diseases* **2005**, *41* (Supplement\_2), S113–S119. <https://doi.org/10.1086/428051>.
- (74) Domagala, J. M. Structure-Activity and Structure-Side-Effect Relationships for the Quinolone Antibacterials. *Journal of Antimicrobial Chemotherapy* **1994**, *33* (4), 685–706. <https://doi.org/10.1093/JAC/33.4.685>.
- (75) Ledoussal, B.; Almstead, J. K.; Flaim, C. P. Presented in Part at the Program and Abstracts of the 39th Interscience Conference on Antimicrobial Agents and Chemotherapy; San Francisco, 1999.
- (76) MacGowan, A. P.; Wootton, M.; Holt, H. A. The Antibacterial Efficacy of Levofloxacin and Ciprofloxacin against Pseudomonas by Combining Antibiotic Exposure and Bacterial Susceptibility. *Journal of Antimicrobial Chemotherapy* **1999**, *43* (3), 345–349. <https://doi.org/10.1093/JAC/43.3.345>.
- (77) Fu, K. P.; Lafredo, S. C.; Foleno, B.; Isaacson, D. M.; Barrett, J. F.; Tobia, A. J.; Rosenthale, M. E. In Vitro and in Vivo Antibacterial Activities of Levofloxacin (l-Ofloxacin), an Optically Active Ofloxacin. *Antimicrob Agents Chemother* **1992**, *36* (4), 860–866. <https://doi.org/10.1128/AAC.36.4.860>.
- (78) Naber, K. G.; Adam, D. Classification of Fluoroquinolones. *Int J Antimicrob Agents* **1998**, *10* (4), 255–257. [https://doi.org/10.1016/S0924-8579\(98\)00059-4](https://doi.org/10.1016/S0924-8579(98)00059-4).

- (79) Tillotson, G. S. Quinolones: Structure-Activity Relationships and Future Predictions. *J Med Microbiol* **1996**, *44* (5), 320–324. <https://doi.org/10.1099/00222615-44-5-320/CITE/REFWORKS>.
- (80) Pham, T. D. M.; Ziora, Z. M.; Blaskovich, M. A. T. Quinolone Antibiotics. *Med. Chem. Comm.* **2019**, *10*, 1719–1739.
- (81) Lin, H.; Dai, C.; Jamison, T. F.; Jensen, K. F. A Rapid Total Synthesis of Ciprofloxacin Hydrochloride in Continuous Flow. *Angewandte Chemie International Edition* **2017**, *56* (30), 8870–8873. <https://doi.org/10.1002/ANIE.201703812>.
- (82) Tosso, N. P.; Desai, B. K.; De Oliveira, E.; Wen, J.; Tomlin, J.; Gupton, B. F. A Consolidated and Continuous Synthesis of Ciprofloxacin from a Vinylogous Cyclopropyl Amide. *Journal of Organic Chemistry* **2019**, *84* (6), 3370–3376. [https://doi.org/10.1021/ACS.JOC.8B03222/SUPPL\\_FILE/JO8B03222\\_SI\\_001.PDF](https://doi.org/10.1021/ACS.JOC.8B03222/SUPPL_FILE/JO8B03222_SI_001.PDF).
- (83) Senger, N. A.; Bo, B.; Cheng, Q.; Keeffe, J. R.; Gronert, S.; Wu, W. The Element Effect Revisited: Factors Determining Leaving Group Ability in Activated Nucleophilic Aromatic Substitution Reactions. *Journal of Organic Chemistry* **2012**, *77* (21), 9535–9540. [https://doi.org/10.1021/JO301134Q/SUPPL\\_FILE/JO301134Q\\_SI\\_001.PDF](https://doi.org/10.1021/JO301134Q/SUPPL_FILE/JO301134Q_SI_001.PDF).
- (84) Sato, M.; Katagiri, N.; Takayama, K.; Hirose, M.; Kaneko, C. Synthesis of 1, 3-Dioxin-4-Ones and Their Use in Synthesis. XVI. : 4-Oxo-1, 3-Dioxin-5-Carboxylic Acids and Related Compounds : Versatile Synthetic Intermediates for the Synthesis of 6-Unsubstituted Six-Membered Heterocyclic Compounds. *Chem Pharm Bull (Tokyo)* **1989**, *37* (3), 665–669. <https://doi.org/10.1248/CPB.37.665>.
- (85) Brinkerhoff, R. C.; Tarazona, H. F.; De Oliveira, P. M.; Flores, D. C.; Montes D'Oca, C. D. R.; Russowsky, D.; Montes D'Oca, M. G. Synthesis of  $\beta$ -Ketoesters from Renewable Resources and Meldrum's Acid. *RSC Adv* **2014**, *4* (91), 49556–49559. <https://doi.org/10.1039/C4RA08986C>.
- (86) Zicane, D.; Ravinya, I.; Teter, Z.; Rijkure, I.; Gudriniece, E.; Kalejs, U. Exotic Amino Acids. 4. Synthesis of Methyl Esters of Some N-Heteroamino-Methylenemalononic Acids. *Chem Heterocycl Compd (N Y)* **2000**, *36* (6), 754–757. <https://doi.org/10.1007/BF02297688/METRICS>.
- (87) Zicane, D.; Ravina, I.; Teter, Z.; Rijkure, I.; Petrova, M.; Kalejs, U. Exotic Amino Acids. 8. Synthesis of Monomethyl Esters of N-Aryl-Aminomethylenemalononic Acids. *Chem Heterocycl Compd (N Y)* **2002**, *38* (7), 840–845. <https://doi.org/10.1023/A:1020641922707/METRICS>.
- (88) Brown, H. C.; Jungk, H. The Isomerization of O- and p-Xylenes and Some Related Alkylbenzenes Under the Influence of Hydrogen Bromide and Aluminum Bromide; the Relative Isomerization Aptitudes of Alkyl Groups. *J Am Chem Soc* **1955**, *77* (21), 5579–5584. [https://doi.org/10.1021/JA01626A038/ASSET/JA01626A038.FP.PNG\\_V03](https://doi.org/10.1021/JA01626A038/ASSET/JA01626A038.FP.PNG_V03).
- (89) Lee, C. C.; Zohdi, H. F.; Sallam, M. M. M. Hydrogen-Deuterium Exchanges in a Friedel-Crafts Reaction. *Journal of Organic Chemistry* **1985**, *50* (5), 705–707. [https://doi.org/10.1021/JO00205A034/ASSET/JO00205A034.FP.PNG\\_V03](https://doi.org/10.1021/JO00205A034/ASSET/JO00205A034.FP.PNG_V03).
- (90) Method for Coproducing Key Intermediates of Quinolone Medicines by Using O-Dichlorobenzene as Raw Material. CN102249881A, 2011.
- (91) Kürti, L.; Czakó, Barbara. *Strategic Applications of Named Reactions in Organic Synthesis : Background and Detailed Mechanisms*; Elsevier Academic Press, 2005.
- (92) Price, C. C. The Alkylation of Aromatic Compounds by the Friedel-Crafts Method. *Organic Reactions* **1946**, 1–82. <https://doi.org/10.1002/0471264180.OR003.01>.

- (93) Xu, T.; Barich, D. H.; Torres, P. D.; Nicholas, J. B.; Haw, J. F. Carbon-13 Chemical Shift Tensors for Acylium Ions: A Combined Solid State NMR and Ab Initio Molecular Orbital Study. *J Am Chem Soc* **1997**, *119* (2), 396–405. [https://doi.org/10.1021/JA962944N/SUPPL\\_FILE/JA396.PDF](https://doi.org/10.1021/JA962944N/SUPPL_FILE/JA396.PDF).
- (94) Tarakeshwar, P.; Lee, J. Y.; Kim, K. S. Role of Lewis Acid( $\text{AlCl}_3$ )-Aromatic Ring Interactions in Friedel-Craft's Reaction: An Ab Initio Study. *Journal of Physical Chemistry A* **1998**, *102* (13), 2253–2255. <https://doi.org/10.1021/JP9807322/ASSET/IMAGES/LARGE/JP9807322F00002.JPEG>.
- (95) Gothelf, A. S.; Hansen, T.; Jørgensen, K. A. Studies on Aluminium Mediated Asymmetric Friedel–Crafts Hydroxyalkylation Reactions of Pyridinecarbaldehydes. *J Chem Soc Perkin 1* **2001**, No. 8, 854–860. <https://doi.org/10.1039/B009669P>.
- (96) Olah, G. A.; Török, B.; Joschek, J. P.; Bucsi, I.; Esteves, P. M.; Rasul, G.; Prakash, G. K. S. Efficient Chemoselective Carboxylation of Aromatics to Arylcarboxylic Acids with a Superelectrophilically Activated Carbon Dioxide- $\text{Al}_2\text{Cl}_6/\text{Al}$  System. *J Am Chem Soc* **2002**, *124* (38), 11379–11391. [https://doi.org/10.1021/JA020787O/SUPPL\\_FILE/JA020787O\\_S.PDF](https://doi.org/10.1021/JA020787O/SUPPL_FILE/JA020787O_S.PDF).
- (97) Brown, H. C.; Grayson, M. Kinetics of the Reaction of Representative Benzyl Halides with Aromatic Compounds; Evidence for a Displacement Mechanism in the Friedel-Crafts Reactions of Primary Halides. *J Am Chem Soc* **1953**, *75* (24), 6285–6292. [https://doi.org/10.1021/JA01120A052/ASSET/JA01120A052.FP.PNG\\_V03](https://doi.org/10.1021/JA01120A052/ASSET/JA01120A052.FP.PNG_V03).
- (98) Brown, H. C.; Jungk, H. The Reaction of Benzene and Toluene with Methyl Bromide and Iodide in the Presence of Aluminum Bromide; Evidence for a Displacement Mechanism in the Methylation of Aromatic Compounds. *J Am Chem Soc* **1955**, *77* (21), 5584–5589. [https://doi.org/10.1021/JA01626A039/ASSET/JA01626A039.FP.PNG\\_V03](https://doi.org/10.1021/JA01626A039/ASSET/JA01626A039.FP.PNG_V03).
- (99) Yamase Yoshiaki. On the Studies of the Friedel-Crafts Acylation. II. The Relative Reactivity for Some Acyl Halides. <https://doi.org/10.1246/bcsj.34.480> **2006**, *34* (4), 480–484. <https://doi.org/10.1246/BCSJ.34.480>.
- (100) Pretsch, E.; Clerc, T.; Seibl, J.; Simon, W. *Tables of Spectral Data for Structure Determination of Organic Compounds*; Fresenius, W., Huber, J. F. K., Pungor, E., Rechnitz, G. A., Simon, W., West, Th. S., Eds.; Chemical Laboratory Practice; Springer Berlin Heidelberg: Berlin, Heidelberg, 1983. <https://doi.org/10.1007/978-3-662-22455-7>.
- (101) Brown, A. C.; Gibson, J. XXX.—A Rule for Determining Whether a given Benzene Mono-Derivative Shall Give a Meta-Di-Derivative or a Mixture of Ortho- and Para-Di-Derivatives. *Journal of the Chemical Society, Transactions* **1892**, *61* (0), 367–369. <https://doi.org/10.1039/CT8926100367>.
- (102) Otake, C.; Namba, T.; Tabata, H.; Makino, K.; Hirano, K.; Oshitari, T.; Natsugari, H.; Kusumi, T.; Takahashi, H. Conformational Preference of 2'-Fluoro-Substituted Acetophenone Derivatives Revealed by Through-Space  $^1\text{H}$ - $^{19}\text{F}$  and  $^{13}\text{C}$ - $^{19}\text{F}$  Spin-Spin Couplings. *Journal of Organic Chemistry* **2021**, *86* (6), 4638–4645. [https://doi.org/10.1021/ACS.JOC.1C00051/ASSET/IMAGES/LARGE/JO1C00051\\_0007.JPEG](https://doi.org/10.1021/ACS.JOC.1C00051/ASSET/IMAGES/LARGE/JO1C00051_0007.JPEG).
- (103) Vedachalam, S.; Muruges, N.; Chakraborty, P.; Karvembu, R.; Liu, X. W. NHC Catalyzed Enantioselective Coates-Claisen Rearrangement: A Rapid Access to the Dihydropyran Core for Oleuropein Based Secoiridoids. *New Journal of Chemistry* **2018**, *42* (3), 1832–1839. <https://doi.org/10.1039/C7NJ04057A>.

- (104) Cavalli, E. S.; Mies, T.; Rzepa, H. S.; White, A. J. P.; Parsons, P. J.; Barrett, A. G. M. Pyrimidine Nucleosides Syntheses by Late-Stage Base Heterocyclization Reactions. *Org Lett* **2022**, *24* (49), 8931–8935. [https://doi.org/10.1021/ACS.ORGLETT.2C03152/SUPPL\\_FILE/OL2C03152\\_SI\\_001.PDF](https://doi.org/10.1021/ACS.ORGLETT.2C03152/SUPPL_FILE/OL2C03152_SI_001.PDF).
- (105) Ko, T. Y.; Youn, S. W. Cooperative Indium(III)/Silver(I) System for Oxidative Coupling/Annulation of 1,3-Dicarbonyls and Styrenes: Construction of Five-Membered Heterocycles. *Adv Synth Catal* **2016**, *358* (12), 1934–1941. <https://doi.org/10.1002/ADSC.201600280>.
- (106) Wang, D. J.; Lu, L. Y.; Zheng, C. Y.; Zheng, J. Synthesis and Crystal Structure of Methyl 2-(2,4-Dichloro-5-Fluorobenzoyl)-3-(Pyrimidin-2-Ylamino)Acrylate. *Research on Chemical Intermediates* **2012**, *38* (9), 2355–2363. <https://doi.org/10.1007/S11164-012-0551-8/FIGURES/3>.



## Vita

Jeffrey Michael Noble was born and raised in northeast, New Jersey. He graduated from Pope John XXIII Regional High School in Sparta, New Jersey. After high school, he studied biochemistry and molecular biology at the University of Richmond in Richmond, Virginia. During his undergraduate studies, Jeffrey performed research in synthetic organic chemistry under his advisors Dr. Raymond Dominey, and Dr. Emma Goldman. He earned a Bachelor of Science in Biochemistry and Molecular Biology from UR in May of 2018

In August of 2018, Jeffrey began graduate studies in chemistry at Virginia Commonwealth University. He initially began work at the Medicines for All Institute under Dr. Thomas Roper, but shortly switched investigators to Dr. B. Frank Gupton in early 2019. Jeffrey completed his graduate studies in May of 2023.